Czech Technical University in Prague
Faculty of Biomedical Engineering
Department of Biomedical Technology

EFFECT OF VENTILATION PARAMETERS ON MECHANICAL POWER DELIVERY TO THE LUNGS

Doctoral Thesis

Ing. Šimon Walzel

Kladno, September 2025

Ph.D. Programme: Biomedical Engineering

Supervisor: prof. Ing. Karel Roubík, Ph.D.
Supervisor-Specialist: doc. MUDr. Petr Waldauf, Ph.D.

DECLARATION

I hereby declare that I have completed this thesis having the topic “Effect of ventilation parameters on mechanical power delivery to the lungs” independently, and that I have attached an exhaustive list of citations of the employed sources.

Generative AI tools were used solely for grammar correction and language refinement. All content, including study design, data analysis, interpretation, and conclusions, was developed by the author based on cited resources.

I do not have a compelling reason against the use of the dissertation thesis within the meaning of Section 60 of the Act No. 121/2000 Sb., on copyright, rights related to copyright and amending some laws (Copyright Act).

In Kladno 10. 9. 2025 …….

Ing. Šimon Walzel

ACKNOWLEDGEMENTS

I would like to express my sincere gratitude to my dissertation supervisor, Professor Karel Roubík, who has accompanied me throughout my studies since my undergraduate years. Since 2017, we have shared not only professional collaboration, but also many moments of both work and free time. Under his mentorship, I have learned to work independently, master scientific writing, develop practical skills with bench tools, and cultivate precision and often patience in my work.

I am also deeply grateful to my closest colleagues from the Non-Conventional Ventilatory Team and the Amateur Radio Club Bídná vlna: MUDr. Lenka Horáková, Ph.D. (OK1DRL), Ing. Václav Ort, Ph.D. (OK1TRO) and Ing. Ladislav Bís (OK1BIS), who accompanied me during my studies and research projects. Special thanks to my colleagues from the Department of Biomedical Technology (Associate Professor Ing. Martin Rožánek, Ph.D., Ing. Veronika Ráfl-Huttová, Ph.D., and Ing. Jakub Ráfl, Ph.D.) for their invaluable cooperation in teaching and research projects.

I am also grateful to the Military University Hospital in Prague and MUDr. David Novotný for providing me with the opportunity to validate my research findings in a clinical environment.

Finally, I would like to express my sincere gratitude to my wife and family, whose unwavering support has been an important factor in my academic journey.

This dissertation was supported by grants from the CTU Student Grant Competition, specifically SGS23/198/OHK4/3T/17 and SGS20/202/OHK4/3T/17.

ABSTRACT

Mechanical ventilation (MV) is a life-saving intervention but is often associated with ventilator-induced lung injury. Recently, the concept of mechanical power (MP), defined as the rate of mechanical energy delivery from the ventilator to the respiratory system, has emerged as a tool for assessing lung protective ventilation. However, current bedside MP calculation methods are based on simplified equations that have important limitations, potentially misrepresenting the actual stresses acting on the lung parenchyma. The aims of this dissertation were to develop a passive physical model of the respiratory system able to independently simulate tissue resistance (R_t) or airway flow resistance (R_{aw}), to quantify the effect of R_t on MP delivery, to compare and evaluate different simplified MP estimation methods in the presence of R_t and R_{aw}, and to investigate the clinical relevance of the findings in a pilot clinical study.

The novel physical model with R_t was developed by connecting a low-friction glass syringe with a throttle valve in parallel to the artificial lung of a bellow-based simulator, creating a mechanical damper that mimics viscoelastic behavior as a Maxwell body. Experiments were performed on physical lung models with a compliance of 30 $mL \cdot cmH_2O^{-1}$, configurable R_{aw} (0–15 $cmH_2O \cdot s \cdot L^{-1}$), and a Maxwell-type viscoelastic element representing R_t. The models were ventilated in volume-controlled mode at varying inspiratory flow rates. Flow, pressure at the airway opening and inside the artificial lung were measured at 100 Hz. Mechanical energy was calculated using the geometric method from pressure-volume (PV) loops and from several published simplified MP equations. Dissipated energy was computed from PV loop hysteresis. Results showed that when R_{aw} and R_t were tuned to produce identical maximum airway pressures, both the simplified MP equations and the geometric method produced nearly identical MP estimates from airway opening pressure measurements. However, measurements inside the artificial lung revealed up to 20% higher delivered energy in the presence of R_t compared to R_{aw}. Dissipated energy analysis indicated that R_t contributed predominantly to energy losses at the lung level, while R_{aw} primarily increased energy dissipation at the airway opening. Increasing R_{aw} increased MP estimates at the airway opening but did not proportionally increase lung-level energy. The pilot clinical study suggested that the duration of the inspiratory hold may affect MP estimates and indicated the possible presence of tissue resistance, as shown by measurable pressure decrease during inspiratory hold maneuvers.

Current simplified MP equations, as well as geometric energy calculation from the inspiratory phase only, may misinterpret the energy delivered to lung tissue. Distinguishing between R_t and R_{aw}, using prolonged inspiratory holds, could assist in adjusting ventilation parameters toward more individualized lung protective strategies.

Keywords

Mechanical ventilation; Mechanical power; Tissue resistance; Viscoelasticity; Physical model of respiratory system

ABSTRAKT

Umělá plicní ventilace (MV) je život zachraňující metoda, která může být spojena se vznikem ventilátorem indukovaného poranění plic. Nedávno se objevujil koncept mechanického výkonu (MP), definovaného jako množství dodávané mechanické energie z ventilátoru do respiračního systému, který slouží jako nástroj pro hodnocení protektivity ventilace. Současné metody výpočtu MP jsou založeny na zjednodušených rovnicích, které mají významná omezení a mohou zkreslovat skutečný tlak působící na plicní parenchym. Cílem této disertační práce bylo vyvinout pasivní fyzický model respiračního systému, který umožní samostatně simulovat tkáňový odpor (R_t) nebo průtočný odpor dýchacích cest (R_{aw}), kvantifikovat vliv R_t na přenos MP, porovnat a vyhodnotit různé zjednodušené metody odhadu MP v přítomnosti R_t a R_{aw} a ověřit klinickou relevanci zjištění v pilotní klinické studii.

Fyzický model s R_t byl vytvořen za pomoci borosilikátové injekční stříkačky (s nízkým třecím odporem) a škrticího ventilu připojených paralelně k umělé plíci měchového simulátoru, čímž vznikl mechanický tlumič napodobující viskoelastické chování typu Maxwellova tělesa. Experimenty byly provedeny na fyzikálních modelech plic s poddajností 30 $mL \cdot cmH_2O^{-1}$, konfigurovatelným R_{aw} (0–15 $cmH_2O \cdot s \cdot L^{-1}$) a viskoelastickým prvkem reprezentujícím R_t. Modely byly ventilovány v objemově řízeném režimu při různých inspiračních průtocích. Byl měřen průtok, tlak na vstupu do dýchacích cest a tlak uvnitř umělé plíce s frekvencí 100 Hz. Mechanická energie byla vypočítána geometrickou metodou z tlakově-objemových (PV) křivek a z několika publikovaných zjednodušených rovnic pro MP. Disipovaná energie byla určena z hystereze PV křivek. Při nastavení R_{aw} a R_t na stejné maximální tlaky na vstupu do dýchacích cest byly výsledné hodnoty získané ze zjednodušených rovnice MP i geometrické metody téměř shodné při měření tlaku na vstupu do dýchacích cest. Měření uvnitř umělé plíce však poukázalo na až o 20 % vyšší dodanou energii v přítomnosti R_t oproti R_{aw}. Analýza disipované energie naznačila, že R_t přispívá převážně ke ztrátám energie na úrovni plic, zatímco R_{aw} zvyšuje zejména disipaci energie na vstupu do dýchacích cest. Zvýšení R_{aw} vedlo k vyšším odhadům MP na vstupu do dýchacích cest, ale na úrovni plic ke změnám MP nedocházelo. Pilotní klinická studie naznačila, že délka inspirační pauzy může ovlivnit odhady MP a poukázala na možnou přítomnost tkáňového odporu, jak ukázal pokles tlaku během inspirační pauz.

Současné zjednodušené rovnice MP, stejně jako výpočet energie geometrickou metodou pouze z inspirační fáze, mohou nesprávně interpretovat energii dodanou do plic. Rozlišení mezi R_t a R_{aw}, například pomocí prodloužených inspiračních pauz, by mohlo pomoci při úpravě ventilačních parametrů směrem k více individualizovaným strategiím protektivity ventilace.

Klíčová slova

Umělá plicní ventilace; Mechanická energie; Tkáňový odpor; Viskoelasticita; Fyzický model respiračního systému

Contents

List of Symbols and Abbreviations

List of Symbols

Symbol	Unit	Meaning
C	$mL \cdot cmH_2O^{-1}$	Compliance
C_1	$mL \cdot cmH_2O^{-1}$	Static compliance of the lung
C_2	$mL \cdot cmH_2O^{-1}$	Viscoelastic compliance of the lung
C_L	$mL \cdot cmH_2O^{-1}$	Lung compliance
C_t	$mL \cdot cmH_2O^{-1}$	Tissue compliance
E	J	Mechanical energy
E_{aw}	J	Mechanical energy measured at the airway opening
E_d	J	Driving mechanical energy measured at the airway opening
E_L	J	Mechanical energy at the lung level
i	-	Number of a sample
I_{insp}	-	Set of indices i that belong to the inspiratory part of the cycle
$I{:}E$	-	Inspiratory-to-expiratory time ratio
MP	$J \cdot min^{-1}$	Mechanical power
P_1	cmH_2O	Alveolar pressure at the start of the inspiratory hold
P_{aw}	cmH_2O	Airway pressure
P_d	cmH_2O	Driving pressure
$PEEP$	cmH_2O	Positive end-expiratory pressure
P_{es}	cmH_2O	Esophageal pressure
P_{max}	cmH_2O	Maximum airway pressure
P_{mean}	cmH_2O	Mean airway pressure
P_{plat}	cmH_2O	Plateau pressure
P_{transp}	cmH_2O	Transpulmonary pressure
P_L	cmH_2O	Pressure at the lung level
Q	$L \cdot min^{-1}$	Flow
Q_{insp}	$L \cdot min^{-1}$	Inspiratory flow
R	$cmH_2O \cdot s \cdot L^{-1}$	Resistance
R_{aw}	$cmH_2O \cdot s \cdot L^{-1}$	Airway flow resistance
R_t	$cmH_2O \cdot s \cdot L^{-1}$	Tissue resistance
t	s	Time
T_i	s	Inspiratory time
T_e	s	Expiratory time
T	s	Total time
VT_i	mL	Inspiratory tidal volume
VT	mL	Tidal volume

List of Abbreviations

Abbreviation	Meaning
ARDS	Acute respiratory distress syndrome
COPD	Chronic Obstructive Pulmonary Disease
CT	Computed Tomography
ECMO	Extracorporeal Membrane Oxygenation
EIT	Electrical Impedance Tomography
FCV	Flow-Controlled Ventilation
FiO_2	Fraction of Inspired Oxygen
FOT	Forced Oscillatory Technique
HFJV	High-Frequency Jet Ventilation
HFOV	High-Frequency Oscillatory Ventilation
HME	Heat and Moisture Exchanger
ICU	Intensive Care Unit
MBW	Multiple-Breath Washout
MFOV	Multi-Frequency Oscillatory Ventilation
MP	Mechanical Power
MRI	Magnetic Resonance Imaging
MV	Mechanical Ventilation
PaO_2	Partial Pressure of Oxygen in Arterial Blood
PCV	Pressure-Controlled Ventilation
PV	Pressure-Volume
SARS	Severe Acute Respiratory Syndrome
SPECT	Single Photon Emission Computed Tomography
VCV	Volume-Controlled Ventilation
VILI	Ventilator-induced lung injury

1 Introduction

Mechanical ventilation (MV) is an advanced method of artificial respiratory support that plays a crucial role in intensive care. However, even after more than 200 years of study, MV remains associated with high mortality rates and numerous complications, making it a persistent focus of investigation. This field is highly complex and can be studied from multiple perspectives, ranging from the technical aspects of ventilators and their physiological effects on patients to the optimization of ventilation strategies. Numerous research teams worldwide are dedicated to this topic, and an extensive body of literature aims to enhance understanding and improve therapeutic approaches.

A relatively new approach to optimizing lung protective ventilator settings, while minimizing the adverse effects of MV, is the estimation of mechanical power (MP) delivered to the respiratory system. However, methods for determining MP are inconsistent, rely on various assumptions and simplifications, and differ in what portion of the delivered energy is considered potentially harmful.

The main focus of this dissertation is to investigate the effect of lung tissue viscoelasticity on MP delivery during MV and to examine the limitations of simplified MP estimation methods under varying airway flow resistance and tissue resistance. The findings may contribute to improving MV efficiency and reducing the risk of ventilator-induced lung injury (VILI).

Chapter 2 provides an overview of the current state of research on MV, covering its clinical implications, various alternative and non-conventional ventilator types designed to mitigate its adverse effects, and the mechanical properties of the respiratory system. It also discusses the concept of mechanical power delivered to the respiratory system, including different calculation methods and their limitations. Chapter 4 describes the design of a physical viscoelastic model of the respiratory system, its validation, and the effect of tissue viscoelasticity on delivered MP, with the potential to distinguish tissue resistance from airway flow resistance using proximal pressure measured at the airway opening. Chapter 5 then compares various simplified methods for calculating MP delivery when applied to a physical model with airway flow resistance and tissue resistance. Chapter 6 presents the methods, results, and discussion of a pilot clinical study validating the laboratory findings. Finally, Chapters 7–9 provide a discussion and summary, including the contributions of the study and its significance for biomedical engineering.

A version of Chapters 2 and 4 has previously been published as: *Walzel S & Roubik K. (2025) Effect of tissue viscoelasticity on delivered mechanical power in a physical respiratory system model: Distinguishing between airway and tissue resistance. Biomedical Physics & Engineering Express, 11(1), 015026. DOI: 10.1088/2057-1976/ad974b.* Walzel S was the primary author and played the principal role in the design of the physical viscoelastic respiratory system model and its verification, data analysis and manuscript preparation.

A version of Chapters 2 and 5 has previously been published as: *Walzel S, Roubik K. (2025) Evaluation of simplified mechanical power and dissipated energy calculations in physical respiratory models with tissue and airway resistance. Lékař a technika-Clinician and Technology. 55(1). DOI: 10.14311/CTJ.2025.1.03. (in print).* Walzel S was the primary author and played the principal role in the preparation of the study methodology and its execution.

As part of broader research related to the effects of ventilation parameters and individualized ventilation strategies, a novel inspiratory flow generation system was developed. This system enables precise control of flow profiles and allows ventilator settings to be adapted across different patient populations, and it is briefly discussed in Chapter 7. The results of this research have also been published in Applied Sciences (*Walzel S, Bis L, Ort V & Roubik K. Simple design of mechanical ventilator for mass production may offer excellent performance, precise monitoring, and advanced safety. DOI: 10.3390/app15105631*) and Scientific Reports (*Roubik K, Ort V, Horakova L & Walzel S. Novel design of inspiratory flow generation and gas mixing for critical care ventilators suitable for rapid production and mass casualty incidents. DOI: 10.1038/s41598-023-34300-x).*

2 Overview of the current state

Respiratory diseases represent a global health challenge, with conditions such as chronic obstructive pulmonary disease (COPD), acute respiratory distress syndrome (ARDS), pneumonia, and neuromuscular disorders often leading to severe respiratory failure. In cases where spontaneous breathing is not sufficient to maintain adequate gas exchange, mechanical ventilation (MV) is a crucial life-support intervention. Indications for MV usually include acute hypoxemic or hypercapnic respiratory failure. Despite its life-saving role, MV is associated with potential complications, including ventilator-induced lung injury (VILI).

2.1 Respiratory diseases

COPD is a lung disease characterized by chronic airflow limitation. In acute exacerbations, patients may develop hypercapnic respiratory failure due to increased airway flow resistance and dynamic hyperinflation. Non-invasive ventilation is often preferred, but invasive MV may be required in severe COPD cases, though its management is challenging due to the risk of air trapping or barotrauma [1]. Bacterial or viral pneumonia, including cases such as influenza, tuberculosis, severe acute respiratory syndrome (SARS), or COVID-19, can cause extensive lung inflammation, alveolar damage, and hypoxemic respiratory failure [2]. Common respiratory diseases include also asthma, which requires prolonged expiratory time during MV [3]. MV may also be required for trauma-related respiratory failure, neuromuscular disorders that cause respiratory muscle weakness, management of postoperative respiratory complications, or respiratory failure due to drug overdose.

ARDS is one of the most difficult respiratory diseases to treat, with a mortality rate of approximately 40% [4]. Most patients with early acute lung injury experience shortness of breath, but early diagnosis of ARDS remains difficult despite the 2012 Berlin definition, which outlines its criteria based on oxygenation, chest radiographs, disease origin, and time course [5]. In healthy lungs, alveolar cells form a very tight barrier that restricts the passage of small, dissolved substances but allows the diffusion of carbon dioxide and oxygen. These cells produce a surfactant that lowers the surface tension, allowing the alveoli to remain open and facilitating gas exchange [6]. As a result of damage to the barrier properties of the alveolar epithelium and endothelium, the edematous fluid enters the alveoli. This leads to pulmonary edema with acute respiratory failure due to decreased oxygenation (caused by ventilation/perfusion mismatch) and respiratory failure (carbon dioxide not adequately removed from the body). Increased dead space and decreased compliance are independent predictors of mortality in ARDS, with heterogeneous structural lung tissue damage being a key pathological feature [6]. Despite the natural asymmetry of the bronchial tree, the distribution of ventilation to each part of the healthy lungs is relatively homogeneous. However, diseased lungs can increase the degree of structural heterogeneity by altering mechanical properties. If the lungs are not homogeneous (e.g., due to the presence of local atelectasis), regions of the lungs adjacent to the collapsed lung compartments must bear additional load, thereby locally

increasing their tension (stress), as previously and theoretically described in the study by Mead et al. [7]. This means that even within the same patient, the most appropriate ventilation setting for one compartment of the lungs may not necessarily be the same for another.

In the study by Cressoni et al. [8], lung heterogeneity in ARDS patients was assessed using computed tomography (CT) scans by comparing regions of lung parenchyma with adjacent areas. The study found that abnormal lung heterogeneity, defined as a ratio greater than 1.61, affected 14–23% of lung volume, with correlations between heterogeneity and physiological variables such as PaO_2/FiO_2, plateau pressure, and dead space fraction, suggesting that lung homogeneity improves with higher airway pressures. The authors speculate that the load on these regions of the lung may be nearly twice that of the whole lung, and that positive end-expiratory pressure (*PEEP*) settings may reduce or paradoxically increase lung heterogeneity, depending on whether they improve or worsen tissue aeration.

2.2 Mechanical ventilation

MV can be divided into several categories according to various characteristics. The use of positive pressure ventilation is preferred over negative pressure ventilation. Although negative pressure ventilation has a number of advantages, its use is inappropriate mainly because of limited access to the patient. If the disease is not too severe, non-invasive ventilation is used, where the patient is assisted in breathing with some pressure support and a fraction of the inhaled oxygen. If the disease is more severe, intubation, and therefore an invasive type of mechanical ventilation, is used. Invasive positive pressure ventilation can be further subdivided according to the patient's degree of dependence on ventilation. If the patient does not breathe spontaneously, mandatory ventilation is used, where the ventilator controls the entire respiratory cycle. When weaning from the ventilator, the patient is then switched from fully mandatory ventilation to assisted ventilation, where the ventilator monitors the patient's spontaneous breathing activity [9].

Conventional ventilators, which use tidal volumes and frequencies similar to spontaneous human breathing, remain the mainstay of treatment for ARDS, despite the risk of exacerbating existing lung injury and causing VILI. VILI arises from various sources, including high pressures (barotrauma), excessive and cyclic lung expansion (volutrauma), repeated asynchronous opening and closing of air compartments with each inflation (atelectrauma), and the release of cytokines and other inflammatory mediators (biotrauma) [10].

2.2.1 Lung protective ventilation

There are several recommendations to provide the lung protective ventilation, such as: low tidal volumes (*VT*), low driving and plateau pressures, appropriately chosen *PEEP*, pronation, alveolar recruitment (opening maneuvers), reasoned (based on careful monitoring of target physiological parameters), or minimization of mechanical power delivery to the lungs [11].

Objectively, the easiest way to ensure lung protective ventilation is to minimize its duration. MV basically aims to bridge the period when the patient is unable to breathe spontaneously. Next, setting MV parameters to avoid excessive distension at the end of inspiration, by using lower tidal volumes, and alveolar derecruitment at the end of expiration, by setting *PEEP* appropriately, has significantly reduced mortality in ARDS [12]. The compliance of diseased lungs is much less than that of healthy lungs because some compartments of the lungs are consolidated by edema and inflammation associated with atelectasis. Therefore, lower tidal volumes are needed in ARDS to avoid regional over-distension. The optimal level of *PEEP* must be balanced between preventing alveolar collapse and avoiding overdistension. While recruitment maneuvers may temporarily improve oxygenation in some patients, their long-term clinical benefit remains uncertain [13]. A study of lung injury in sheep found that PEEP levels between 15–17.5 cmH_2O optimized recruitment while minimizing overdistension, maximizing oxygenation, and reducing ventilatory pressures [14].

Then, the study by Amato et al. [15] found that driving pressure (P_d)—calculated as plateau pressure minus *PEEP*—is the strongest predictor of survival in ARDS patients, independent of tidal volume and *PEEP* settings. Lowering P_d was associated with improved survival, suggesting that optimizing mechanical ventilation based on P_d may be more effective than focusing solely on low tidal volumes or high *PEEP*.

Prone positioning is now recommended for most patients with severe ARDS [16]. Pronation is beneficial in obese patients by reducing ventilatory heterogeneity and improving lung ventilation. The authors believe that obesity is a key factor in the progression of pneumonia in COVID-19 and that this risk can be reduced by effective pronation strategies early in the course of the disease [17].

The role of high inspiratory flow in the development of VILI has received less attention than other factors. Higher inspiratory flow rates have been found to require more pressure to inflate the lungs to a given volume than lower inspiratory flow rates [18], and more recently, higher pressures resulting from higher flow rates have been found to be associated with the development of VILI [19]. These findings are also supported by the studies of Maeda et al. [20] and Santini et al. [21], which suggest that when tidal volume is delivered at a higher peak flow rate, gas exchange and respiratory mechanics are impaired, and pulmonary histology appears to be more pronounced than when tidal volume is delivered at a lower peak flow rate. Furthermore, MV using high pressures for 6 hours using conventional flow patterns was found to result in severe lung injury regardless of respiratory rate or inspiratory time. However,

reducing inspiratory flow at similar maximum pressures provides greater lung protective ventilation [22].

As summarized in the review by Gattinoni et al. [23], the adverse effects of MV in ARDS are due to unphysiological changes in transpulmonary and pleural pressures. Excessive strain and stress, resulting in volutrauma and barotrauma, are the main damaging factors, influenced not only by tidal volume and pressure, but also by respiratory rate and inspiratory flow. To improve patient outcomes, a personalized approach that takes into account mechanical properties of the respiratory system, recruitability, inhomogeneity and mechanical power thresholds is essential.

As noted earlier, MV support is usually necessary for survival. There are many approaches to MV that differ in principle. However, they all have in common that they always damage the lung to some extent and cannot simultaneously address the requirements for optimal ventilation. Alternative and unconventional methods of MV to improve lung protective ventilation are also the subject of research.

2.2.2 Alternative and non-conventional methods of mechanical ventilation

In an effort to provide adequate oxygenation and carbon dioxide removal while minimizing the adverse effects of conventional MV, several alternative and non-conventional strategies have been explored. Some of these methods still rely on ventilatory support, albeit in a modified or unconventional form—such as high-frequency ventilation, liquid ventilation, or tracheal gas insufflation—while others, like extracorporeal membrane oxygenation (ECMO), function independently of the lungs by using extracorporeal circuits to ensure gas exchange. Among these, ECMO has become widely adopted in clinical practice, whereas the other methods are used only rarely today.

High-frequency ventilation can be subdivided into and high-frequency jet ventilation (HFJV) and high-frequency oscillatory ventilation (HFOV). HFJV delivers small tidal volumes at very high frequencies using brief pulses of pressurized gas injected into the airway, typically through a specialized jet nozzle. HFOV is an alternative form of MV where tidal volumes are less than the anatomical dead space and respiratory cycle frequencies are greater than 1 Hz. The method is based on several different physical mechanisms: turbulence, pendelluft, Taylor dispersion, asymmetric velocity profiles, molecular diffusion or collateral ventilation [24]. Generally, lower maximum pressures at the alveolar level and higher mean airway pressures are used. Thus, HFOV appears to achieve several goals of lung protective ventilation by utilizing appropriate mean airway pressures and small tidal volumes. However, recent multicenter studies, the OSCILATE and OSCAR trials [25, 26], do not support the routine use of HFOV in adult patients with moderate to severe ARDS because the benefit of this alternative non-conventional method has not been proven. A study by Ferguson et al. [25] found that early use of HFOV was associated with higher mortality than conventional MV with low tidal volumes and high *PEEP* levels. HFOV was associated with higher mean airway pressures and

greater use of sedatives, neuromuscular blocking agents, and vasoactive drugs. In the study by Young et al. [26], the authors found no benefit or harm from the use of HFOV in adult patients with ARDS. However, they recommended that this mode of ventilation should not be used in routine care. According to a study by Meade et al. [27], HFOV increases mortality in most patients with ARDS, but may improve survival in patients with severe hypoxemia. These findings add to the uncertainty about the role of HFOV. In carefully selected patients, HFOV may still have a role in severe ARDS, but only after trying conventional MV and considering the prone position.

Some studies suggest that multifrequency HFOV (MFOV) may improve gas exchange more effectively than single-frequency HFOV by ensuring a more even distribution of ventilation across heterogeneous lung regions [28, 29]. Experimental study in preterm lambs showed that MFOV led to significantly better oxygenation, CO_2 elimination, and lung recruitment at lower airway pressures, reducing regional stress and potentially minimizing the risk of VILI compared to single-frequency HFOV [29].

Another approach, called "Twinstream", combines conventional MV with superimposed HFJV, allowing lung ventilation at two different pressure levels. This method improves gas exchange, particularly CO_2 removal, and is beneficial for a wide range of patients, including neonates, obese adults, and those with severe obstructive or restrictive lung disease [30]. HFJV should improve oxygenation at lower ventilation pressures and without adverse effects on hemodynamics, increase alveolar recruitment, increase functional residual capacity, and decrease transpulmonary pressure.

A rather interesting alternative approach is the so-called Three-Level ventilation. Three-Level ventilation can be defined as MV at three programmable pressure levels, whereby the pressure levels alternate and the duration of the pressure levels in the lungs is controlled by the ventilator software once set by the operator. The inhomogeneity of the ventilation distribution is due to different time constants of lung compartments with different mechanical properties, in which single-level ventilation (pressure- or volume-controlled) cannot achieve optimal ventilation settings without a critical decrease in minute ventilation by reducing the ventilation rate [31].

One of the currently discussed approaches to lung protective ventilation is flow-controlled ventilation (FCV). It differs from volume-controlled ventilation (VCV) only in the setting of a constant flow rate in the expiratory phase. According to a study by Wenzel et al. [32], the pressure distribution in the inhomogeneous lung is more homogeneous during linearized expiration than during conventional passive expiration. This may be another mechanism to increase lung protective ventilation. The effect of FCV on respiratory mechanics and regional ventilation in obese and morbidly obese patients showed that linearized expiratory flow during FCV provides better lung aeration at comparable tidal volume, plateau pressure and *PEEP* compared to VCV [33].

2.3 Mechanical properties of the respiratory system

Respiratory system can be described as a pneumatic circuit, simply defined by resistance (R) and compliance (C). The relationship between the pressure drop across a pneumatic system and the gas flow can be described by a parameter called flow resistance, which indicates the volume flow rate Q resulting from the pressure difference Δp. This relationship is given by:

$$R = \frac{\Delta p}{Q}. \tag{1}$$

This formula for flow resistance is the pneumatic equivalent of electrical resistance, where pressure and flow are analogous to voltage and current. The unit of flow resistance R is $\mathrm{Pa \cdot s \cdot m^{-1}}$. In pneumatic systems, the resistance value often depends on the gas flow rate, making the system description more complex. The compliance C of a pneumatic system describes how easily the system can accumulate gas and is defined as:

$$C = \frac{\Delta V}{\Delta p}, \tag{2}$$

where ΔV is the volume of gas delivered to the system and Δp is the pressure increase due to the volume change. Compliance is a typical property of the lungs, with units of $\mathrm{m^3 \cdot Pa^{-1}}$ (or $\mathrm{mL \cdot cmH_2O^{-1}}$). Assuming negligible gas compression in the lungs, the volume of gas delivered is equivalent to the increase in lung volume, and lung compliance is defined as the change in lung volume per change in transpulmonary pressure, i.e., the difference between alveolar and pleural pressures. The higher the pressure needed to deliver a given volume, the lower the system's compliance.

However, simple linear models consisting of only R and C, which are crucial for understanding the fundamentals of mechanical behavior, may have limited validity due to the nonlinearities, inhomogeneities, and structural complexity that characterize the entire respiratory system. Numerous studies have been conducted to develop reliable physical models [32, 34, 35] and computer models [36–38] of the respiratory system, e.g., to outline some of the mechanical properties of the respiratory system or to compare different ventilation modes.

2.3.1 Viscoelasticity

One of the properties complicating the description of the respiratory system is the viscoelasticity of the lung parenchymal tissue. The total resistance of the respiratory system is determined not only by the flow resistance in the airways but also by the resistance of the lung tissue [39]. Tissue resistance (R_t) can be attributed to several factors, including viscoelasticity [40, 41], nonlinear viscoelasticity [42, 43], fractional viscoelasticity [44], poroelasticity [45, 46], pendelluft [21] or, for example, surface tension [47]. Then, the changes in total resistance

can be caused, for example, by an obstructed endotracheal tube, an airway narrowing or the tissue resistance of the respiratory system [48].

The single compartment linear model is linear because its independent variables (volume and flow) have a linear relationship with the dependent variable (pressure). This means that if only one of these independent variables changes while the other remains constant, there is a linear relationship between pressure and that variable. If the model included a variable for which this condition was not true, the model would be nonlinear [39].

The single airway of the viscoelastic model in Fig. 2.1 represents the entire airway tree R_{aw}. The mechanical properties of the tissues are described by three components: a resistor (known as a dashpot) and two springs. Together, these three elements—R_t, C_1, and C_2—form what is known as a Kelvin body. The stiffness of the spring C_1 represents the static elastic compliance of the lung, while the combination of R_t and C_2 in series (which together form a Maxwell body) accounts for its viscoelastic behavior. The model represents a single homogenous physical compartment, but still has two degrees of freedom, because the magnitude of the pressure at any moment in time is defined by two factors: the volume in the alveolar compartment and the extension of the spring C_2 or the dashpot R_t [39].

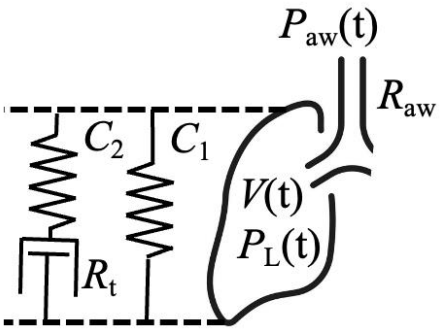

Figure 2.1: The viscoelastic single compartment model of the respiratory system.

2.3.2 Measurement of the mechanical properties of the respiratory system

To understand the state of the respiratory system and ensure optimal lung protective ventilation, it is essential to determine several mechanical properties of the respiratory system. In addition to basic parameters such as resistance R and compliance C of the respiratory system, several other factors play a key role in optimizing MV. These include auto-*PEEP*, lung recruitability, lung viscoelasticity, hysteresis of the pressure-volume loop, regional ventilation heterogeneity, stress distribution in the lung parenchyma and others.

Many parameters can be obtained simply by analyzing the pressure, flow, or volume waveforms of MV. However, a seemingly simple measurement of compliance can be problematic due to tissue resistance. The method for measuring tissue resistance involves

maintaining a constant volume during inspiratory hold and measuring the pressure. When inspiratory flow is stopped, the pressure drops rapidly from its maximum value (P_{max}) to a lower value P_1, which represents the alveolar pressure. This rapid drop in pressure is caused by flow resistance, both artificial and anatomical. During inspiratory hold, a slower decrease in pressure to the plateau pressure (P_{plat}) value is observed [49]. This additional pressure decrease is mainly caused by the stress relaxation in the parenchyma, usually assigned to viscoelasticity [19, 21, 50]. Under dynamic conditions, P_1 reflects alveolar pressure more accurately than P_{plat} and therefore, it can be used to predict the actual pressures acting on the lung parenchyma [21]. Therefore, the P_{plat} readings taken at 0.5 s and 5 s of inspiratory hold, used to calculate the total resistance and compliance of the respiratory system, can produce significantly different results due to the lung tissue viscoelasticity [51]. And further, static measurements of compliance using P_{plat} have been shown to underestimate the maximum pressure experienced by lung parenchymal tissue during dynamic inflation and that the inspiratory slope as a dynamic measure may provide a more accurate estimate of maximum alveolar pressure [52].

Assessing the mechanical properties of individual lung compartments is complicated due to the lung recruitability and heterogeneity or stress distribution, with several approaches varying in accuracy, complexity, and information obtained. One method for determining lung heterogeneity could be done by the evaluation of the time constants of individual compartments during expiration. As the time constant is the product of airway flow resistance and lung compliance, it links structural mechanics to lung function. In healthy lungs, the variation in time constants between lung compartments is relatively small. However, in lung compartments that are heterogeneous in terms of mechanical properties, the differences in time constants can be so large that the optimal setting of MV parameters for one compartment makes the setting of parameters for other compartments significantly inappropriate [53]. Although many methods exist to determine time constants [54], linear single compartment models poorly describe the lung during ARDS, where significant mechanical and structural heterogeneity exists [55].

Functional imaging methods allow for the visualization of ventilation heterogeneity based on its topographic distribution. Single-photon emission computed tomography (SPECT) measures the distribution of inhaled ^{99m}Tc, reflecting ventilation, where areas with low activity indicate poorly ventilated or non-ventilated lung compartments. Oxygen and hyperpolarized gases such as xenon (^{129}Xe) or helium (^{3}He) can also be used with magnetic resonance imaging (MRI) to assess ventilation distribution without ionizing radiation [56]. Cressoni et al. analyzed lung heterogeneity in ARDS patients using CT scans, comparing lung regions voxel by voxel based on gas-to-tissue ratios, but this assessment remains relative due to the lack of an absolute reference standard [8].

Multiple breath washout (MBW) and the forced oscillation technique (FOT) are both used to assess lung heterogeneity, though they offer different insights. MBW evaluates ventilation heterogeneity by tracking the washout of an inert gas (such as nitrogen or helium) and analyzing the temporal distribution of ventilation, making it particularly sensitive to

detecting the extent of airway constriction. In contrast, FOT assesses respiratory mechanics by measuring resistance and reactance across a range of frequencies, thus providing information on airway impedance and structural changes [56]. While MBW is more effective at quantifying how much the airways are constricted, FOT is better suited for characterizing the nature and location of the constriction [57]. Additionally, FOT has been shown to serve as a non-invasive tool for monitoring lung volume recruitment and derecruitment [58].

The assessment of lung recruitability and appropriate *PEEP* titration during MV, as well as the determination of heterogeneities in the mechanical properties of individual lung compartments, is possible with electrical impedance tomography [59, 60]. This imaging modality offers more potential and is likely to be the future in intensive care for monitoring lung protective ventilation and individualizing MV strategy.

2.4 Mechanical power

Tidal volume, pressure, and flow are components of the energy load that contribute to the amount of mechanical power (MP) delivered to the lungs and it was recently suggested that MP is also a strong predictor of VILI risk [61, 62, 63]. A study by Cressoni et al. [61] showed that transpulmonary MP higher than 12 $J \cdot min^{-1}$ induced VILI in healthy pigs and the study by Serpa Neto et al. [64] showed that MP (> 17.0 $J \cdot min^{-1}$) was independently associated with higher in-hospital mortality in ICU patients receiving invasive ventilation for at least 48 h.

The mechanical energy (E) delivered to the lungs by the mechanical ventilator can be calculated from the pressure-volume (PV) loop as the area enclosed under the inspiratory curve of airway pressure against inspired volume, expressed in joules [65]. This is usually referred to as the geometric method and requires numerical integration of airway pressure (P_{aw}) with respect to changes in inspired volume (VT_i):

$$E = \int_0^{VT_i} P_{aw} \cdot dVT. \tag{3}$$

Simply multiplying E delivered during one respiratory cycle by the respiratory rate per minute then gives the value of the delivered MP. The use of the geometric method, however, is computationally challenging and requires special equipment with a high sampling rate to record pressure and flow waveforms. Various simplifications of mechanical power calculations for VCV have been proposed in the last years to facilitate bedside calculations in clinical environments [62, 66–70].

In a study by Gattinoni et al. [66], the authors proposed a simple equation to quantify E delivered to the respiratory system during mechanical ventilation based on the equation of motion. The authors noted that the benefit of the equation is its ability to quantify the individual contributions of its various components. At any given time, the pressure (P_{aw}) in the whole respiratory system is equal to:

$$P_{\mathrm{aw}} = \frac{VT}{C_{\mathrm{rs}}} + R_{\mathrm{aw}} \cdot Q + PEEP, \tag{7}$$

where VT represents the delivered tidal volume, C_{rs} is the compliance of the respiratory system, R_{aw} is the airway flow resistance and Q is the inspiratory flow. Each component in the equation actually represents a pressure:

$$\frac{VT}{C_{rs}} = P_{\mathrm{aw}} \; = \; P_{\mathrm{plat}} - \; PEEP, \tag{8}$$

$$R_{\mathrm{aw}} \cdot Q = \; P_{\mathrm{max}} - \; P_{\mathrm{plat}}. \tag{9}$$

PEEP itself is not associated with movement but represents the basic tension of the lungs because it is the pressure present in the respiratory system when VT and Q are zero. Conversion factor 0.098 was used to recalculate cmH_2O to Pa. After a few more mathematical operations we can calculate the energy delivered per one cycle E by multiplying each pressure in the equation by VT, as follows:

$$E = 0.098 \cdot VT^2 \cdot \left(\frac{1}{2 \cdot C_{\mathrm{rs}}} + \frac{R_{\mathrm{aw}}}{T_{\mathrm{i}}}\right) + VT \; \cdot \; PEEP, \tag{10}$$

where T_{i} is the inspiratory time. Considering the ratio of T_{i} to the whole respiratory cycle, expressing the volume in liters, the pressure in cmH_2O, their product multiplied by the respiratory rate (RR), we already obtain the following well-known equation:

$$MP = \; 0.098 \; \cdot RR \cdot \left(VT^2 \cdot \left(\frac{1}{2 \cdot C_{\mathrm{rs}}} + RR \; \cdot \frac{R_{\mathrm{aw}}\,(1+I{:}E)}{60 \cdot I{:}E}\right) + VT \; \cdot \; PEEP\right). \tag{11}$$

Another approach that simplifies the integration is based on equation (11) but reduces significantly the computational effort. The disadvantage, however, is the persistent need for an inspiratory hold. This method is usually referred to as "simplified" or "comprehensive" [66, 67]:

$$E = 0.098 \cdot VT \cdot \left[\left(P_{\mathrm{max}} - 0.5 \cdot \left(P_{\mathrm{plat}} - PEEP\right)\right]\right. . \tag{12}$$

The following methods of calculating E delivery do not require any intervention during mechanical ventilation and can therefore be calculated from the ventilation parameters still shown on the ventilator display. By modifying the "simplified" equation (12) by substituting P_{plat} for P_{max}, we obtain the so-called dynamic mechanical power equation [68]:

$$E = 0.098 \cdot VT \cdot [(P_{\mathrm{max}} - 0.5 \cdot (P_{\mathrm{max}} - PEEP)]. \tag{13}$$

However, in VCV, P_{plat} can differ significantly from P_{max} due to flow resistance, so its use is probably more appropriate for pressure-controlled ventilation.

The so-called "surrogate" equation proposed by Giosa et al. [67] simplifies the calculation of E delivery by replacing the resistive component with an average flow resistance value of 10 $cmH_2O \cdot s \cdot L^{-1}$:

$$E = VT \cdot \left(\frac{P_{\max} + PEEP + \left(\frac{Q}{6}\right)}{20} \right), \tag{14}$$

where the inspiratory flow rate (Q) divided by six is obtained by multiplying the flow rate by the flow resistance and converting from seconds to minutes. However, a significant limitation of this approach is the assumption of a stable airway flow resistance of 10 $cmH_2O \cdot s \cdot L^{-1}$.

The equation of Chi et al. [70] assumes that the pressure fractions in the formula of Gattinoni et al. [66] can be replaced by the mean airway pressure over the entire respiratory cycle, weighted by the ratio of expiratory to inspiratory pressure due to the inclusion of the entire respiratory cycle. As there is no P_{plat} in the equation, no inspiratory hold is required for this calculation.

$$E = 0.098 \cdot VT \cdot \left(P_{\text{mean}} + \frac{T_e}{T_i} (P_{\text{mean}} - PEEP) \right), \tag{15}$$

where P_{mean} is the mean airway pressure, T_e is the expiratory time and T_i is the inspiratory time. The mathematical derivation of the simplified MP equations is accessible in Appendix A.

All the equations presented so far used only the measured parameters at the airway opening to determine the delivered E. The equation by Silva et al. [62], which is based on the studies by Guerin et al. [71] and Marini et al. [72], uses the so-called transpulmonary driving pressure (P_{transp}) to determine the delivered E. P_{transp} was calculated as the difference between alveolar pressure and pleural pressure at end-inspiration and end-expiration. This equation estimates E without taking into account resistive properties and $PEEP$:

$$E = \frac{1}{2} \cdot VT \cdot P_{\text{transp}} \, . \tag{16}$$

In another study [73], the authors examined different methods of calculating MP in mechanically ventilated patients, comparing MP calculated from P_{aw} and including $PEEP$, MP calculated from P_d, and MP calculated from transpulmonary P_d. MP calculated from P_{aw} and including $PEEP$ produced significantly higher MP delivery estimates than the other two but only calculations considering P_d predicted 28-day mortality.

2.4.1 Dissipated energy

Recently, the so-called dissipated energy, which is represented by the hysteresis area of the PV loop, and which might be potentially harmful, has been taken into account [19, 66, 74]. During inspiratory phase, a part of the energy is stored as elastic energy, and a part is dissipated by various mechanisms in the airways and lung tissue. The remaining energy is then recovered during expiration. In physical terms, dissipated energy reflects the irreversible loss of mechanical energy in the respiratory system during a respiratory cycle, while mechanically it is the portion of inspiratory energy not recovered during expiration. Mathematically, it corresponds to the area enclosed by the inspiratory and expiratory limbs of the PV loop.

According to the results of Gotti et al. [75, 76], it appears that the amount of energy that may be associated with the development of VILI is static dissipated energy (i.e., the flow resistance of the respiratory system is excluded from the dissipated energy calculation) and that less energy is dissipated with lower tidal volumes with an unchanged minute ventilation.

This is further supported by Massari et al. [77] who suggested that higher energy loads during mechanical ventilation lead to VILI, with dissipated energy in the lung parenchyma being related to lung recruitability, strain and lung inhomogeneity. The dissipated energy was primarily influenced by high tidal volumes, but lung inhomogeneities and alveolar opening and closing also played a significant role.

Another study [74] reported that numerical calculations indicate that energy dissipation can be significantly reduced by controlling the ventilation flow to be constant and continuous during both inspiration and expiration, and by ventilating at an I:E ratio very close to 1:1, that is, by using FCV. This statement was then verified when both inspiratory and expiratory flows were kept nearly constant at 12 ± 0.98 $L \cdot min^{-1}$, and the I:E ratio was 1:1 with a minute ventilation of 6.23 ± 0.15 $L \cdot min^{-1}$. The authors recorded PV loops using pressure measured directly in the patient's trachea and calculated the energy dissipated in the patient from the hysteresis area of the PV loops. The energy dissipation was 0.17 ± 0.02 J, which, according to the authors, is close to the minimum energy dissipation achievable for this minute ventilation [78].

Spraider et al. [79] in their long-term porcine ventilation study demonstrated the applicability of compliance-guided individualization of FCV settings, resulting in lower tidal volumes, more efficient gas exchange with improved oxygenation, more efficient CO_2 elimination, and more homogeneous gas distribution without signs of overinflation compared to pressure-controlled ventilation (PCV). According to the authors, their results for individualized FCV and the underlying concept of reducing dissipated energy and minimizing stress and strain suggest a more lung protective ventilation strategy than the current best clinical practice of PCV.

However, different results were found in the study by Busana et al. [80]. Twenty-two healthy pigs were randomized to a control group (n = 11) and a valve group (n = 11) with controlled expiratory flow. Both groups had identical ventilation settings. Total energy

dissipation differed significantly (4.34 ± 0.66 vs. 2.62 ± 0.31 J·min^{-1}), mainly through the endotracheal tube (2.87 ± 0.3 vs. 1.88 ± 0.2 J·min^{-1}), while energy dissipation in the respiratory system was lower in the valve group (0.73 ± 0.16 vs. 1.45 ± 0.5 J·min^{-1}). Despite similar respiratory mechanics, gas exchange and histology, the control group had a greater decrease in end-expiratory lung impedance. The authors conclude that with their experimental conditions, the reduction of energy dissipated in the respiratory system did not lead to appreciable differences in VILI.

Thus, how to quantify injurious dissipated energy in the lung from PV loops measured at the bedside is a matter for future research [81].

2.4.2 Assumptions and limitations

MP calculations are based on several assumptions that limit their general use, and their application is still subject to several limitations. First, only constant inspiratory flow in VCV and linear respiratory system compliance are assumed for the use of simplified equations.

Next, airway flow resistance is not explicitly distinguished from tissue resistance in any of these methods of calculating mechanical power delivery to the lungs. Therefore, the P_{plat} used in the calculations may not accurately quantify the forces and injurious energy that cause damage. The small pressure difference between P_1 and P_{plat}, which probably corresponds to viscoelastic losses [19, 23, 48, 63], is buried in what is usually clinically assigned to the difference between maximum pressure and P_{plat}, which caregivers use to calculate airway flow resistance. This hidden pressure difference involves unmeasured energy spent on viscoelastic losses and potentially on the direct infliction of damage by microfractures of extracellular matrix elements [63].

Another limitation of using some MP calculations is that there is no defined length of the inspiration hold. This limitation is basically based on the tissue resistance mentioned above. As discussed, under dynamic conditions, P_1 provides a more accurate alveolar pressure than P_{plat} and can thus serve as a predictor of the actual pressures acting on the lung parenchyma [21]. Consequently, the P_{plat} readings taken at 0.5 s and 5 s of inspiratory hold, used to calculate the total resistance and compliance of the respiratory system, can produce significantly different results [51].

Next, the inclusion of *PEEP* into simplified MP calculations despite no mechanical movement is debated. *PEEP* sets a baseline level of lung inflation, meaning that every additional breath starts from a higher lung volume. This baseline energy contributes to lung stress and ignoring it in MP calculations would underestimate the total mechanical load on lung tissue [82]. On the other hand, reducing *PEEP* to lower MP may be misleading because *PEEP* has both protective and adverse effects depending on its relationship to pleural pressure [73]. *PEEP* has the ability to modify the lung surface area (due to the recruitability of the patient's lungs) able to receive the stress released by the mechanical ventilator. If an increase in *PEEP*

will lead to a decrease in P_d and respiratory system elastance, MP will decrease, and vice versa [62].

Whether MP dissipated in the airway is related to the development of VILI is questionable [83]. Amato et al. [15] found that P_d calculated is the strongest predictor of survival in ARDS patients, and a retrospective study of 8,207 critically ill patients found that high MP in the first 48 hours of ventilation was associated with higher mortality, fewer ventilator-free days, and longer ICU and hospital stays, with *RR* and P_d being the key factors associated with mortality [64]. Therefore, it is unclear whether the inclusion of resistive MP in MP calculations is justified. Evaluation of MP as a measure of VILI development would be most relevant when volume and related pressure changes are measured directly at the lung parenchyma [83]. The magnitude of the pressure acting on the lung parenchyma is indicated by P_{transp}, which is not commonly available in clinical practice. To calculate P_{transp}, both alveolar pressure and pleural pressure must be estimated. The most widely accepted surrogate for alveolar pressure is P_{aw} during end-inspiratory or end-expiratory hold maneuvers. Direct measurement of pleural pressure is invasive and impractical for clinical use, so esophageal pressure (P_{es}), despite its limitations, is an accepted surrogate for pleural pressure [84]. It allows estimation of transpulmonary pressure by calculating the difference between esophageal pressure and P_{aw}:

$$P_{\mathrm{transp}} = P_{\mathrm{aw}} - P_{\mathrm{es}} \,. \tag{17}$$

Another unresolved limitation of the use of MP is the unknown MP threshold when VILI is already developing. It seems that the solution could be normalization to a standard lung volume or to the amount of aerated lung tissue [23, 72]. The study by Zhang et al. [85] suggested that MP normalized to predicted body weight or lung compliance may be an appropriate solution. Other assumptions made when using the equations to calculate the delivered MP include the absence of spontaneous respiratory activity by the patient and homogeneous mechanical properties of the individual lung compartments.

3 Aims of dissertation thesis

The most effective way to achieve lung protective ventilation is to minimize its duration, but this is not always possible in clinical practice. The invasive positive pressure conventional mechanical ventilation leads to progressive lung injury. In recent years, mortality in ARDS patients on mechanical ventilation has been reduced mainly by individualized care. One of the pillars of individualized care is the effort to minimize the delivery of mechanical power to the lungs. This dissertation deals with the optimization of ventilatory parameter settings and diagnostic capabilities of mechanical ventilators, especially with regard to providing increased lung protective ventilation.

The first aim was to develop a passive physical model of the respiratory system that simulates lung tissue viscoelasticity and airway flow resistance, and to use this model to determine whether it is possible to distinguish tissue resistance from airway flow resistance using proximal pressure measured at the airway opening.

The next aim was to mathematically analyze the effect of lung tissue viscoelastic properties on mechanical power delivery during mechanical ventilation, and to compare and evaluate different simplified estimation methods for determining delivered mechanical power in the presence of tissue and airway flow resistance, assessing their accuracy and limitations.

And finally, the aim was to investigate the clinical relevance of the findings through a pilot clinical study, thereby validating the results from laboratory models in real patient scenarios.

4 Effect of Tissue Viscoelasticity on Delivered Mechanical Power in a Physical Respiratory System Model: Distinguishing Between Airway and Tissue Resistance

A version of this chapter has previously been published as: *Walzel S & Roubik K. (2025) Effect of tissue viscoelasticity on delivered mechanical power in a physical respiratory system model: Distinguishing between airway and tissue resistance. Biomedical Physics & Engineering Express, 11(1), 015026. DOI: 10.1088/2057-1976/ad974b.*

The aim of this study was to develop a passive physical model of the respiratory system that simulates lung tissue viscoelasticity and airway flow resistance, and to use this physical model to determine whether it is possible to distinguish tissue resistance from airway flow resistance using proximal pressure measured at the airway opening.

4.1 Abstract

A precise understanding of respiratory system mechanics is essential for optimizing ventilator settings and maintaining patient safety. Conventional simplified models usually account only for airway flow resistance and lung compliance, while tissue resistance is often disregarded. In this study, the impact of lung tissue viscoelastic properties on delivered mechanical power was assessed using a physical respiratory system model, along with the feasibility of differentiating tissue resistance from airway flow resistance through proximal pressure measured at the airway opening. Three passive physical model configurations were employed, each representing distinct mechanical properties: a Tissue resistance model, an Airway resistance model, and a No-resistance model. Identical volume-controlled ventilation settings were applied across all configurations, with inspiratory flow rates varied. Pressure and flow were recorded using a Datex-Ohmeda S/5 vital signs monitor (Datex-Ohmeda, Madison, WI, USA). Tissue resistance was adjusted so that peak pressures and mechanical energy delivered at the airway opening were comparable between the Tissue and Airway resistance models. Nevertheless, measurements within the artificial lung revealed notable discrepancies, with the Tissue resistance model exhibiting up to 20% higher delivered mechanical energy. These findings highlight the necessity of reconsidering current approaches to mechanical power calculation, as the inability to separate tissue resistance from airway flow resistance complicates the assessment and interpretation of mechanical power in relation to lung-protective ventilation.

4.2 Viscoelastic respiratory system model

A dedicated apparatus was constructed, consisting of a passive bellow-based Adult Lung Simulator (Michigan Instruments, Kentwood, MI, USA), a 20 mL borosilicate glass syringe (Socorex, Ecublens, Switzerland), and a throttle valve. The throttle valve was attached to the syringe's Luer adapter to control airflow into the syringe, thereby generating tissue resistance. Using custom 3D-printed components and fixtures, the syringe with the throttle valve was mounted in parallel to one artificial bellow lung of the Simulator, as illustrated in Fig. 4.1. Due to the low friction coefficient of borosilicate glass, the syringe functions as a mechanical damper with negligible frictional resistance. Further details on the testing protocol and confirmation of the negligible effect of friction on measured pressure and flow are provided in Appendix B.

The viscoelastic respiratory system model is therefore characterized by two elements: a linear compliance C_L (the spring incorporated in the Simulator), which represents the static elastic properties, and a compliance C_t in combination with a dashpot resistance R_t (the syringe and throttle valve), which together form a Maxwell body (a type of mechanical rheological model) representing the viscoelastic properties. Although the physical model corresponds to a single homogeneous compartment, it retains two degrees of freedom, as described by Bates [39]. The instantaneous pressure within the respiratory system model is determined by two parameters—the gas volume in the artificial lung and the flow entering or leaving the syringe, i.e., the pressure in the syringe chamber. During inspiration, a negative pressure is generated in the syringe chamber, whereas during expiration, a positive pressure develops.

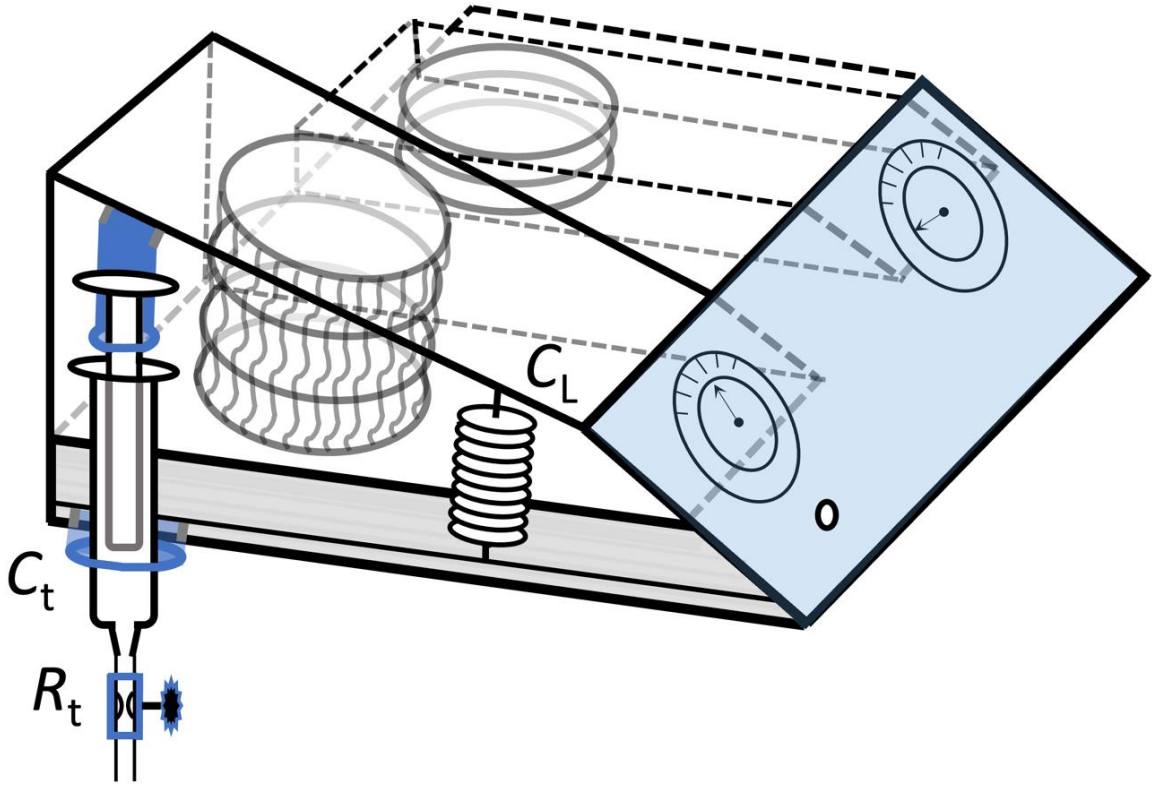

Figure 4.1: The Adult Lung Simulator with the glass syringe and the throttle valve mounted parallel to the one artificial bellow lung representing the tissue resistance of the viscoelastic respiratory system model. The spring represents the static elastic properties of the viscoelastic respiratory system model. Reproduced from [Walzel et al., 2025], published under the CC BY 4.0 license.

4.3 Testing

Three distinct configurations of a passive physical respiratory system model were evaluated, each representing different mechanical properties:

1. Tissue resistance model: viscoelastic respiratory system model including tissue resistance ($R_t + C_t$) but without airway flow resistance (R_{aw}),
2. Airway resistance model: system with linear airway flow resistance (R_{aw}) of 5 $cmH_2O \cdot s \cdot L^{-1}$ (Model 7100R, Hans Rudolph Inc., Shawnee, KS, USA) without tissue resistance ($R_t + C_t$),
3. No-resistance model: respiratory system without airway flow resistance (R_{aw}) and without tissue resistance ($R_t + C_t$).

For all configurations, the artificial lung's linear compliance (C_L) was fixed at 30 mL·cmH_2O^{-1}.

To examine whether proximal pressure at the airway opening can differentiate tissue resistance from airway flow resistance, Airway resistance model with R_{aw} of 5 cmH_2O·s·L^{-1} was used as a reference. In Tissue resistance model, the throttle valve was adjusted so that the maximum proximal airway pressure matched that of the reference model.

Ventilation was provided with a Veolar lung ventilator (Hamilton Medical, Bonaduz, Switzerland) operating in volume-controlled mode. The following parameters were applied: tidal volume VT = 1000 mL, constant flow during inspiration, $PEEP$ = 5 cmH_2O, inspiratory to expiratory time ratio (I:E) = 1:1, inspiratory hold = 20%, and RR = 6, 12 or 18 min^{-1}, corresponding to inspiratory flow rates (Q_{insp}) of approximately 20, 40 and 60 L·min^{-1}. Identical settings were maintained across all configurations.

Airway pressure (P_{aw}) and flow (Q) were monitored using a D-Lite spirometric sensor of the Datex-Ohmeda S/5 vital signs monitor (Datex-Ohmeda, Madison, WI, USA). As the monitor lacked an additional gas pressure port, the pressure inside the artificial lung (P_L) was measured using the haemodynamic module E-PSMP, which recorded pressures in millimeters of mercury (mmHg). These values were subsequently converted into cmH_2O. The sampling frequency for P_{aw}, Q and P_L was set to 100 Hz. The complete experimental setup is presented in Fig. 4.2.

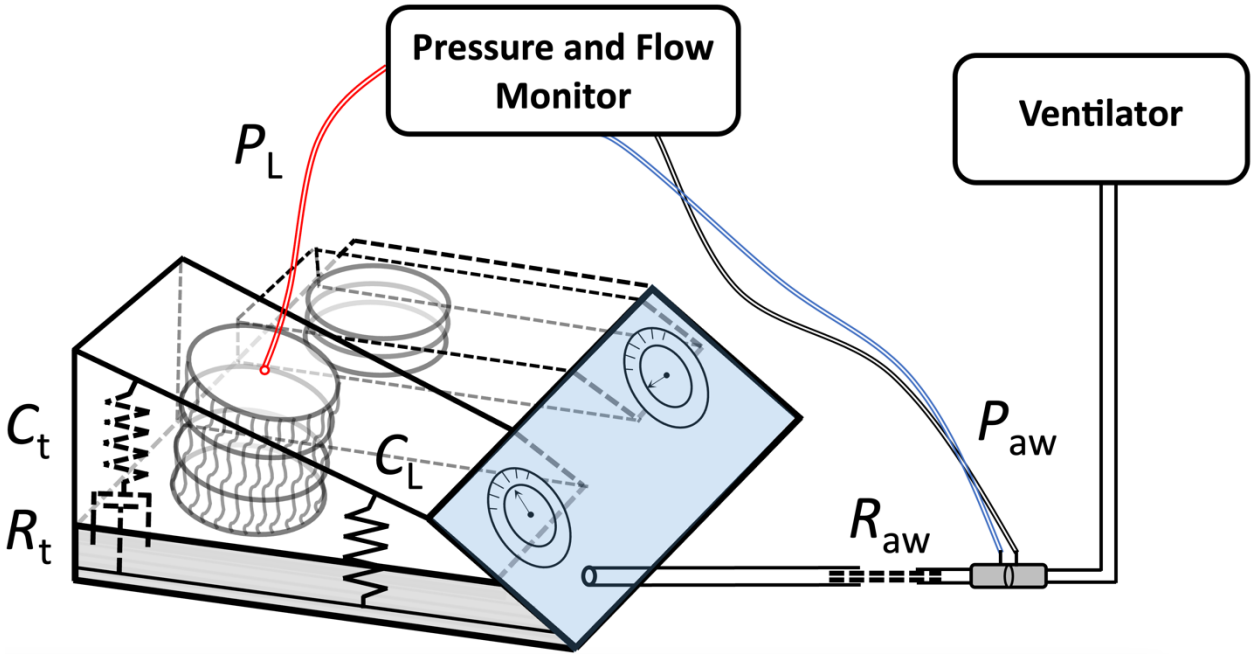

Figure 4.2: A scheme of the measuring system consisting of a lung ventilator, flow and pressure monitor and configurations of the passive physical respiratory system model representing different mechanical properties. The components representing the dynamic viscous ($R_t + C_t$) and the static elastic (C_L) properties are replaced by the symbols for mechanical rheological models. The connection or disconnection of R_{aw}, R_t or C_t was determined by the tested configuration. Reproduced from [Walzel et al., 2025], published under the CC BY 4.0 license.

4.4 Data processing and statistical analysis

Pressure and flow signals from five representative respiratory cycles were recorded for each respiratory system model configuration and respiratory rate. These curves were averaged and subsequently analyzed. Flow data were integrated over time to obtain delivered tidal volumes.

From the averaged data, curves of P_{aw}, Q and P_L, as well as plots of P_{aw} and P_L as functions of delivered volume, were generated for every respiratory rate and model configuration. Although standard deviations were computed, their values were negligible and therefore not displayed in the graphs.

To enable a quantitative comparison between Tissue resistance model and Airway resistance model, the mechanical energy delivered during the inspiratory phase of the respiratory cycle was determined using a formula based on the geometric method [65, 66]. Numerical integration was applied for the calculation:

$$E = \frac{0.098}{1000} \cdot \sum_i \left[0.5 \cdot \left((P_{\mathrm{aw}_i} + P_{\mathrm{aw}_{i+1}}) - 2 \cdot PEEP\right) \cdot (VT_{i+1} - VT_i)\right], \quad (18)$$

where E denotes the delivered mechanical energy during the inspiratory phase of the respiratory cycle in J, P_{aw} represents the measured airway pressure at a given time in cmH_2O, $PEEP$ is the positive end-expiratory pressure in cmH_2O, VT corresponds to the measured volume at a given time in mL and i indicates the number of samples within the inspiratory phase.

The calculation was performed using both P_{aw} and P_L, allowing for comparison between the mechanical energy delivered as measured at the airway opening of the respiratory system model (E_{aw}) and that measured inside the artificial lung (E_L) across all tested configurations.

4.5 Results

Connecting the glass syringe with the tuned airflow resistance of the throttle valve in parallel to the artificial lung of the Simulator (Tissue resistance model) led to a progressive rise in the measured maximum pressures (P_{aw} and P_L) as Q_{insp} increased from 20 $L \cdot min^{-1}$ to 60 $L \cdot min^{-1}$.

As designed, the P_{aw} curves during the inspiratory phase and the maximum P_{aw} values closely overlapped in Tissue resistance model and Airway resistance model. In both configurations, the maximum P_{aw} reached approximately 36 cmH_2O for Q_{insp} of 20 $L \cdot min^{-1}$ (RR = 6 min^{-1}) and 42 cmH_2O for Q_{insp} of 60 $L \cdot min^{-1}$ (RR = 18 min^{-1}), as illustrated in Fig. 4.3. By contrast, the P_L curves overlapped during the inspiratory phase in Airway resistance model and No-resistance model. During the inspiratory hold, however, only Tissue resistance model displayed an exponential decline from maximum P_{aw} and P_L toward P_{plat}.

In the expiratory phase of the respiratory cycle, the steepest initial pressure decrease occurred in Tissue resistance model. Toward the end of expiratory phase, the slope of this decline diminished, whereas No-resistance model exhibited the most rapid overall pressure decrease to $PEEP$.

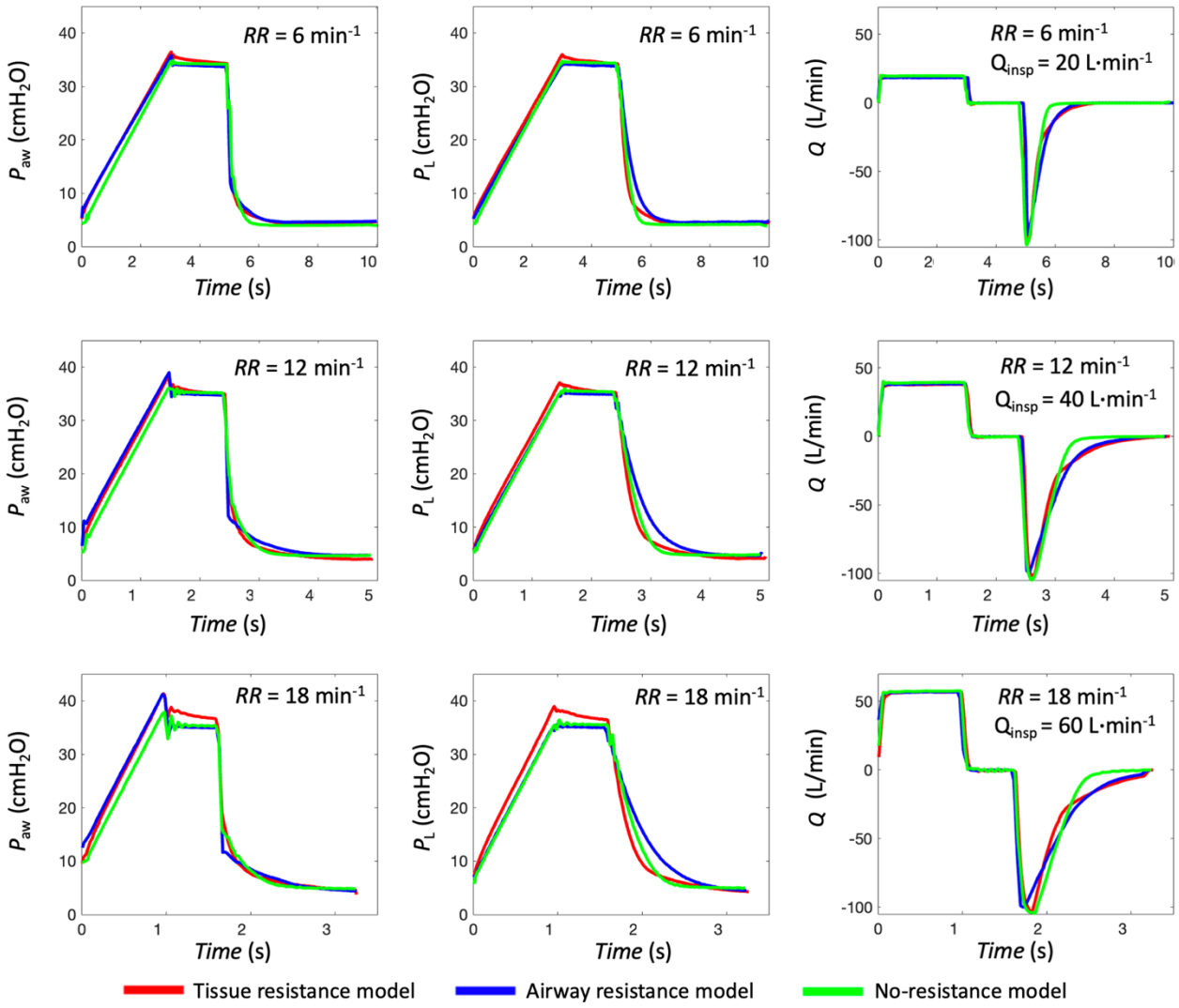

Figure 4.3: Time dependence of P_{aw}, P_L and Q at RR of 6, 12 and 18 min^{-1}, representing Q_{insp} = 20, 40 a 60 $L \cdot min^{-1}$, for the respiratory system model configurations tested. Reproduced from [Walzel et al., 2025], published under the CC BY 4.0 license.

A closer examination of the inspiratory phase showed that the maximum P_{aw} did not differ significantly between Tissue resistance and Airway resistance models, as intended. However, maximum P_L values showed marked differences between these models, which increased with rising Q_{insp} (averaging 1.6–3.3 cmH_2O depending on Q_{insp}), as depicted in Fig. 4.4. During the inspiratory hold, in Airway resistance model, P_{aw} fell rapidly to P_{plat} level, which then remained constant throughout the hold. In contrast, Tissue resistance model exhibited an exponential pressure decay, with values gradually approaching those measured in Airway resistance model and No-resistance model. At RR = 18 min^{-1}, the inspiratory hold lasted about 0.8 s, which was insufficient to allow a complete decay to P_{plat}.

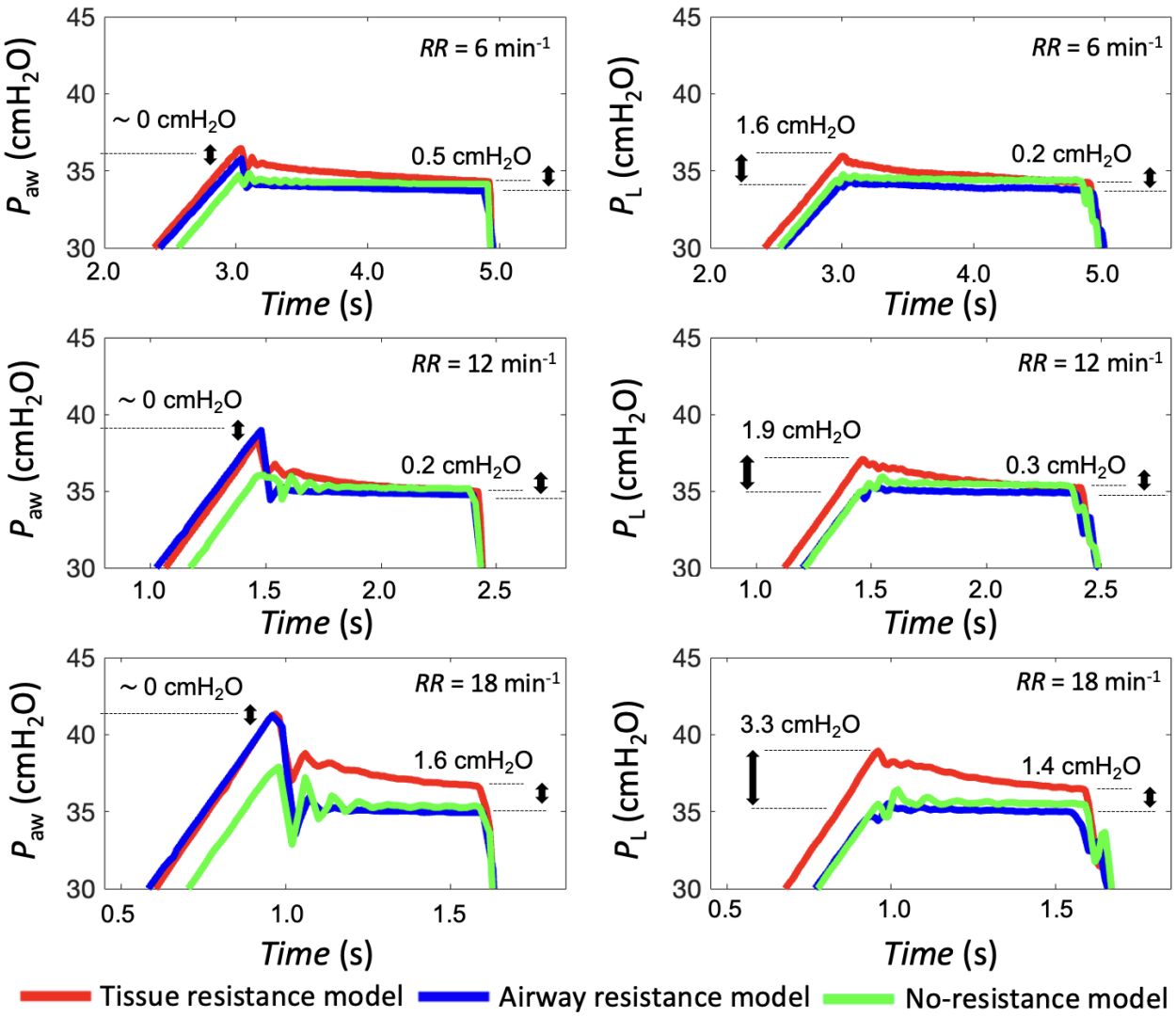

Figure 4.4: A detailed view of the time courses of P_{aw} and P_L during the inspiratory phase at respiratory rates of 6, 12 and 18 min^{-1} for the tested respiratory system model configurations. Reproduced from [Walzel et al., 2025], published under the CC BY 4.0 license.

The PV loops for P_{aw} during the inspiratory phase in Tissue resistance and Airway resistance models shifted from the loop of No-resistance model as Q_{insp} increased, reaching higher maximum pressures (Fig. 4.5). No significant differences were observed between Tissue resistance and Airway resistance models in the inspiratory phase.

In contrast, the PV loops for P_L showed a different pattern. With increasing Q_{insp}, the loop in the inspiratory phase in Tissue resistance model progressively shifted from the loops of Airway resistance and No-resistance models. At the same time, no differences were detected between Airway resistance and No-resistance models in the inspiratory phase.

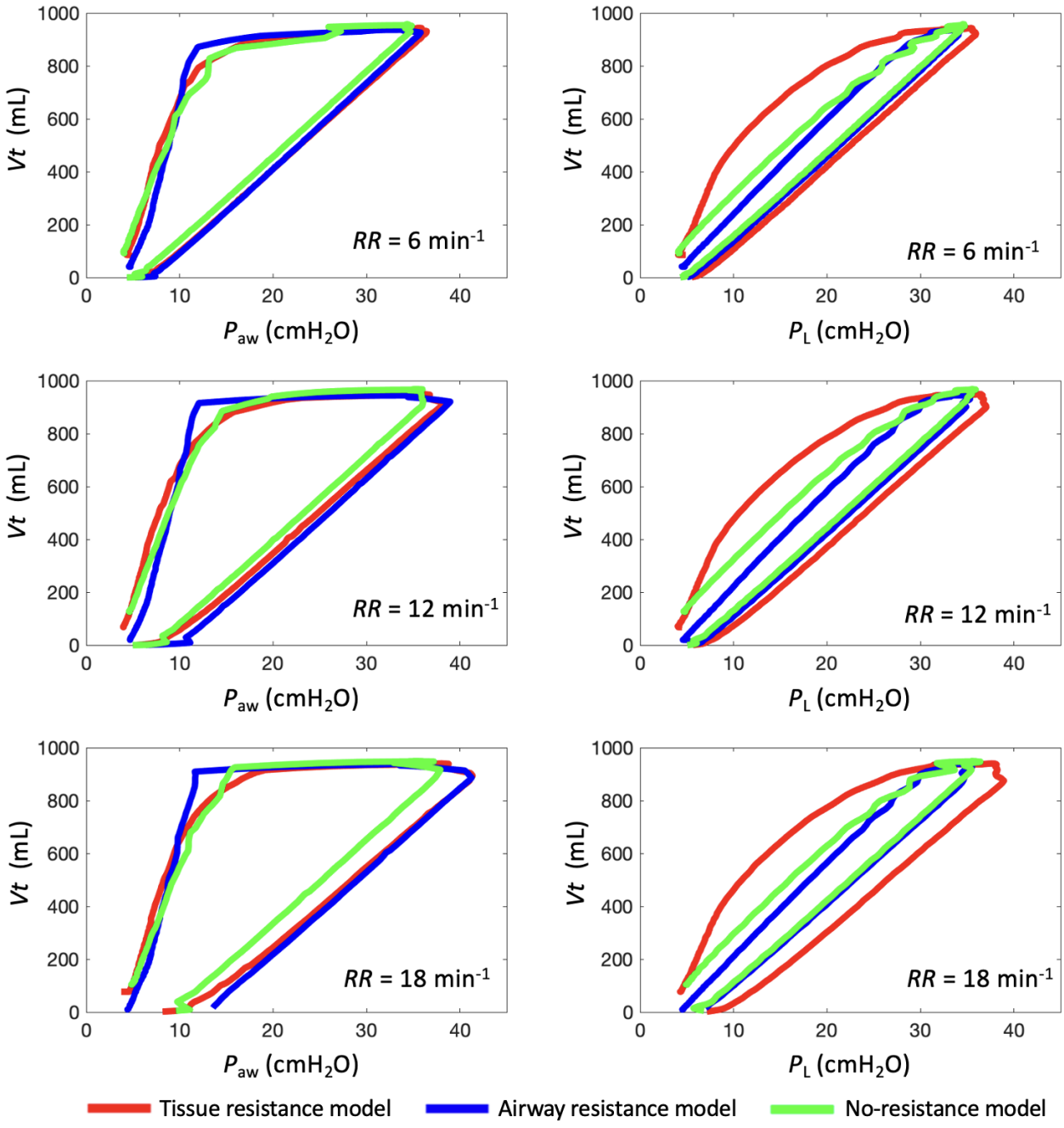

Figure 4.5: PV loops for P_{aw} and P_L during the whole respiratory cycle at RR of 6, 12 and 18 min^{-1} for all the three tested respiratory system model configurations. Reproduced from [Walzel et al., 2025], published under the CC BY 4.0 license.

As shown in Table 1, no substantial differences were observed in E_{aw}, calculated from P_{aw}, between Tissue resistance model and Airway resistance model at any respiratory rate (2.08 J vs. 2.16 J, 1.86 J vs. 1.88 J, and 1.63 J vs. 1.59 J). Different results emerged when the delivered mechanical energy E_L was calculated from P_L. For all respiratory rates, the differences between Tissue resistance model and Airway resistance model were significant, up to 20% higher in Tissue resistance model (1.93 J vs. 1.60 J, 1.78 J vs. 1.57 J, and 1.63 J vs.

1.46 J). By comparison, the differences in E_L between Airway resistance and No-resistance models were negligible (1.60 J vs. 1.55 J, 1.57 J vs. 1.57 J, and 1.46 J vs. 1.51 J).

Table 4.1: Mechanical energy delivered (E_{aw}, E_L) in the different respiratory system model configurations at varying respiratory rates, calculated from measured P_{aw} and P_L.

Respiratory system model configuration	***RR*** **(min^{-1})**	E_{aw} **(J)**	E_L **(J)**
Tissue resistance	18	2.08 ± 0.01	1.93 ± 0.02
	12	1.86 ± 0.02	1.78 ± 0.02
	6	1.63 ± 0.03	1.63 ± 0.03
Airway resistance (5 cmH$_2$O·s·L^{-1})	18	2.16 ± 0.01	1.60 ± 0.01
	12	1.88 ± 0.03	1.57 ± 0.02
	6	1.59 ± 0.01	1.46 ± 0.01
No-resistance	18	1.81 ± 0.01	1.55 ± 0.02
	12	1.72 ± 0.04	1.57 ± 0.04
	6	1.56 ± 0.04	1.51 ± 0.04

4.6 Discussion

The main finding of this study is that identical inspiratory P_{aw} waveforms, maximum P_{aw}, and delivered mechanical energy can be obtained in Tissue resistance model and Airway resistance model, even though the resistances arise from different mechanisms and are located at different sites. In contrast, when evaluating the delivered mechanical energy based on the pressure measured inside the artificial lung, Tissue resistance model produced values up to 20% higher than those of Airway resistance model, reflecting the specific impact of viscoelasticity.

As the artificial lung of the Simulator expands, its volume increase displaces the syringe plunger, forcing air through the throttle valve in Tissue resistance model. The rapid rise in lung volume generates a negative pressure within the syringe chamber, caused by the high airflow resistance of the throttle valve. This negative pressure, which effectively reduces the compliance of the artificial lung, depends on both the throttle valve's airflow resistance and the rate of volume change in the syringe chamber. During the inspiratory hold, once the artificial lung volume ceases to increase, the pressure difference between the syringe chamber and ambient air decays exponentially, accompanied by an exponential decrease in pressure inside the artificial lung.

During the inspiratory hold, the pressure in Tissue resistance model decreased by an average of 2 to 3 cmH$_2$O, depending on the ventilation parameters. This observation is in line with the findings of Santini et al. and Mezidi et al., who reported a similar average decline of 2 to 3 cmH$_2$O during a 2-second inspiratory hold under varying ventilation settings [21, 49]. In a study on piglets, pressure differences between the beginning and the end of a 5-second inspiratory hold ranged from 2 to 8 cmH$_2$O, depending on Q_{insp} (15–96 L·min^{-1}) [19]. Furthermore, Barberis et al. demonstrated that measuring P_{plat} immediately at the start of the

inspiratory hold led to an overestimation of the true P_{plat} by 11% in ARDS patients and by 17% in patients with Chronic Obstructive Pulmonary Disease [51].

Increasing Q_{insp} while maintaing all other parameters constant (*VT*, *PEEP*, *I*:*E,* C_L) led to a higher maximum airway pressures and greater delivered mechanical energy. In No-resistance model, however, the increase was minimal, most likely due to the short narrowing at the airway opening of the artificial lung. Although maximum pressures and the delivered mechanical energy at the airway opening did not differ between Tissue resistance and Airway resistance models, a significant difference emerged when mechanical energy was calculated from the pressure measured inside the artificial lung. This distinction is likely critical for assessing the degree of lung ventilation protectivity. Specifically, the mechanical energy derived from the measured P_L was approximately 10% higher at lower Q_{insp} and up to 20% higher at higher Q_{insp} in Tissue resistance model compared with Airway resistance model.

The findings of this study suggest that current methods of calculating delivered mechanical power from proximal airway pressure do not adequately account for the influence of tissue resistance or the duration of the inspiratory hold, despite the established evidence of parenchymal relaxation and the associated pressure decay during this phase [19, 21, 50]. As a result, routine measurements of pressure at the airway opening may underestimate the actual pressure acting on the lung parenchyma, since part of the measured pressure may be incorrectly attributed to airway flow resistance. These results therefore indicate that the conditions under which mechanical power calculations are applied should be reconsidered, or at the very least, the limitations of using proximal pressure alone for estimating mechanical power delivery to the lungs should be clearly acknowledged.

Assuming a purely viscoelastic system, a possible revision would be to introduce a sufficiently long inspiratory hold and to monitor the pressure curve at the airway opening during this period in order to distinguish airway flow resistance from tissue resistance. Previous work has shown that a 5-second inspiratory hold is adequate to achieve a stabilized P_{plat} within the lung parenchyma [51]. Careful evaluation of the entire pressure curve is particularly important, since isolated maximum pressure values or single P_{plat} measurements may appear identical and therefore fail to provide a complete interpretation of respiratory mechanics. The extent of pressure decay during the inspiratory hold may also have clinical relevance. For instance, Protti et al. demonstrated that the strain rate, which produces a pressure difference between the start and end of the inspiratory hold due to viscous resistance, significantly influenced the incidence of pulmonary edema [19]. Thus, incorporating the magnitude of this pressure decay into assessments, together with delivered mechanical power, could provide a more accurate evaluation of lung stress during mechanical ventilation.

Another possible approach to estimating the protectivity of lung ventilation is the calculation of dissipated mechanical energy, defined as the difference between delivered and returned mechanical energy [74]. This method, however, also requires a sufficiently long inspiratory hold.

Overall, unawareness of additional natural or pathological mechanical properties of the respiratory system, such as tissue resistance, may influence not only the calculation of mechanical power delivered to the lungs but also other parameters, including the static compliance displayed on the ventilator, and thereby affect the clinician's assessment of the patient's condition. Moreover, the presence of air leaks in the breathing circuit must always be considered, as these can further distort measured values. In this context, esophageal pressure monitoring [86] may be valuable, as it provides pressure measurements corrected for airway flow resistance. However, the use of an esophageal balloon catheter introduces further challenges and carries considerable costs.

While the detrimental effects of elevated pressures within the lung parenchyma are well established, higher pressures in the proximal airways may not necessarily be harmful unless they correspond to increased pressures in the parenchymal tissue. A widely cited study [15] demonstrated a relationship between driving pressure—defined as the difference between P_{plat} and *PEEP*—and survival in ARDS patients. The driving pressure calculation does not consider the effects of pressures acting in the proximal airways, possibly suggesting negligible harmful effects to the proximal airways. Conversely, high strain rates (velocity) have been shown to increase stress and induce distortion of epithelial cells in both peripheral [87, 88] and distal airways [89]. Taken together, the current evidence suggests that pressures in both the airways and the lung tissue should be carefully monitored and minimized.

The expiratory phase of the respiratory cycle was not examined in detail in this study. Nevertheless, we speculate that the developed physical viscoelastic respiratory system model could be applied in future investigations of expiratory curve morphology and in the determination of expiratory time constants, which are commonly used to estimate respiratory system compliance and resistance [90]. However, apart from potential technical limitations such as the influence of expiratory valve design and ventilator control algorithms, we consider these methods for estimating compliance and resistance to be overly simplistic, as they fail to capture the complexity of lung mechanics.

In this study, we assumed that tissue resistance was determined solely by viscoelasticity. In reality, tissue resistance may also be influenced by additional factors such as poroelasticity [45, 46], while the pressure decay observed during the inspiratory hold may be affected by airflow through distal airways or by chest wall mechanics [19].

5 Evaluation of Simplified Mechanical Power and Dissipated Energy Calculations in Physical Respiratory Models with Tissue and Airway Resistance

A version of this chapter has been published as: *Walzel S, Roubik K. (2025) Evaluation of simplified mechanical power and dissipated energy calculations in physical respiratory models with tissue and airway resistance. Lékař a technika-Clinician and Technology. 55(1). DOI: 10.14311/CTJ.2025.1.03. (in print).*

The aim of this study was to evaluate how simplified mechanical power equations differ in their estimates of delivered mechanical energy in physical respiratory models with either tissue viscoelastic or airway flow resistance. The second objective was to assess how increasing airway flow resistance affects the calculated mechanical energy and whether this corresponds to the actual energy measured at the lung level, and to analyze the contribution of tissue and flow resistance to energy dissipation.

5.1 Abstract

Mechanical power (MP) calculation is a promising predictor of ventilator-induced lung injury, yet simplified bedside equations rely on airway opening pressure, potentially missing key information about tissue-level stresses, and involve unclear contributions of *PEEP* and airway flow resistance. This study compared simplified MP equations in physical models of the respiratory system with either tissue viscoelastic (R_t) or airway flow (R_{aw}) resistance, evaluating how pressure measurement location affects delivered and dissipated energy estimates. Six physical models (No-resistance, Tissue resistance, Flow resistance, and three combinations of R_t with different R_{aw}) were ventilated with the same volume-controlled parameters. Pressure was measured at the airway opening and at an artificial lung level with vital signs monitor, sampled at 100 Hz. Mechanical energy was calculated using both simplified equations and a geometric method based on the pressure-volume loops. Simplified MP equations produced similar mechanical energy estimates for Tissue resistance model and Flow resistance model (R_{aw} = 5 $cmH_2O \cdot s \cdot L^{-1}$) when pressure was measured at the airway opening. However, measurements at the artificial lung level revealed marked differences in delivered and dissipated energy. Simplified MP equations may misrepresent tissue-level energy, particularly when R_{aw} dominates. Future studies should focus on refining energy estimation methods, considering driving transpulmonary pressures, inspiratory hold duration, and tissue versus flow resistance.

5.2 Testing of lung models combining tissue and airway resistance

Physical models of the respiratory system were formed from combinations of tissue viscoelastic resistance (R_t) and different airway flow resistances (R_{aw}). The linear compliance (C_L) of the artificial lung of Adult Lung Simulator (Michigan Instruments, Kentwood, MI, USA), set at 30 mL·cmH_2O^{-1}, was utilized for each model of the respiratory system. R_{aw} was represented by linear resistances of 5, 10 and 15 cmH_2O·s·L^{-1} (Hans Rudolph Inc., Shawnee, KS, USA).

R_t was represented by a Maxwell body, comprising a compliance and a dashpot resistance, to simulate viscoelastic properties. This was achieved by a glass syringe (Socorex, Ecublens, Switzerland) with a throttle valve, acting as a mechanical damper and the airflow resistance of the throttle valve was adjusted to achieve the same maximum airway pressure measured at the airway opening as in the model with the linear airway flow resistance of 5 cmH_2O·s·L^{-1} [95]. The system models a single homogenous compartment with two degrees of freedom, where pressure depends on the gas volume in the artificial lung and the flow to or from the syringe.

Six different physical models of the respiratory system were used: No-resistance (without R_t and without R_{aw}), Flow resistance 5 (without R_t and with R_{aw} of 5 cmH_2O·s·L^{-1}), Tissue resistance (with R_t and without R_{aw}), Tissue + Flow resistance 5 (with R_t and R_{aw} of 5 cmH_2O·s·L^{-1}), Tissue + Flow resistance 10 (with R_t and R_{aw} of 10 cmH_2O·s·L^{-1}) and Tissue + Flow resistance 15 (with R_t and R_{aw} of 15 cmH_2O·s·L^{-1}). Mechanical ventilation was performed using a Veolar ventilator (Hamilton Medical, Bonaduz, Switzerland) set to volume-controlled mode with tidal volume VT = 1000 mL, $PEEP$ = 5 cmH_2O, inspiratory to expiratory time ratio ($I:E$) = 1:1, inspiratory hold = 30%, and RR of 10 min^{-1}, corresponding to constant inspiratory flow rates of approximately 51 L·min^{-1}. P_{aw} and VT were measured at the airway opening using a D-Lite spirometry sensor connected to the E-CAiOVX anesthesia and spirometry module of the Datex-Ohmeda S/5 vital signs monitor (Datex-Ohmeda, Madison, WI, USA). Pressure at the lung level (P_L) was recorded in mmHg via the invasive blood pressure port of the E-PSMP hemodynamic module and converted to cmH_2O. All signals were collected using S/5 Collect software on a laptop computer and sampled at 100 Hz.

5.3 Data processing and statistical analysis

The averaged waveforms of P_{aw}, P_L and V over the entire respiratory cycle from five representative respiratory cycles for each respiratory system model were plotted in Fig. 5.1. Standard deviations were calculated but were too small to be shown in the graphs. The values of P_{max}, P_{plat}, compliance C, airway flow resistance R_{aw}, and P_{mean}, calculated from the measured waveforms of five representative respiratory cycles, were listed in Table C1 in Appendix C.

Next, the dependence of P_{aw} and P_L on VT were plotted in the form of PV loops for each respiratory system model in Fig. 5.2A and 5.2B. Using the PV loops, the mechanical energy (E) delivered during the inspiratory phase of the respiratory cycle was calculated for each respiratory system model using the geometric method, i.e., by numerically integrating the area under the respective curve. Dissipated energy was calculated as the hysteresis area of the PV loop, obtained from the difference between inspiratory and expiratory pressures over the corresponding volume changes. The calculation was performed using the pressure measured at the airway opening with *PEEP* (E_{aw}), pressure at the airway opening without *PEEP* (E_d), and pressure measured at the artificial lung level without *PEEP* (E_L). The equations used for these calculations are provided in Appendix D. The measured pressure at the airway opening with *PEEP* (P_{aw}) and without *PEEP* (P_d), as well as the measured pressure at the artificial lung level without *PEEP* (P_L), were used. Finally, E was calculated according to simplified mechanical energy equations (10, 12–15) for each model of the respiratory system, and the average values of E were included in Table C2 of Appendix C.

The calculated inspiratory E_{aw}, E_d, E_L by the geometric method and the E obtained from the simplified equations (10, 12–15) for Tissue resistance and Flow resistance 5 models were plotted on a graph for comparison (Fig. 5.3A). A two-tailed paired t-test was used to evaluate the statistical difference between Tissue resistance and Flow resistance 5 models for each simplified E equation. A p-value less than 0.05 was considered statistically significant. In addition, E_L, which represents the driving energy acting directly at the lung level, was used as a reference. The ratio of each calculated E to the reference E_L was then determined (Fig. 5.3B).

Lastly, models of the respiratory system consisting of only R_t or R_t with R_{aw} of 5, 10, and 15 $cmH_2O \cdot s \cdot L^{-1}$ were used to investigate the effect of increasing flow resistance on the calculated E in simplified equations (Fig. 5.4).

5.4 Results

The time course of the measured pressure P_{aw} at the airway opening (Fig. 5.1A) at RR = 10 min^{-1} showed that the highest maximum pressure was measured in Tissue + Flow resistance model 15 (appx. 50 cmH_2O) and the lowest in No-resistance model (appx. 36 cmH_2O). The curves for Tissue resistance and Flow resistance 5 models overlapped during the inspiratory phase and reached the same P_{max} and P_{plat}, as intended. However, the decrease in pressure during inspiratory hold was different for these two models. Similar P_{plat} was measured for all models.

Looking at Fig. 5.1B, where the pressure was measured at the artificial lung level, the results were different. The lowest P_{max} was again measured in No-resistance model, but now also in Flow resistance 5 model (appx. 36 cmH_2O). The curves for the other models (containing R_t) overlapped throughout the inspiratory phase, reached similar P_{max} (appx. 39 cmH_2O) and P_{plat} during the inspiratory hold.

Fig. 5.1C showed that the inspiratory *VT* did not differ between the models. However, the rate of expired tidal volume varied between the models, with the slowest rate in Tissue + Flow resistance 15 model and the fastest in No-resistance model.

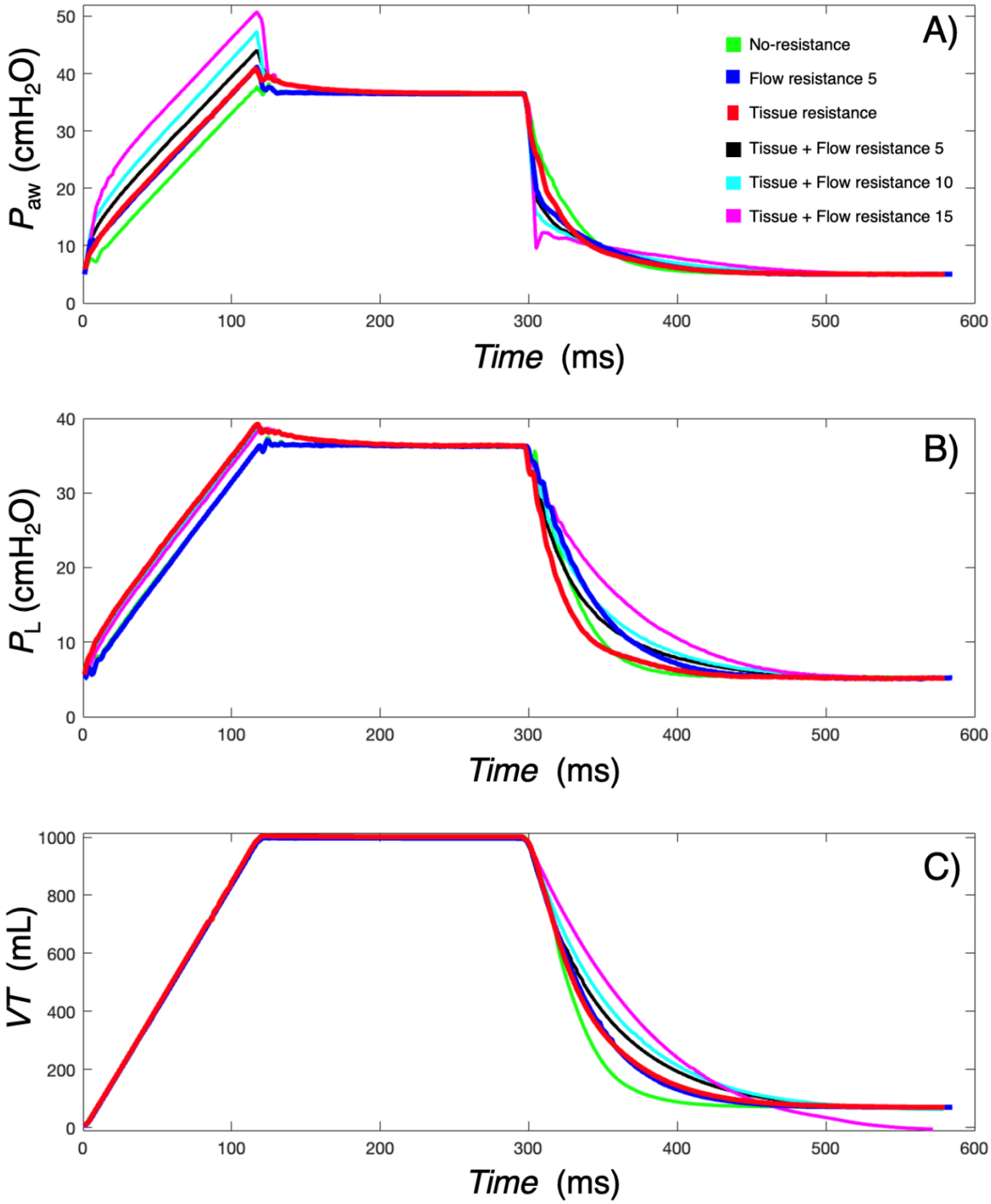

Figure 5.1: Time dependence of P_{aw} (A), P_L (B) and *VT* (C) during the whole respiratory cycle for each respiratory system model. No-resistance (green), Flow resistance 5 (blue), Tissue resistance (red), Tissue + Flow resistance 5 (black), Tissue + Flow resistance 10 (cyan), Tissue + Flow resistance 15 (magenta). Reproduced from [Walzel et al., 2025], published under the CC BY 4.0 license.

The PV loops in Fig. 5.2A showed the lowest inspiratory E (simply put, the product of pressure and volume) and the narrowest hysteresis area in No-resistance model. By adding R_t or R_{aw}, the inspiratory curves shifted from No-resistance model, resulting in an increase in inspiratory E and a larger hysteresis area (increase in dissipated energy). In Tissue resistance and Flow resistance 5 models, the inspiratory E were the same and the hysteresis areas were similar.

The resulting PV loops in Fig. 5.2B for the pressure measured at the artificial lung level (P_L) did not follow the same trend. The hysteresis area was the largest for Tissue resistance model (0.87 ± 0.07 J), whereas the hysteresis areas for No-resistance and Flow resistance 5 models were very similar and narrow (appx. 0.20 J). There was no difference in all models with R_t in the inspiratory phase of the PV loop, where the curves mostly overlapped, indicating nearly identical pressure–volume behavior across models in this part of the cycle, but in the expiratory phase, increasing R_{aw} narrowed the hysteresis area.

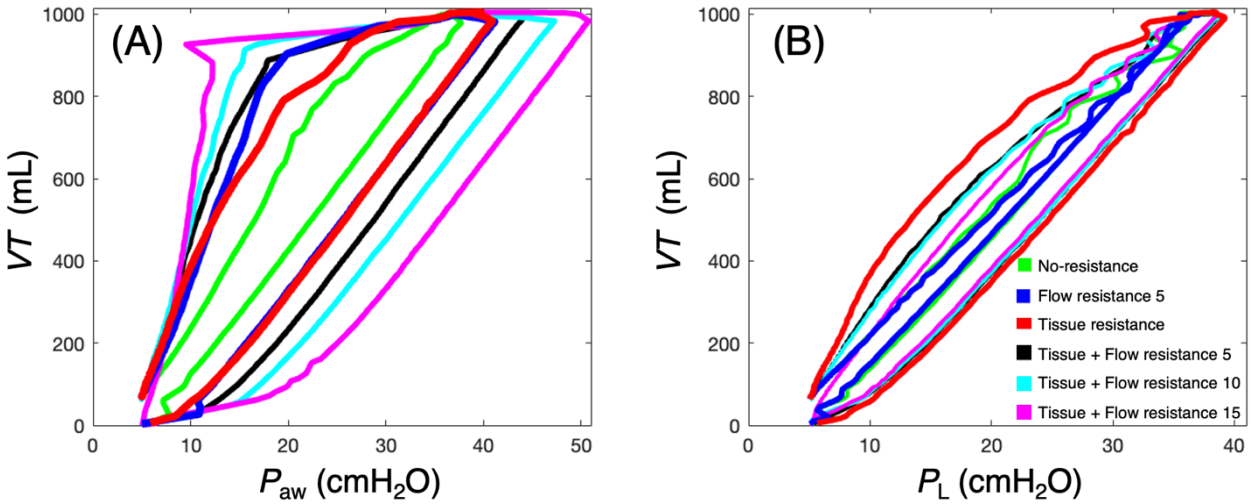

Figure 5.2: PV loops for P_{aw} (A) and P_L (B) during the whole respiratory cycle for each respiratory system model. No-resistance (green), Flow resistance 5 (blue), Tissue resistance (red), Tissue + Flow resistance 5 (black), Tissue + Flow resistance 10 (cyan), Tissue + Flow resistance 15 (magenta). Reproduced from [Walzel et al., 2025], published under the CC BY 4.0 license.

Table 5.1, which presents the inspiratory and dissipated E_{aw}, E_d, and E_L calculated from the PV loops using the geometric method, showed that the inspiratory E_{aw} and E_d differed by approximately 0.5 J for all models. The difference is due to the omission of *PEEP* from the calculation of E_d. However, the dissipated E_{aw} and E_d did not differ between the models. Next, for Tissue resistance and Flow resistance 5 models, the results were very similar for inspiratory E_{aw} (2.49 ± 0.04 J versus 2.51 ± 0.03 J), inspiratory E_d (2.00 ± 0.04 J versus 2.01 ± 0.03 J), dissipated E_{aw} (1.25 ± 0.12 J versus 1.15 ± 0.10 J), and dissipated E_d (1.21 ± 0.12 J versus 1.11 ± 0.10 J), as briefly described in Fig. 5.2A. But the results were again clearly different for E_L. The inspiratory E_L is about 20% higher for Tissue resistance model than for Flow resistance 5 model (1.88 J versus 1.57 J). The dissipated E_L was about 4 times higher for Tissue resistance

model than for Flow resistance 5 model (0.87 J versus 0.18 J). And lastly, increasing flow resistance resulted in such a significant increase in dissipated E_{aw} and E_d that both were even higher than inspiratory E_L for Tissue + Flow resistance 10 model and Tissue + Flow resistance 15 model, despite dissipated E_L decreasing with the increasing flow resistance.

Table 5.1: The inspiratory and dissipated E_{aw}, E_d and E_L for all models of the respiratory system calculated using the geometric method (18).

Model of the respiratory system	**Inspiratory E_{aw} (J)**	**Dissipated E_{aw} (J)**	**Inspiratory E_d (J)**	**Dissipated E_d (J)**	**Inspiratory E_L (J)**	**Dissipated E_L (J)**
No-resistance	2.20 ± 0.08	0.56 ± 0.12	1.70 ± 0.08	0.53 ± 0.12	1.61 ± 0.04	0.21 ± 0.01
Flow resistance 5	2.49 ± 0.04	1.25 ± 0.12	2.00 ± 0.04	1.21 ± 0.12	1.57 ± 0.03	0.18 ± 0.06
Tissue resistance	2.51 ± 0.03	1.15 ± 0.10	2.01 ± 0.03	1.11 ± 0.10	1.88 ± 0.02	0.87 ± 0.07
Tissue + Flow resistance 5	2.77 ± 0.07	1.60 ± 0.13	2.28 ± 0.07	1.57 ± 0.13	1.83 ± 0.06	0.62 ± 0.10
Tissue + Flow resistance 10	3.03 ± 0.08	1.98 ± 0.15	2.55 ± 0.08	1.94 ± 0.15	1.82 ± 0.07	0.59 ± 0.14
Tissue + Flow resistance 15	3.40 ± 0.05	2.36 ± 0.06	2.91 ± 0.05	2.36 ± 0.06	1.81 ± 0.02	0.47 ± 0.03

A statistically significant difference between Tissue resistance and Flow resistance 5 models was found only for inspiratory E_L and the simplified Chi (15) equation, as shown in Fig. 5.3A. At the same time, E_L was the lowest for both models compared to other equations. It is also evident that there was no difference between E_{aw} and Gattinoni (10) and Comprehensive (12) equations for either Tissue resistance or Flow resistance 5 models, where E is equal to 2.5 J. Inspiratory E_d was lower than inspiratory E_{aw} for both models by the aforementioned 0.5 J, while Dynamic (13) and Surrogate (14) equations showed values approximately 10% lower and 10% higher than E_{aw}, respectively.

The calculated E from all equations exhibited a higher value in comparison to E_L, which was used as a reference in this case, as demonstrated in Fig. 5.3B. Of the simplified equations, Dynamic (13) overestimated the least by 20% for Tissue resistance model and 45% for Flow resistance 5 model, and Chi (15) overestimated the most by 85% for Tissue resistance model and 120% for Flow resistance 5 model. However, E_d values calculated by the geometric method were closest to the E_L for both models.

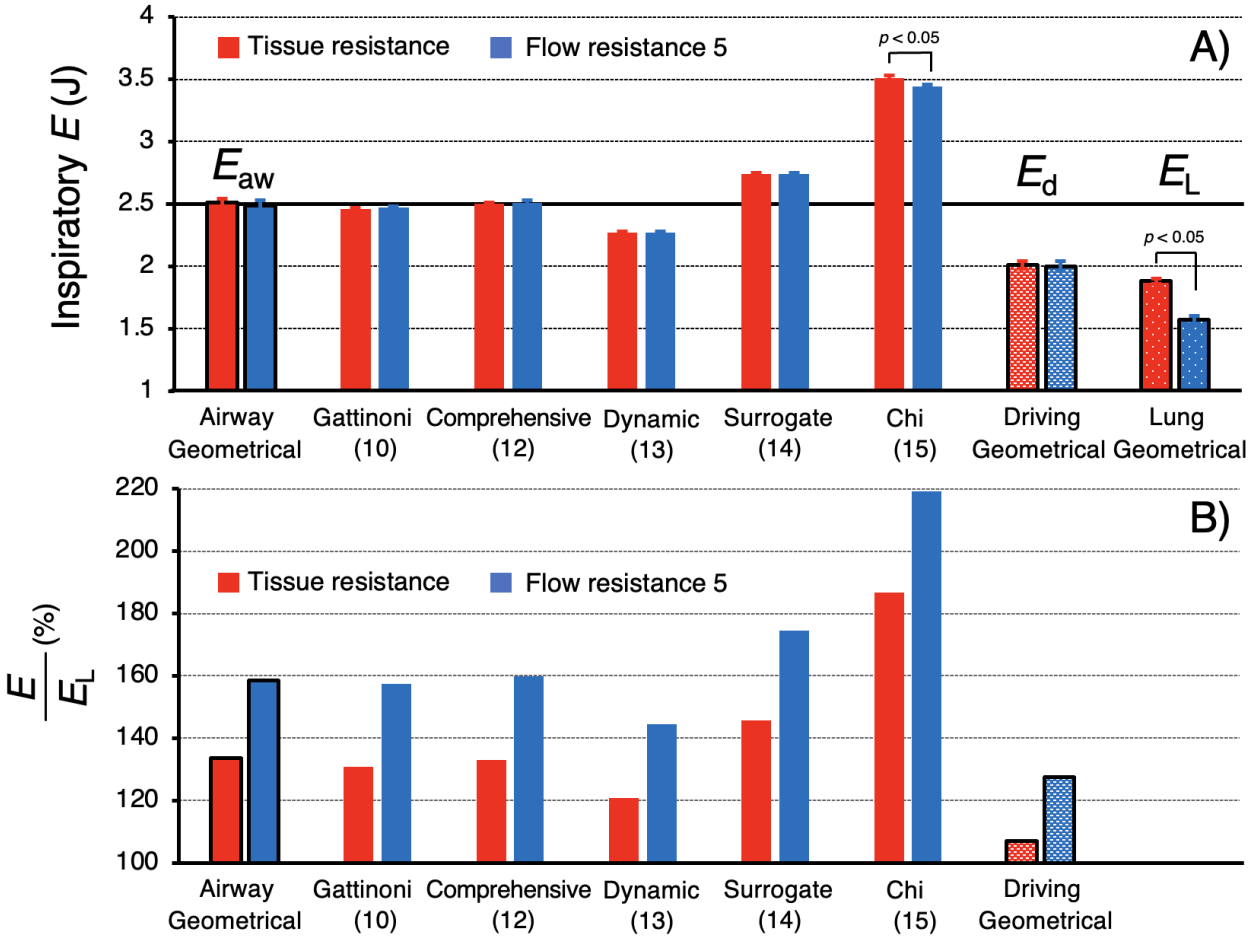

Figure 5.3: The calculated inspiratory E_{aw}, E_d, E_L by the geometric method and the mechanical energy obtained from the simplified equations (10, 12–15) for Tissue resistance and Flow resistance 5 (A); The ratio of each calculated E to the reference E_L (B). Reproduced from [Walzel et al., 2025], published under the CC BY 4.0 license.

Although there was no increase in E_L due to increasing R_{aw}, the increase in E was significant for all simplified equations (Fig. 5.4). The highest increase in E due to increasing R_{aw} occurred for the Comprehensive (12) equation, where the difference between the lowest and highest E was equal to 1 J. In contrast, the smallest difference was observed for the Gattinoni (10) equation, where the difference was only 0.4 J.

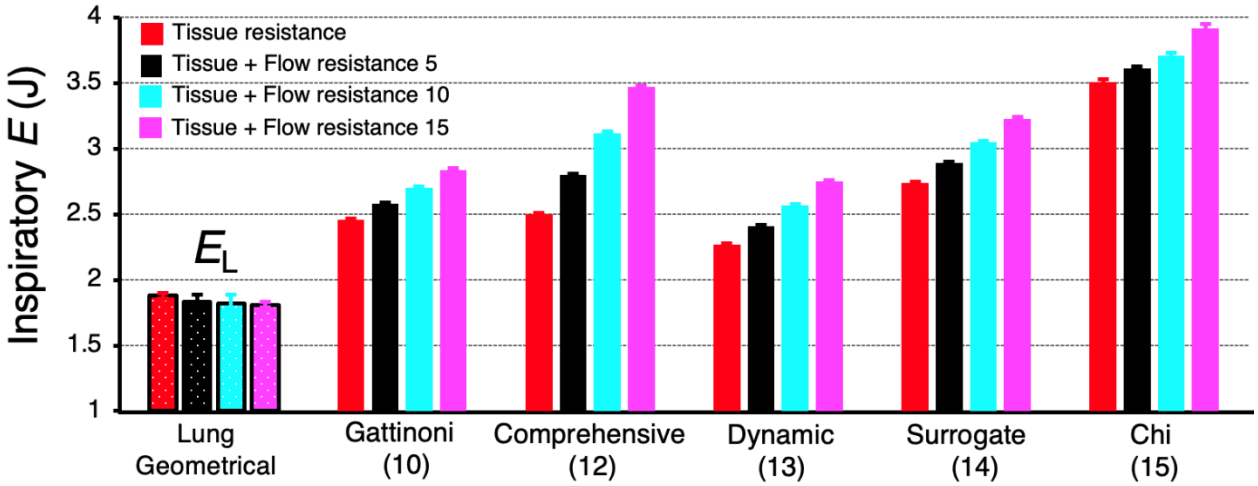

Figure 5.4: The effect of increasing flow resistance on E in simplified equations in models of the respiratory system consisting of only tissue resistance or tissue resistance with flow resistances of 5, 10, and 15 $cmH_2O \cdot s \cdot L^{-1}$. Reproduced from [Walzel et al., 2025], published under the CC BY 4.0 license.

5.5 Discussion

The main findings of this study are that simplified mechanical power (MP) calculations provide similar estimates of delivered mechanical energy (E) in physical respiratory models with either tissue viscoelastic (R_t) or airway flow (R_{aw}) resistance, despite significant differences observed at the lung level and different origins of the resistances situated at distinct locations. Furthermore, the simplified MP calculations overestimate E when R_{aw} dominates compared to the E measured at the lung level. Increasing R_t or R_{aw} elevated dissipated energy measured at the airway opening, whereas only R_t increased the dissipated energy at the lung level. In contrast, increased R_{aw} paradoxically decreased energy dissipation at the lung level.

The unique setup of the respiratory model with R_t allowed the evaluation of E associated with the viscoelastic behavior of the lung parenchyma, a known [23, 48, 63] but overlooked characteristic. Rapid inflation of the artificial lung of the Simulator induces a transient negative pressure inside the syringe due to the high flow resistance of the throttle valve, temporarily reducing model compliance. This effect is time-dependent and is influenced by the resistance of the throttle valve and the volume increase of the syringe. When an inspiratory hold is applied, the pressure inside the syringe equilibrates to atmospheric pressure while the pressure at the artificial lung level decreases exponentially [95]. This results in a plateau pressure similar to that of models with no resistance or R_{aw} only (Fig. 5.1). This unique feature was achieved by the low coefficient of friction of the borosilicate glass of the syringe [95]. Baseline E dissipation was quantified in No-resistance model. Table 5.1 showed that the minimum achievable hysteresis using the artificial lung of the Adult Lung Simulator was approximately 0.56 ± 0.12 J for E_{aw} and 0.53 ± 0.12 J for E_d, while the artificial lung alone exhibited a hysteresis of 0.21 ± 0.01 J. This suggests that roughly 0.3 J originates from the intrinsic flow resistance of the

test apparatus, with the remaining E dissipation likely attributable to the hysteresis of the rubber of the artificial lung of the Simulator and the use of a not fully thermocompensated model. Thus, the small difference between the inspiratory E_d and E_L in Tissue resistance model (with no added R_{aw}) was due only to the limitations of the apparatus.

The simplified MP equations analyzed here rely on several assumptions—linear compliance and airway flow resistance, constant inspiratory flow during volume-controlled ventilation, or homogeneous mechanical properties in each lung compartment. Although newer simplified MP equations for spontaneous breathing or MP normalization to lung size, compliance, or functional residual capacity have emerged [23, 72, 85], none account for the viscoelastic properties of lung tissue or the duration of inspiratory holds, both of which can significantly affect the calculation of delivered E.

In our study, E_L served as a reference for potentially harmful mechanical energy as it reflects the E acting directly at the lung level [73 83]. However, in clinical practice, E_L is difficult to measure and requires measurement using an esophageal catheter [84]. For Tissue resistance model, the so-called Dynamic equation (13), proposed in the study by Urner et al. [68], overestimated the least among the simplified equations compared to the geometrically calculated E_L (Fig. 5.3B). This is due to the fact that only P_{max} was used for the calculation, which showed almost no difference between the pressure measured at the airway opening and at the artificial lung level (the small difference was due to the limitations of the test apparatus). Furthermore, if the energy component for *PEEP* (static elastic energy) of approximately 0.5 J is removed from the calculation (13), E would be essentially the same.

Although the simplified equation (15) of Chi et al. [70] does not require an inspiratory hold, its application significantly increased the calculated E. Notably, the inspiratory hold revealed a difference between Tissue resistance model and Flow resistance 5 (Fig. 5.3A), due to the use of P_{mean} in the equation and the presence of the exponential pressure decrease during the hold in Tissue resistance model. However, when the results were analyzed without the inclusion of the inspiratory hold, as assumed by equation (15), the E between Tissue resistance model and Flow resistance 5 model was identical, as shown in the Appendix C.

Our results are consistent with those of Chiumello et al. [67], who found strong correlations between simplified MP equations (Comprehensive and Surrogate) and a reference geometric method based on PV loops in 40 sedated and paralyzed ventilated patients. However, our data show that simplified equations may misrepresent the E acting at the lung level. Increasing R_{aw} caused an increase in E for all simplified equations, despite no change at the lung level (Fig. 5.4). The effect of increasing R_{aw} was least pronounced with the Gatinnoni equation (10) and most significant with the Comprehensive equation (12). This discrepancy may hinder the setting of appropriate ventilation parameters in patients with high R_{aw} if MP thresholds are strictly followed. However, this does not negate the potential harm of elevated airway pressures, which can contribute to distal lung injury [89].

While dissipated energy has been suggested as a possible contributor to VILI [19, 66, 74], it is unclear how to quantify the harmfulness of this energy. Our findings

emphasize that the location of the measurement significantly affects the interpretation. PV loops recorded at the airway opening showed increasing hysteresis with higher R_{aw} in both inspiratory and expiratory phases (Fig. 5.2). However, the energy dissipation in the inspiratory phase of the PV loop is largely driven by R_{aw}, the effect of which on VILI is not straightforward [83]. Measured at the lung level, high R_{aw} decreased the energy dissipated in the expiratory phase of the PV loop, similar to mechanical control of expiratory flow [78–80]. R_t increased energy dissipation across both phases at the lung level but behaved similarly to R_{aw} when measured at the airway opening. In addition, the duration of the inspiratory hold may significantly affect energy dissipation. During the hold, parenchymal stress relaxation induces a pressure drop that may alter the shape and area of the expiratory PV loop. This mechanism further underscores the role of tissue viscoelasticity in energy dissipation. Taken together, R_t appears to be a dominant contributor to energy dissipation at the lung level, while R_{aw} predominantly affects measurements at the airway opening—highlighting the risk of misinterpretation if only proximal measurements are considered.

It is also important to note that the calculation of E using simplified equations that rely on values provided on the ventilator display may be affected by proprietary algorithms of the ventilator. For example, the length of the inspiratory hold may or may not affect the calculated values of P_{plat}, compliance, and R_{aw} [51], thereby affecting the values calculated using the simplified equations. Additionally, since the effect of *PEEP* on E is definitely not linear [83] and the contribution of airway flow resistance to VILI remains unclear, driving transpulmonary pressure may be a more appropriate parameter for estimating energy delivery and dissipation. A possible surrogate for this difficult-to-measure value could be the pressure measured at the airway opening immediately after the start of the inspiratory hold, as it may reflect alveolar pressure acting on the lung tissue. A longer inspiratory hold could help monitor viscoelastic relaxation of the parenchyma; however, leaks in the breathing circuit may confound these measurements and caregiver interpretation. Ultimately, large clinical studies are needed to determine whether different methods of calculating delivered or dissipated energy correlate with outcomes such as mortality, development of VILI, or pulmonary edema. Potential approaches include randomized trials, which could be appropriate if ventilator settings were prospectively adjusted to minimize mechanical energy delivery to the respiratory system according to a selected equation, or large observational cohorts with high-resolution ventilator data, which would probably be more feasible and would allow both comparison of simplified equations with a geometric reference and direct comparison among the simplified equations themselves to assess their prognostic accuracy.

This study has several limitations. First, although physical models offer controlled conditions to isolate and analyze specific variables, they are simplifications and cannot fully replicate the complexity of human lung mechanics. Despite this, the effects described here are consistent with phenomena observed in clinical practice. Second, pressure and volume curves during the expiratory phase may be influenced by the design of the expiratory valve and ventilator control algorithms. However, this influence is unlikely to have significantly affected the main findings. A possible limitation of this study is the use of relatively high tidal volumes compared with typical clinical practice. This setting was chosen because smaller tidal volumes

produced only minimal displacement of the bellow-based lung Simulator from its resting position. Such small displacement would have amplified the effect of mechanical imperfections of the Simulator, making it difficult to reliably separate the elastic, resistive, and viscoelastic components. The physical model with tissue resistance could, however, be further optimized in future work, for example by using a syringe of different size or employing a custom-built simulator designed to achieve greater displacement at lower tidal volumes. Finally, this study did not evaluate energy dissipation due to recruitment during inspiration, which has been recently suggested as a possible contributor to VILI [96].

6 Pilot Clinical Study

The aim of this pilot study was to verify, under clinical conditions, the effect of inspiratory hold duration on the calculation of mechanical energy delivery and dissipated energy. Another objective was to compare various simplified equations for calculating mechanical energy delivery and to perform the calculation of delivered mechanical energy using transpulmonary pressure. The final objective was to determine whether viscoelastic properties of the lung tissue (tissue resistance) can be assessed from the measured parameters.

6.1 Methods

This prospective interventional study was registered on ClinicalTrials.gov under the identifier NCT06236685, titled "*Optimizing the Assessment of Mechanical Ventilation by Integrating Advanced Monitoring Techniques*" (Appendix E). The aim of the whole study is to collect synchronized data from multiple monitoring techniques of mechanical ventilation (pressure/flow waveforms from the ventilator, electrical impedance tomography, esophageal pressure, capnography) in patients ventilated either on intensive care units or during anesthesia and to evaluate the data by detailed mathematical analysis. The study protocol was approved by the Ethics Committee of the Central Military Hospital Prague (approval number 108/19-1/2024). All procedures were performed in accordance with the principles of the Declaration of Helsinki. Informed consent was obtained from each patient or their legal representative prior to inclusion in the study.

All included patients in intensive care units underwent repeated inspiratory hold maneuvers during passive, fully controlled ventilation while maintaining constant ventilator settings (*VT*, *PEEP*, *RR*, and Q_{insp}). During each inspiratory hold, the airway pressure and flow waveforms were recorded. Simultaneously, esophageal pressure measurements were used to estimate the pleural pressure and derive the transpulmonary pressure. All acquired data were anonymized and synchronized for subsequent offline analysis. Exclusion criteria included patients or their representatives who did not provide informed consent, those unable to understand the study information or the informed consent form, and patients for whom any of the monitoring methods could not be applied. This included cases with dermatological conditions preventing the placement of EIT electrodes, or specific clinical circumstances requiring a ventilation mode incompatible with the study protocol.

Mechanical ventilation was performed using a critical care ventilator (Infinity® C500; Drägerwerk AG & Co. KGaA, Lübeck, Germany). Vital signs were monitored using a multiparameter monitor (CARESCAPE™ B450; GE Healthcare, Chicago, IL, USA). Airway pressure (P_{aw}) and flow (Q) were recorded using a D-Lite spirometric sensor (Datex-Ohmeda S/5, Madison, WI, USA). Esophageal pressure was measured using a balloon catheter (Nutrivent; Sidam, Mirandola, Italy) through the TrachCare system, and the data were acquired using a hemodynamic module (E-PSMP) in mmHg and later converted to cmH_2O. The

sampling frequency for P_{aw}, Q, and P_{es} was set to 100 Hz. The patient circuit arrangement is shown in Fig. 6.1.

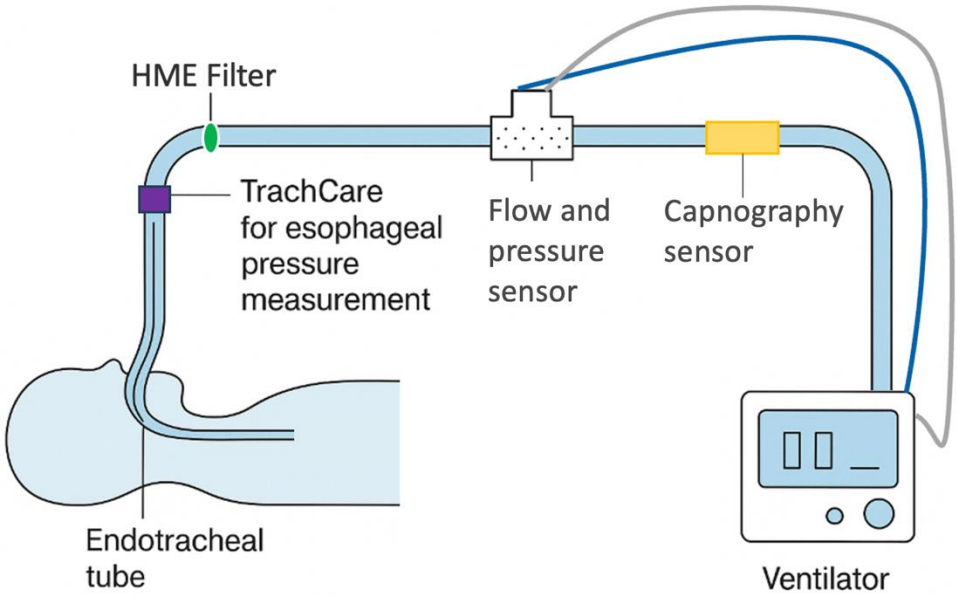

Figure 6.1: The patient circuit included an endotracheal tube, a TrachCare system for esophageal pressure measurement, an HME filter, a flow and pressure sensor, and a capnography sensor.

For each patient and ventilator setting, the entire respiratory cycle was analyzed. Waveforms of P_{aw}, Q, and P_{es} were plotted and the following parameters were calculated: P_{max}, P_{plat}, $PEEP$, P_{mean}, VT, C, R_{aw}, $I:E$. PV loops for both P_{aw} and P_{es} were constructed, and the delivered mechanical energy (E_{aw}, E_{es}, E_{transp}) per breath and dissipated E_{aw} and E_{es} during the respiratory cycle were computed using the geometric method (18). For the calculations, the measured pressure at the airway opening with $PEEP$ (P_{aw}) and P_{es} were used. Finally, E was calculated according to simplified mechanical energy equations (10, 12–16).

6.2 Results

Two patients met the eligibility criteria for inclusion in the pilot study at the Central Military Hospital Prague in 2025. Eligibility required the ability to undergo repeated inspiratory hold maneuvers during passive, fully controlled mechanical ventilation with constant ventilator settings. Patient 1 was admitted to the ICU with a traumatic diaphragmatic rupture, while Patient 2 was treated for severe pneumonia of infectious origin.

Patient 1 was ventilated with a VT of 618 mL, resulting in P_{max} of approximately 26–27 cmH_2O. In contrast, Patient 2 was ventilated with a lower VT of 240 mL, yet P_{max} reached up to 36 cmH_2O due to reduced lung compliance, as shown in Table 6.1. In both patients, $PEEP$

was maintained at 8 cmH_2O and the *I:E* ratio was approximately 1:2 to 1:2.5. It can also be observed that the use of an inspiratory hold was associated with an increase in both compliance and flow resistance.

Tissue resistance, calculated as the difference between R_{aw} during the 10-second inspiratory hold and the minimum inspiratory hold, was determined to be 2.1 $cmH_2O \cdot L^{-1} \cdot s^{-1}$ in Patient 1 and 17.8 $cmH_2O \cdot L^{-1} \cdot s^{-1}$ in Patient 2.

Table 6.1: The key ventilation parameters measured in two patients during two settings – with a 10s inspiratory hold and with minimum inspiratory hold.

Patient No.	Inspiratory hold	P_{max}	*PEEP*	P_{plat}	P_{mean}	*VT*	*Q*	*C*	R_{aw}	*I:E*
		cmH_2O				mL	$L \cdot min^{-1}$	$mL \cdot cmH_2O^{-1}$	$cmH_2O \cdot L^{-1} \cdot sec^{-1}$	(-)
1	10-s	26.4	8.2	18.1	17.3	618	48	34	10.4	1:2.5
1	Minimum	26.6	8.4	20.0	12.8	618	48	31	8.3	1:2.5
2	10-s	35.9	8.6	24.5	25.9	240	28	10	24.4	1:2
2	Minimum	34.9	8.6	31.8	15.8	240	28	8	6.6	1:2

In Fig. 6.2, it is noticeable that both P_{aw} and P_{es} decreased exponentially by approximately 2 cmH_2O during the 10-second inspiratory hold. In the setting with a minimum inspiratory hold, the same maximum pressure was reached, and during the minimum inspiratory hold, P_{aw} dropped to P_1 (alveolar pressure). The inspiratory flow did not differ between the two settings, while during the expiratory phase, the peak flow was higher in the setting with the minimum inspiratory hold, possibly due to higher P_{aw}. P_{transp}, the difference between P_{aw} and P_{es}, remained around 3 cmH_2O during the inspiratory hold.

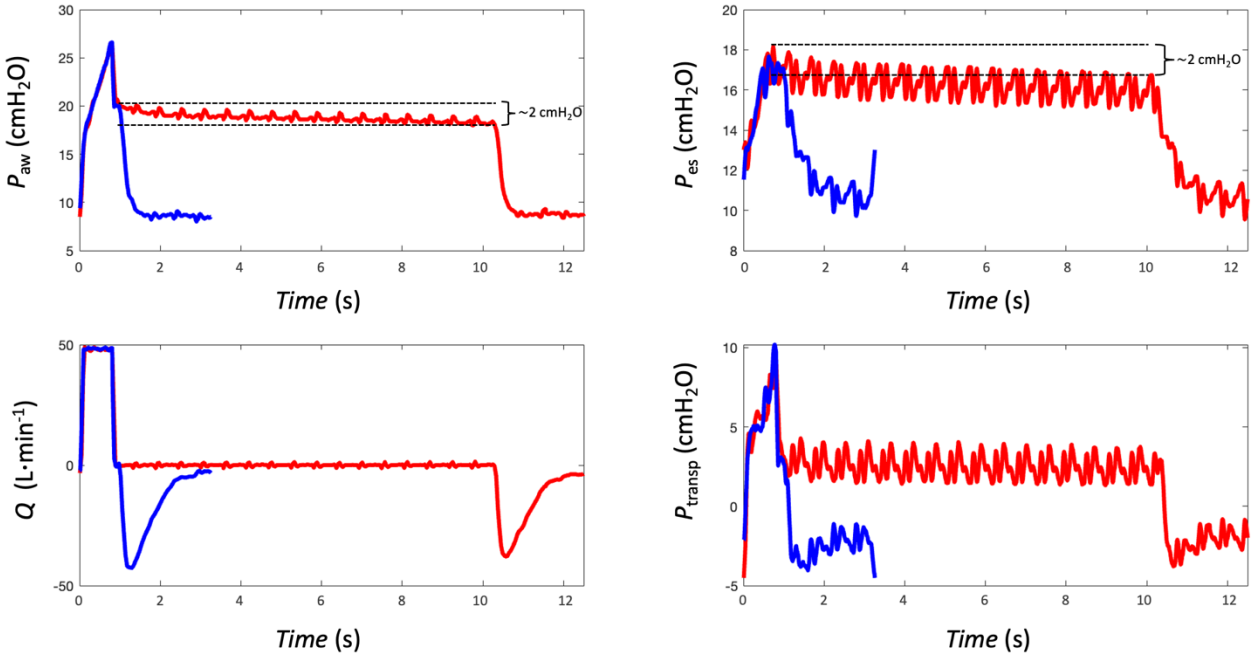

Figure 6.2: Time course of P_{aw}, P_{es}, Q, and P_{transp} during the respiratory cycle in Patient 1 with an inspiratory hold (in red) and without an inspiratory hold (in blue).

P_{aw} decreased by approximately 6 cmH_2O during the 10-second inspiratory hold, while P_{es} decreased by only 1 cmH_2O, as depicted in Fig. 6.3. In the setting with a minimum inspiratory hold, the same maximum pressure was reached, and during the minimum inspiratory hold, P_{aw} dropped to indistinct P_1. The inspiratory flow did not differ between the two settings, while during the expiratory phase, the peak flow was again higher in the setting with the minimum inspiratory hold. P_{transp} reached a maximum pressure of 24 cmH_2O.

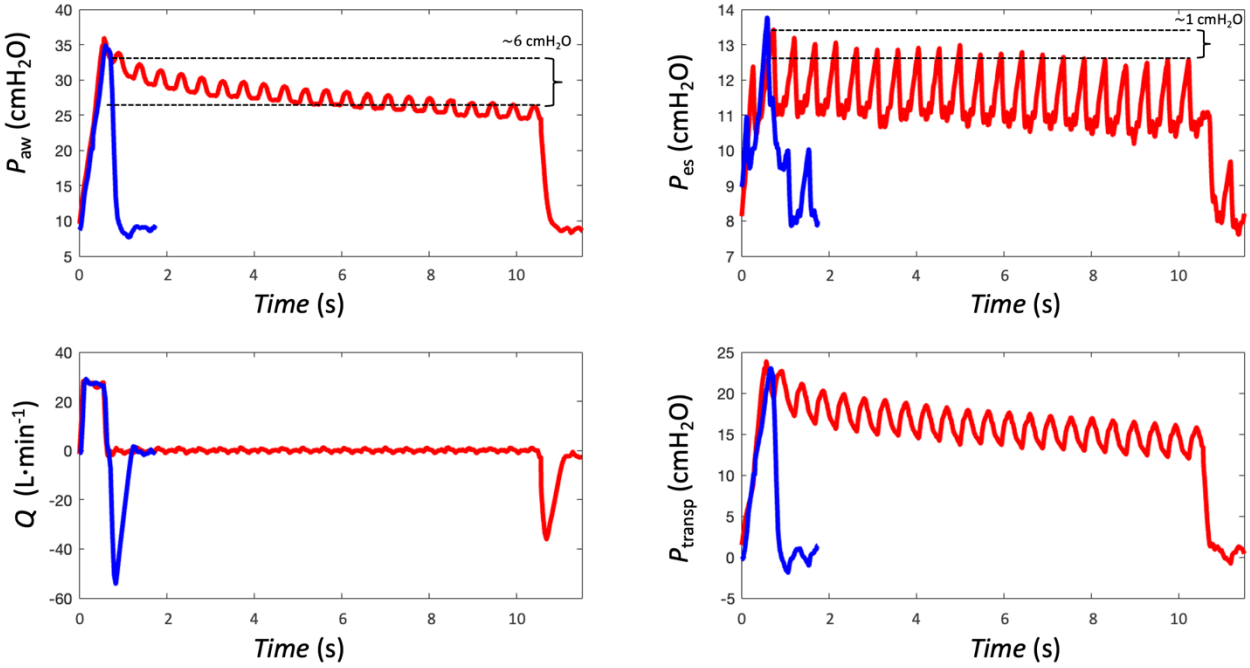

Figure 6.3: Time course of P_{aw}, P_{es}, Q, and P_{transp} during the respiratory cycle in Patient 2 with an inspiratory hold (in red) and without an inspiratory hold (in blue).

The PV loops for P_{aw} and P_{es} in the inspiratory phase did not differ for settings with 10-second inspiratory hold and with minimum inspiratory hold for both patients, as depicted in Fig. 6.4 and numerically shown in Table 6.2. However, the dissipated E_{aw} and E_{es} was higher for the setting with 10-second inspiratory hold for both patients. E_{transp} was around 0.3 J in both patients.

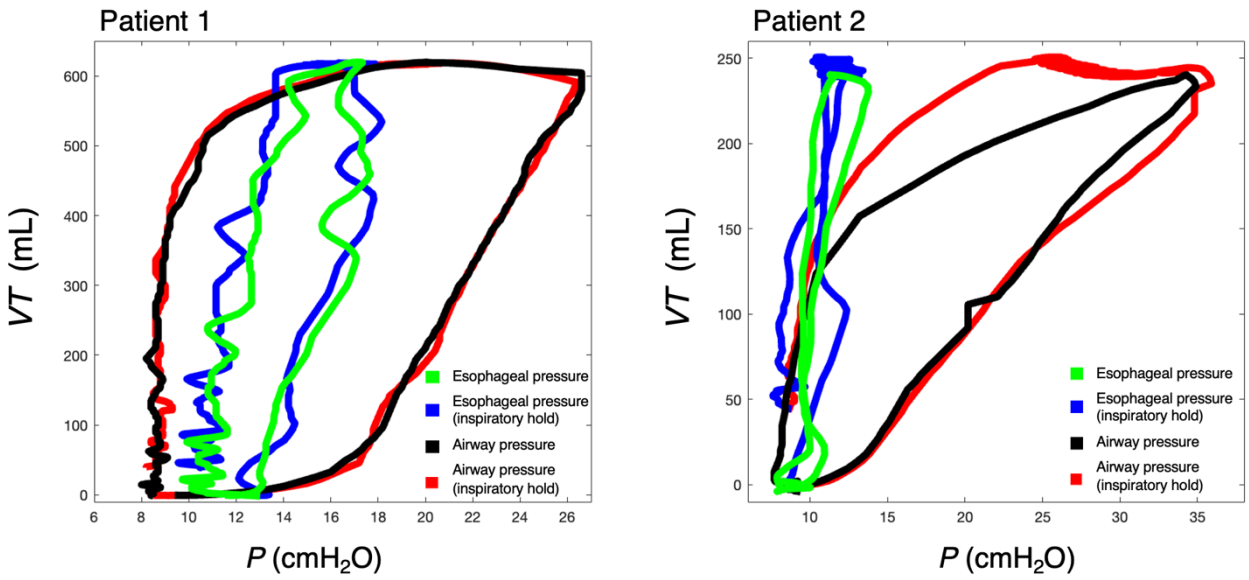

Figure 6.4: PV loops for P_{aw} and P_{es} with 10-s inspiratory hold a minimum inspiratory hold during the whole respiratory cycle for both patients.

Table 6.2: The calculated inspiratory E_{aw}, E_{es}, and E_{transp} and dissipated E_{aw} and E_{es} by the geometric method for both patients with 10-s inspiratory hold and minimum inspiratory hold.

Patient No.	Inspiratory hold	Inspiratory E_{aw} (J)	Dissipated E_{aw} (J)	Inspiratory E_{es} (J)	Dissipated E_{es} (J)	Inspiratory E_{transp} (J)
1	10-s	1.30	0.75	0.95	0.27	0.35
1	Minimum	1.30	0.70	0.95	0.19	0.35
2	10-s	0.57	0.34	0.26	0.07	0.31
2	Minimum	0.54	0.21	0.26	0.03	0.28

As shown in Table 6.3, in Patient 1, the effect of inspiratory hold duration resulted in a significant difference in delivered mechanical energy only for the Chi equation (15). In Patient 2, where the decrease in P_{aw} during the inspiratory hold was more pronounced, the differences between the individual simplified equations were greater. According to equations (10) and (12), the difference was as much as 20%. Signifficant differences were also observed between the simplified equations.

Table 6.3: The mechanical energy obtained from the simplified equations (10, 12–15) for both patients with 10-s inspiratory hold and minimum inspiratory hold.

Patient No.	Inspiratory hold	Airway Geometrical	Gattinoni (10)	Comprehensive (12)	Surrogate (13)	Chi (14)	Dynamic (15)
1	10-s	1.30	1.49	1.30	1.32	2.41	1.05
1	Minimum	1.30	1.47	1.26	1.33	1.06	1.06
2	10-s	0.57	0.75	0.68	0.61	1.48	0.55
2	Minimum	0.54	0.63	0.55	0.58	0.71	0.51

6.3 Discussion

The pilot clinical study demonstrated that the duration of the inspiratory hold did not affect the estimation of delivered mechanical energy when calculated using the geometric method based solely on the inspiratory phase. However, the length of the inspiratory hold significantly affected the calculated dissipated energy and highlighted the discrepancies among the simplified mechanical energy estimation methods. The results confirmed several key findings previously observed in viscoelastic physical models of the respiratory system.

During a 10-second inspiratory hold, both patients exhibited a gradual decrease in airway pressure (P_{aw}) and esophageal pressure (P_{es}). This pattern, which corresponds to viscoelastic stress relaxation in lung tissue as previously shown in physical models, highlights the importance of tissue resistance as a contributor to total respiratory resistance. The duration of the inspiratory hold had a notable effect on P_{plat}, and consequently on calculated compliance and airway resistance. In patients with elevated tissue resistance, the difference in P_{plat} values obtained after short versus prolonged inspiratory holds was significant. For example, in Patient 2, P_{plat} measured after a short hold was approximately 6 cmH_2O higher than after a 10-second hold, resulting in up to 20% variability in estimated mechanical energy depending on the equation used.

A comparison of simplified mechanical power equations revealed marked differences between them. While some of these equations are convenient for bedside use due to minimal measurement requirements and the absence of the need for inspiratory holds, the estimates may be affected in the presence of significant tissue resistance or when inspiratory hold duration varies.

To estimate mechanical energy delivered to the lung parenchyma, transpulmonary pressure—calculated as the difference between P_{aw} and P_{es}—was employed. Although this method, consistent with the approach described by Silva et al. [62], theoretically provides a more precise assessment of stress exerted on lung tissue, its routine clinical use is limited. Esophageal manometry, while considered the best available surrogate for pleural pressure [84], is invasive, technically demanding, and often poorly tolerated by patients. Moreover, its accuracy depends on correct catheter placement, appropriate balloon inflation, and the absence of artifacts.

In Patient 1, a persistently negative P_{es} during expiration suggested possible overinflation of the balloon, likely resulting in underestimation of P_{transp}. In Patient 2, a difference between inspiratory and expiratory tidal volumes was noted despite a ventilator gas leak test, suggesting a minor circuit leak. This could have been caused by the complexity of the breathing system, including an HME filter, capnography, flow sensor, TrachCare system, and multiple connectors. Even minor leaks, such as those, for example, around the cannula, may cause pressure decrease during an inspiratory hold that is not attributable solely to viscoelastic tissue resistance. However, these small leaks are generally insufficient to cause observable chest wall movement or significant changes in intrathoracic volume. As a result,

P_{es} may remain nearly constant. Despite these limitations, the measurement of tissue resistance, derived from differences in calculated resistance between short and long inspiratory holds, appears feasible and could provide clinically relevant insights. Incorporating R_t into routine clinical assessments may improve the identification of patients at greater risk for VILI and could guide individualized adjustments of ventilation parameters such as *PEEP*, *VT*, and flow.

An important limitation of this pilot study lies in the small number of participants. Only two patients were included, primarily due to strict inclusion criteria—fully controlled ventilation, availability of esophageal catheter, experienced personnel, patient tolerance for prolonged inspiratory holds, presence of lung injury, and informed consent. Nonetheless, this preliminary study proved sufficient to assess the feasibility of esophageal catheter use, the application of inspiratory holds, the estimation of tissue resistance, and their impact on mechanical energy delivery and the performance of simplified mechanical power equations.

An interesting direction for future research could be to investigate the magnitude of tissue resistance in various lung diseases and its potential implications for respiratory mechanics and lung protective ventilation strategies.

7 Discussion

The physical model of respiratory system showed that identical inspiratory airway pressures and mechanical energy values can result from either tissue resistance or airway flow resistance, despite their different physiological origin. The pilot clinical study confirmed that the duration of the inspiratory hold may affect plateau pressure and derived parameters such as compliance and resistance, particularly in patients with elevated tissue resistance, and thereby affect the mechanical energy delivered to the lungs. Different simplified mechanical energy equations produced different results, highlighting the risk of misinterpretation when viscoelastic properties are overlooked. These findings underline the need to distinguish between airway flow and tissue resistance when assessing mechanical energy load and support the potential of tissue resistance monitoring in personalized lung protective ventilation.

A central contribution of this work is the development and validation of a novel physical model of the respiratory system that enables the isolated study of tissue resistance and airway flow resistance. By incorporating a low-friction borosilicate syringe with a throttle valve in parallel to a bellow-based lung Simulator, the physical model was able to mimic viscoelastic properties of lung tissue. Using this setup, it was possible to directly compare two different configurations—one with tissue resistance and no airway flow resistance, and the other with airway flow resistance only. These comparisons revealed that even when inspiratory airway pressure at the opening was matched between the two physical models, the pressure inside the artificial lung and consequently the calculated mechanical energy was higher. This finding demonstrates that pressure at the airway opening alone can be misleading, as it does not distinguish between the contributions of airway and tissue resistance, and therefore cannot accurately reflect the actual mechanical energy delivered to the lung parenchyma. The physical model's ability to simulate tissue and airway flow resistances independently provides a powerful tool for applications such as testing mechanical ventilation modes, evaluating the impact of inspiratory hold duration, or exploring ventilation strategies aimed at minimizing dissipated energy. On the other hand, the physical respiratory system model represents a single, homogeneous compartment and therefore cannot fully capture the heterogeneity, recruitability, and dynamic complex behavior observed in human lungs in clinical scenarios.

While mechanical power calculations provide a single value representing the energy delivered to the respiratory system, this energy comprises various static and dynamic components (e.g., PEEP, airway flow resistance, and others). Understanding the relative contributions of these components may help identify which portion of the delivered energy is potentially harmful. The inclusion of positive *PEEP* in the calculations remains debated. *PEEP* should be included in mechanical power calculations because it represents a static energy load applied to the respiratory system that contributes to strain and potential lung injury according to Vasques et at. [82]. Energy is required to maintain *PEEP* even before any tidal volume is delivered, adding to the total mechanical load. This can be illustrated by the elevator analogy: lifting an elevator from the second to the third floor requires more energy than from the ground to the first, even if the height difference is the same—similarly, starting from a higher *PEEP* level increases the energy applied with each breath [82]. On the other side, Marini and Jaber

questioned whether *PEEP* should be included in mechanical power calculations, and suggested that incorporating the product of breathing frequency and the hysteresis area of the tidal transpulmonary pressure–volume loop, a variable influenced by *PEEP* and recruitment, may refine the mechanical power concept to more accurately determine the proximate mechanical cause of VILI [72].

Next, the profile of inspiratory flow, such as square versus decelerating, may also directly affect the energy delivery to the lungs and contribute to VILI [91]. Flow magnitude and profile affects the aggressiveness of lung tissue expansion, even when plateau and driving pressures are unchanged, and also interacts with airway flow resistance to determine how much energy is dissipated in the airways versus delivered to the lung tissue. Unfavorable flow patterns can raise stress and strain rates in alveolar units, also increasing VILI risk [72, 91].

Furthermore, including airway flow resistance in mechanical power calculations may lead to misinterpretation of the injurious load on the lung parenchyma. Experimental results showed that increasing airway flow resistance elevated mechanical power estimates derived from airway opening pressure without proportionally increasing lung-level energy. This indicates that energy dissipated in the airways is largely lost before reaching the alveoli. Whether resistive mechanical power dissipated in the airways contributes to VILI remains uncertain, and the most relevant assessment of injurious energy would be based on pressures measured at the lung level by estimationg transpulmonary pressures rather than at the airway opening [15, 64, 83]. Therefore, including airway flow resistance in mechanical power calculations may overestimate energy delivery, limiting the clinical value of mechanical power as a predictor of VILI. This limitation may be further amplified by the inability of current methods to distinguish airway flow resistance from tissue resistance, resulting in misattribution of viscoelastic pressure losses to airway resistance.

Although this dissertation did not directly evaluate regional lung heterogeneity, such heterogeneity is also an important determinant of VILI. The differences between the regions in terms of mechanical properties can be so large that the optimal setting of mechanical ventilation parameters for one region makes the setting of parameters for others significantly inappropriate [53]. Alternative and non-conventional ventilation strategies, such as FCV, MFOV or Three-Level ventilation [28, 29, 31, 33], may reduce the problems associated with heterogeneity. Also, a novel approach to inspiratory flow generation and gas mixing based on pulse-width modulation of fast ON/OFF valves, previously implemented in the CoroVent ventilator, could also be applied in experimental studies testing alternative breathing patterns for their effect on mechanical power and VILI risk [92, 93]. This principle enables not only precise control of *VT* and FiO_2, but also the generation of various inspiratory flow profiles, including square and decelerating waveforms, which could be further explored in future studies assessing their effect on mechanical power and energy delivery to the lungs. The design supports scalability and adaptability across a wide range of patient populations, from neonates to adults or large animals, simply by exchanging the ON/OFF valves for models with different flow capacities.

The estimation of transpulmonary pressure via esophageal manometry is the most straigtforward method for assessing mechanical energy delivery to the lung tissue, but its use

is limited by cost, technical complexity, and patient discomfort. In its absence, simplified equations for estimating mechanical power are attractive in clinical settings due to their ease of use and minimal data requirements. However, the findings of this dissertation reveal substantial variability in the results produced by these equations, particularly in the presence of high airway flow resistance or variable inspiratory hold durations. In the pilot clinical study, different simplified equations yielded different energy estimates, even when applied to the same ventilation parameters and data. Such results highlight the potential for misinterpretation and inaccurate assessment of mechanical load. Relying on simplified equations without considering their limitations may compromise clinical decision-making, particularly when mechanical power is used to guide protective ventilation strategies. For these equations to be applied more reliably, it is essential to standardize the duration of the inspiratory hold used to determine P_{plat} and derived parameters, and to account for the contribution of tissue resistance.

Integrating tissue resistance monitoring into routine practice could help identify patients at higher risk of VILI and guide adjustments to *VT*, inspiratory flow, and *PEEP* based on individual lung mechanics. Taken together, tissue resistance appears to be a dominant contributor to energy dissipation at the lung level, while airway flow resistance predominantly affects dissipation at the airway opening, highlighting the risk of misinterpretation if only proximal measurements are considered. The magnitude of pressure decrease during this inspiratory hold may correlate with subsequent clinical outcomes during mechanical ventilation. For example, in the study by Protti et al., a difference between the measured pressure at the beginning of inspiratory hold and at the end of inspiratory hold due to tissue resistance, had a significant effect on the prevalence of pulmonary edema [19]. This pressure decrease could then be evaluated along with the mechanical power delivery. Larger, more diverse clinical studies are required to validate tissue resistance monitoring and to determine its prognostic value on clinical outcomes. Future research might focus on developing clinical tools for automated estimation of tissue resistance, enabling real-time integration into routine ventilator monitoring.

In addition, limitation of the use of mechanical power is the insufficiently defined threshold above which VILI develops. Cressoni et al. [61] showed that transpulmonary mechanical power greater than 12 $J \cdot min^{-1}$ induced VILI in healthy pigs, while Serpa Neto et al. [64] found that mechanical power greater than 17.0 $J \cdot min^{-1}$ was independently associated with higher in-hospital mortality in ICU patients receiving invasive ventilation. However, such thresholds may depend not only on the mechanical power but also on the distribution of energy across lung regions, the amount of aerated tissue, and the degree of pre-existing lung injury. Normalization to a standard lung volume or to the amount of aerated lung tissue has been proposed as a potential refinement [23, 72], and Zhang et al. [85] suggested to normalize mechanical power to predicted body weight or lung compliance.

The present work focused on fully controlled ventilation. In clinical practice, spontaneous breathing efforts frequently occur in all assisted modes of ventilation, altering measured airway pressures and volumes, and thereby affecting mechanical power calculations

[83]. Spontaneous activity may either mitigate or exacerbate lung stress depending on its synchrony with the ventilator.

The pilot clinical study's small sample size was the result of strict inclusion criteria requiring fully controlled ventilation, patient tolerance of inspiratory holds, availability of experienced personnel, and placement of an esophageal catheter. While sufficient for proof of concept, the limited cohort restricts generalizability, highlighting the need for larger studies across different patient populations and clinical settings.

Finally, it must be acknowledged that mechanical power estimation alone will probably never provide a complete solution for preventing VILI. A comprehensive lung protective approach should combine mechanical power assessment with other physiological measurements, imaging modalities, and clinical judgment, with the aim of tailoring ventilation to the unique mechanical characteristics of each patient while minimizing harm [94].

8 Contribution to Biomedical Engineering

Mechanical ventilation represents a major milestone in the evolution of modern medicine. It has evolved and improved over time, allowing physicians to better manage patients with respiratory difficulties or those dependent on artificial respiratory support. Although the history of mechanical ventilation dates back to the 19th century and there are hundreds to thousands of research teams investigating mechanical ventilation from various perspectives, many challenges remain, indicating that there is still room for optimization that could significantly improve outcomes for patients reliant on mechanical ventilation.

The analysis of current methods for calculating mechanical power delivery does not distinguish between airway flow resistance and tissue resistance, which can significantly affect the evaluation, interpretation, and clinical relevance of mechanical power delivery in terms of lung protective ventilation. The proposed method for determining tissue resistance and incorporating the duration of the inspiratory hold into the calculation of mechanical energy delivery to the lungs, as addressed in this dissertation, could lead to increased reliability and a reduced risk of lung tissue damage and complications associated with mechanical ventilation.

The simplified mechanical power equations, although practical for bedside use, tend to overestimate the actual mechanical energy delivered to the lungs when flow resistance is dominant. Future studies should focus on refining energy estimation methods, which could enable physicians to tailor ventilatory parameters to individual patients based on their physiological characteristics, provide guidance on how to interpret and rationally use data provided by the ventilator, and further contribute to the development of personalized approaches to mechanical ventilation. One possible future engineering direction could be the development of ventilators that automatically estimate tissue resistance, similar to how they currently estimate compliance and flow resistance.

The topic of this dissertation has clinical relevance, and its results may have a direct impact on improving the quality of care provided. A dissertation focused on studying the effects and settings of ventilatory parameters on the calculation of mechanical energy delivery during mechanical ventilation could thus offer potential benefits for both biomedical engineering and clinical practice.

9 Conclusion

A novel viscoelastic physical model was developed to simulate tissue resistance by connecting a low-friction borosilicate glass syringe with a throttle valve in parallel to the artificial lung of a bellow-based Simulator, forming a mechanical damper that mimics viscoelastic behavior. The model functions as a Maxwell body, with static elasticity represented by linear compliance and viscoelastic resistance by the syringe and throttle valve system.

By experimental comparison of physical models with tissue resistance and airway flow resistance during mechanical ventilation, it was found that the resulting values of maximum airway pressures and delivered mechanical energy, calculated using the geometric method, were similar despite the different origins of the resistances situated at different locations. In contrast, when mechanical energy was calculated from the pressure measured inside the artificial lung, the values for the physical model with tissue resistance were up to 20% higher than for the physical model with airway flow resistance for the given setting.

Next, it was demonstrated that, although the simplified mechanical power equations are practical for bedside use, they also yield similar estimates of delivered energy in physical models with either tissue viscoelastic or airway flow resistance. Moreover, the simplified mechanical power equations tend to overestimate the actual mechanical energy delivered to the lung when airway flow resistance is dominant. The results further showed that tissue resistance, rather than airway flow resistance, is the primary contributor to energy dissipation at the lung level, indicating that the calculations based solely on airway pressures may not accurately reflect the mechanical stresses responsible for lung injury.

The pilot study validated selected findings from physical models under clinical conditions and highlighted the limitations of simplified energy equations when tissue resistance is significant. The routine use of esophageal pressure monitoring for mechanical energy delivery estimates remains questionable due to its invasiveness and technical complexity. The measurement of tissue resistance, derived from differences in calculated resistance between short and long inspiratory holds, appears feasible and may offer clinically relevant insights that could improve the identification of patients at greater risk for VILI.

Thus, current methods for calculating mechanical power delivery do not distinguish between tissue resistance and airway flow resistance, which can have a significant impact on the evaluation, interpretation and significance of mechanical power delivery in terms of lung ventilation protectivity. The results underscore the importance of considering tissue resistance and its potential for ventilator-induced lung injury.

Future research should focus on refining energy estimation methods by considering factors such as the duration of the inspiratory hold and by distinguishing between tissue resistance and airway flow resistance. A promising direction may also be the quantification of injurious dissipated energy through measurements of driving transpulmonary pressure.

However, this approach requires advanced and costly equipment, experienced personnel, and large multicenter studies involving a substantial number of patients.

List of Literature

[1] REDDY, Raghu M, GUNTUPALLI, Kalpalatha K. Review of ventilatory techniques to optimize mechanical ventilation in acute exacerbation of chronic obstructive pulmonary disease. *International journal of chronic obstructive pulmonary disease*. 2007, **2**(4), 441–452. DOI: 10.2147/copd.s12159979.

[2] RUUSKANEN, Olli, et al. Viral pneumonia. *The Lancet*. 2011, **377**(9773), 1264–1275. DOI: 10.1016/S0140- 6736(10)61459-6.

[3] LEATHERMAN, James. Mechanical ventilation for severe asthma. *Chest*. 2015, **147**(6): 1671–1680. DOI: 10.1378/chest.14-1733.

[4] CORTEGIANI, Andrea, et al. Immunocompromised patients with acute respiratory distress syndrome: secondary analysis of the LUNG SAFE database. Critical Care, 2018, 22: 1–15. DOI: 10.1186/s13054-018-2079-9.

[5] ARDS Definition Task Force. Acute respiratory distress syndrome. Jama, 2012, 307.23: 2526–2533. 10.1001/jama.2012.5669.

[6] MATTHAY, Michael A., et al. Acute respiratory distress syndrome. *Nature reviews Disease primers*, 2019, 5.1: 18. DOI: 10.1038/s41572-019-0069-0.

[7] MEAD, Jere; TAKISHIMA, TAMOTSU; LEITH, DAVID. Stress distribution in lungs: a model of pulmonary elasticity. *Journal of applied physiology*, 1970, 28.5: 596–608. DOI: 10.1152/JAPPL.1970.28.5.596.

[8] CRESSONI, Massimo, et al. Lung inhomogeneity in patients with acute respiratory distress syndrome. American journal of respiratory and critical care medicine, 2014, 189.2: 149–158. DOI: 10.1164/rccm.201308-1567OC.

[9] TOBIN, Martin J., 2013. Principles and practice of mechanical ventilation. 3rd edition. Mcgraw Hill Education & Medic. ISBN 9780071736268.

[10] TONETTI, Tommaso, et al. Driving pressure and mechanical power: new targets for VILI prevention. Annals of translational medicine, 2017, 5.14. DOI: 10.21037/atm.2017.07.08.

[11] BATTAGLINI, Denise, et al. Challenges in ARDS definition, management, and identification of effective personalized therapies. Journal of Clinical Medicine, 2023, 12.4: 1381. DOI: 10.3390/jcm12041381

[12] ESTEBAN, Andrés, et al. Evolution of mortality over time in patients receiving mechanical ventilation. *American journal of respiratory and critical care medicine*, 2013, 188.2: 220-230. DOI: 10.1164/rccm.201212-2169OC

[13] GOLIGHER, Ewan C., et al. Lung recruitment maneuvers for adult patients with acute respiratory distress syndrome. A systematic review and meta-analysis. *Annals of the American Thoracic Society*, 2017, 14.Supplement 4: S304-S311. DOI: 10.1513/AnnalsATS.201704-340OT

[14] BLACK, Carissa L. Bellardine, et al. Relationship between dynamic respiratory mechanics and disease heterogeneity in sheep lavage injury. Critical care medicine, 2007, 35.3: 870-878. DOI: 10.1097/01.CCM.0000257331.42485.94

[15] AMATO, Marcelo BP, et al. Driving pressure and survival in the acute respiratory distress syndrome. New England Journal of Medicine, 2015, 372.8: 747-755. DOI: 10.1056/NEJMsa1410639

[16] GATTINONI, Luciano, et al. Prone position in acute respiratory distress syndrome. Rationale, indications, and limits. *American journal of respiratory and critical care medicine*, 2013, 188.11: 1286-1293. DOI: 10.1164/rccm.201308-1532CI

[17] FOY, Brody H.; BRIGHTLING, Christopher E.; SIDDIQUI, Salman. Proning reduces ventilation heterogeneity in patients with elevated BMI: implications for COVID-19 pneumonia management?. ERJ Open Research, 2020, 6.2. DOI: 10.1183/23120541.00292-2020

[18] OTIS, Arthur B., et al. Mechanical factors in distribution of pulmonary ventilation. Journal of applied physiology, 1956, 8.4: 427-443. DOI: 10.1152/jappl.1956.8.4.427

[19] PROTTI, Alessandro, et al. Role of strain rate in the pathogenesis of ventilator-induced lung edema. Critical care medicine, 2016, 44.9: e838-e845. DOI: 10.1097/CCM.0000000000001718

[20] MAEDA, Yoshiko, et al. Effects of peak inspiratory flow on development of ventilator-induced lung injury in rabbits. Anesthesiology, 2004, 101.3: 722-728. DOI: 10.1097/00000542-200409000-00021

[21] SANTINI, Alessandro, et al. Effects of inspiratory flow on lung stress, pendelluft, and ventilation heterogeneity in ARDS: a physiological study. Critical Care, 2019, 23: 1-9. DOI: 10.1186/s13054-019-2641-0

[22] RICH, Preston B., et al. Effect of rate and inspiratory flow on ventilator-induced lung injury. Journal of Trauma and Acute Care Surgery, 2000, 49.5: 903-911. DOI: 10.1097/00005373-200011000-00019

[23] GATTINONI, Luciano, et al. The future of mechanical ventilation: lessons from the present and the past. Critical Care, 2017, 21: 1-11. DOI: 10.1186/s13054-017-1750-x.

[24] PILLOW, J. Jane. High-frequency oscillatory ventilation: mechanisms of gas exchange and lung mechanics. Critical care medicine, 2005, 33.3: S135-S141. DOI: 10.1097/01.CCM.0000155789.52984.B7

[25] FERGUSON, Niall D., et al. High-frequency oscillation in early acute respiratory distress syndrome. New England Journal of Medicine, 2013, 368.9: 795-805. DOI: 10.1056/NEJMoa1215554

[26] YOUNG, Duncan, et al. High-frequency oscillation for acute respiratory distress syndrome. New England Journal of Medicine, 2013, 368.9: 806-813. DOI: 10.1056/NEJMoa1215716

[27] MEADE, Maureen O., et al. Severity of hypoxemia and effect of high-frequency oscillatory ventilation in acute respiratory distress syndrome. American journal of respiratory and critical care medicine, 2017, 196.6: 727-733. DOI: 10.1164/rccm.201609-1938OC

[28] HERRMANN, Jacob; TAWHAI, Merryn H.; KACZKA, David W. Parenchymal strain heterogeneity during oscillatory ventilation: why two frequencies are better than one. Journal of Applied Physiology, 2018, 124.3: 653-663. DOI: 10.1152/japplphysiol.00615.2017

[29] KACZKA, David W., et al. Multi-frequency oscillatory ventilation in the premature lung: effects on gas exchange, mechanics, and ventilation distribution. Anesthesiology, 2015, 123.6: 1394. DOI: 10.1097/ALN.0000000000000898

[30] GALMÉN, Karolina, et al. The use of high-frequency ventilation during general anaesthesia: an update. F1000Research, 2017, 6.

[31] TÖRÖK, Pavol, et al. Teória a zjednodušený matematický model viachladinovej umelej ventilácie pľúc. Anesteziologie a intenzivní medicína, 2008, 19.2: 96-104.

[32] WENZEL, Christin, et al. A linearized expiration flow homogenizes the compartmental pressure distribution in a physical model of the inhomogeneous respiratory system. Physiological Measurement, 2020, 41.4: 045005. DOI: 10.1088/1361-6579/ab83e6

[33] WEBER, Jonas, et al. Flow-controlled ventilation (FCV) improves regional ventilation in obese patients–a randomized controlled crossover trial. BMC anesthesiology, 2020, 20: 1-10. DOI: 10.1186/s12871-020-0944-y

[34] HÖHNE, Tobias; WENZEL, Christin; SCHUMANN, Stefan. Flow-controlled expiration (FLEX) homogenizes pressure distribution in a four compartment physical model of the respiratory system with chest wall compliance. Physiological Measurement, 2021, 42.7: 07NT01. DOI: 10.1088/1361-6579/ac0ff8

[35] PASTEKA, Richard, et al. Electro-mechanical lung simulator using polymer and organic human lung equivalents for realistic breathing simulation. Scientific reports, 2019, 9.1: 19778. DOI: 10.1038/s41598-019-56176-6

[36] WALL, Wolfgang A., et al. Towards a comprehensive computational model for the respiratory system. International Journal for Numerical Methods in Biomedical Engineering, 2010, 26.7: 807-827. DOI: 10.1002/cnm.1378

[37] ROTH, Christian J., et al. Computational modelling of the respiratory system: discussion of coupled modelling approaches and two recent extensions. Computer Methods in Applied Mechanics and Engineering, 2017, 314: 473-493. DOI: 10.1016/j.cma.2016.08.010

[38] IONESCU, Clara M.; SEGERS, Patrick; DE KEYSER, Robin. Mechanical properties of the respiratory system derived from morphologic insight. IEEE Transactions on Biomedical Engineering, 2008, 56.4: 949-959. DOI: 10.1109/TBME.2008.2007807

[39] BATES, Jason HT. Lung mechanics: an inverse modeling approach. Cambridge University Press, 2009. ISBN 9780521509602.

[40] SIMILOWSKI, T., et al. Viscoelastic behavior of lung and chest wall in dogs determined by flow interruption. Journal of Applied Physiology, 1989, 67.6: 2219-2229. DOI: 10.1152/jappl.1989.67.6.2219

[41] SUKI, Bela; BARABASI, ALBERT-LASZL; LUTCHEN, Kenneth R. Lung tissue viscoelasticity: a mathematical framework and its molecular basis. Journal of Applied Physiology, 1994, 76.6: 2749-2759. DOI: 10.1152/jappl.1994.76.6.2749

[42] BIRZLE, Anna M.; WALL, Wolfgang A. A viscoelastic nonlinear compressible material model of lung parenchyma–experiments and numerical identification. Journal of the mechanical behavior of biomedical materials, 2019, 94: 164-175. DOI: 10.1016/j.jmbbm.2019.02.024

[43] GOSWAMI, Soumya, et al. Imaging the local nonlinear viscoelastic properties of soft tissues: Initial validation and expected benefits. IEEE transactions on ultrasonics, ferroelectrics, and frequency control, 2022, 69.3: 975-987. DOI: 10.1109/TUFFC.2021.3140203

[44] DAI, Zoujun, et al. A model of lung parenchyma stress relaxation using fractional viscoelasticity. Medical engineering & physics, 2015, 37.8: 752-758. DOI: 10.1016/j.medengphy.2015.05.003

[45] BERGER, Lorenz, et al. A poroelastic model coupled to a fluid network with applications in lung modelling. International journal for numerical methods in biomedical engineering, 2016, 32.1. DOI: 10.1002/cnm.2731

[46] CONCHA, Felipe; HURTADO, Daniel E. Upscaling the poroelastic behavior of the lung parenchyma: A finite-deformation micromechanical model. Journal of the Mechanics and Physics of Solids, 2020, 145: 104147. DOI: 10.1016/j.jmps.2020.104147

[47] ESCOLAR CASTELLÓN, J. de D., et al. Lung histeresis: a morphological view. Histology and histopathology, 2004, 19: 159-166. DOI: 10.14670/HH-19.159

[48] GUERIN, Claude; RICHARD, Jean-Christophe. Measurement of respiratory system resistance during mechanical ventilation. Intensive care medicine, 2007, 33(6): 1046-1049. DOI: 10.1007/s00134-007-0652-9

[49] MEZIDI, M., et al. Effect of end-inspiratory plateau pressure duration on driving pressure. Intensive care medicine, 2017, 43(4): 587-589. DOI: 10.1007/s00134-016-4651-6

[50] GANZERT, Steven, et al. Pressure-dependent stress relaxation in acute respiratory distress syndrome and healthy lungs: an investigation based on a viscoelastic model. Critical Care, 2009, 13: 1-10. DOI: 10.1186/cc8203

[51] BARBERIS, Luigi; MANNO, Emmanuello; GUÉRIN, Claude. Effect of end-inspiratory pause duration on plateau pressure in mechanically ventilated patients. Intensive care medicine, 2003, 29(1): 130-134. DOI: 10.1007/s00134-002-1568-z

[52] TAWFIK, Pierre, et al. Static and dynamic measurements of compliance and driving pressure: a pilot study. Frontiers in physiology, 2022, 13: 773010. DOI: 10.3389/fphys.2022.773010

[53] TÖRÖK, Pavol, et al. Teória a zjednodušený matematický model viachladinovej umelej ventilácie pľúc. Anesteziologie a intenzivní medicína, 2008, 19.2: 96-104.

[54] DEPTA, Filip, et al. Six methods to determine expiratory time constants in mechanically ventilated patients: a prospective observational physiology study. Intensive Care Medicine Experimental, 2024, 12.1: 25. DOI: 10.1186/s40635-024-00612-z

[55] HENDERSON, William Roy. Expiratory time constant heterogeneity in experimental acute respiratory distress syndrome. 2016. PhD Thesis. University of British Columbia.

[56] RUTTING, Sandra, et al. Lung heterogeneity as a predictor for disease severity and response to therapy. Current Opinion in Physiology, 2021, 22: 100446. DOI: 10.1016/j.cophys.2021.05.009

[57] FOY, Brody H.; KAY, David. A computational comparison of the multiple-breath washout and forced oscillation technique as markers of bronchoconstriction. Respiratory physiology & neurobiology, 2017, 240: 61-69. DOI: 10.1016/j.resp.2017.02.016

[58] DELLACA, Raffaele L., et al. Lung recruitment assessed by total respiratory system input reactance. Intensive care medicine, 2009, 35: 2164-2172. DOI: 10.1007/s00134-009-1673-3

[59] LUEPSCHEN, H., et al. Protective ventilation using electrical impedance tomography. Physiological measurement, 2007, 28.7: S247. DOI: 10.1088/0967-3334/28/7/S18

[60] FRERICHS, Inéz, et al. Heterogeneous distribution of pulmonary ventilation in intensive care patients detected by functional electrical impedance tomography. Journal of Intensive Care Medicine, 1998, 13.4: 168-173. DOI: 10.1177/088506669801300404

[61] CRESSONI, Massimo, et al. Mechanical power and development of ventilator-induced lung injury. Anesthesiology, 2016, 124.5: 1100-1108. DOI: 10.1097/ALN.0000000000001056

[62] SILVA, Pedro Leme, et al. Power to mechanical power to minimize ventilator-induced lung injury?. Intensive care medicine experimental, 2019, 7(Suppl 1):38. DOI: 10.1186/s40635-019-0243-4

[63] MARINI, John J., et al. Practical assessment of risk of VILI from ventilating power: a conceptual model. Critical Care, 2023, 27.1: 157. DOI: 10.1186/s13054-023-04406-9

[64] SERPA NETO, Ary, et al. Mechanical power of ventilation is associated with mortality in critically ill patients: an analysis of patients in two observational cohorts. Intensive care medicine, 2018, 44: 1914-1922. DOI: 10.1007/s00134-018-5375-6

[65] MARINI, John J.; RODRIGUEZ, R. Michael; LAMB, Virnita. Bedside estimation of the inspiratory work of breathing during mechanical ventilation. Chest, 1986, 89.1: 56-63. DOI: 10.1378/chest.89.1.56

[66] GATTINONI, Luciano, et al. Ventilator-related causes of lung injury: the mechanical power. Intensive care medicine, 2016, 42: 1567-1575. DOI: 10.1007/s00134-016-4505-2

[67] CHIUMELLO, Davide, et al. Bedside calculation of mechanical power during volume- and pressure-controlled mechanical ventilation. Critical care, 2020, 24: 1-8. DOI: 10.1186/s13054-020-03116-w

[68] URNER, Martin, et al. Time-varying intensity of mechanical ventilation and mortality in patients with acute respiratory failure: a registry-based, prospective cohort study. The Lancet Respiratory Medicine, 2020, 8.9: 905-913. DOI: 10.1016/S2213-2600(20)30325-8

[69] GIOSA, Lorenzo, et al. Mechanical power at a glance: a simple surrogate for volume-controlled ventilation. Intensive care medicine experimental, 2019, 7: 1-13. DOI: 10.1186/s40635-019-0276-8

[70] CHI, Yi; HE, Huaiwu; LONG, Yun. A simple method of mechanical power calculation: using mean airway pressure to replace plateau pressure. Journal of Clinical Monitoring and Computing, 2021, 35: 1139-1147. DOI: 10.1007/s10877-020-00575-y

[71] GUÉRIN, Claude, et al. Effect of driving pressure on mortality in ARDS patients during lung protective mechanical ventilation in two randomized controlled trials. Critical Care, 2016, 20: 1-9. DOI: 10.1186/s13054-016-1556-2

[72] MARINI, John J.; JABER, Samir. Dynamic predictors of VILI risk: beyond the driving pressure. Intensive care medicine, 2016, 42.10: 1597-1600. DOI: 10.1007/s00134-016-4534-x

[73] SCHAEFER, Maximilian S., et al. Comparison of mechanical power estimations in mechanically ventilated patients with ARDS: a secondary data analysis from the EPVent study. Intensive Care Medicine, 2021, 47: 130-132. DOI: 10.1007/s00134-020-06282-1

[74] BARNES, Tom; VAN ASSELDONK, Dirk; ENK, Dietmar. Minimisation of dissipated energy in the airways during mechanical ventilation by using constant inspiratory and expiratory flows–flow-controlled ventilation (FCV). Medical Hypotheses, 2018, 121: 167-176. DOI: 10.1016/j.mehy.2018.09.038

[75] GOTTI, M., et al. Dissipated energy inside the respiratory system during mechanical ventilation. Critical Care, 2014, 18: 1-182. DOI: 10.1186/cc13474

[76] GOTTI, M., et al. Dissipated energy during protective mechanical ventilation. Intensive Care Medicine Experimental, 2015, 3: 1-1. DOI: 10.1186/2197-425X-3-S1-A663

[77] MASSARI, D., et al. Determinants of energy dissipation in the respiratory system during mechanical ventilation. Critical Care, 2015, 19: 1-201. DOI: 10.1186/cc14327

[78] BARNES, T.; ENK, D. Ventilation for low dissipated energy achieved using flow control during both inspiration and expiration. Trends in Anaesthesia and Critical Care, 2019, 24: 5-12. DOI: 10.1016/j.tacc.2018.09.003

[79] SPRAIDER, Patrick, et al. Individualized flow-controlled ventilation compared to best clinical practice pressure-controlled ventilation: a prospective randomized porcine study. Critical Care, 2020, 24: 1-10. DOI: 10.1186/s13054-020-03325-3

[80] BUSANA, Mattia, et al. Energy dissipation during expiration and ventilator-induced lung injury: an experimental animal study. Journal of applied physiology, 2022, 133.5: 1212-1219. DOI: 10.1152/japplphysiol.00426.2022

[81] BATES, Jason HT, et al. Mechanical power and ventilator-induced lung injury: what does physics have to say?. American journal of respiratory and critical care medicine, 2024, 209.7: 787-788. DOI: 10.1164/rccm.202307-1292VP

[82] VASQUES, Francesco, et al. Is the mechanical power the final word on ventilator-induced lung injury?—we are not sure. Annals of translational medicine, 2018, 6.19: 395. DOI: 10.21037/atm.2018.08.17

[83] HUHLE, Robert, et al. Is mechanical power the final word on ventilator-induced lung injury?—no. Annals of translational medicine, 2018, 6.19: 394. DOI: 10.21037/atm.2018.09.65

[84] SHIMATANI, Tatsutoshi, et al. Fundamental concepts and the latest evidence for esophageal pressure monitoring. Journal of Intensive Care, 2023, 11.1: 22. DOI: 10.1186/s40560-023-00671-6

[85] ZHANG, Zhongheng, et al. Mechanical power normalized to predicted body weight as a predictor of mortality in patients with acute respiratory distress syndrome. Intensive care medicine, 2019, 45: 856-864. DOI: 10.1007/s00134-019-05627-9

[86] PIQUILLOUD, Lise; BEITLER, Jeremy R.; BELONCLE, François M. Monitoring esophageal pressure. Intensive care medicine, 2024, 50.6: 953-956. DOI: 10.1007/s00134-024-07401-y

[87] PELOSI, Paolo; ROCCO, Patricia R. Effects of mechanical ventilation on the extracellular matrix. Intensive care medicine, 2008, 34.4: 631-639. DOI: 10.1007/s00134-007-0964-9

[88] GARCIA, Cristiane Sousa Nascimento Baez, et al. Pulmonary morphofunctional effects of mechanical ventilation with high inspiratory air flow. Critical care medicine, 2008, 36.1: 232-239. DOI: 10.1097/01.CCM.0000295309.69123.AE

[89] JAIN, Manu; SZNAJDER, J. Iasha. Bench-to-bedside review: distal airways in acute respiratory distress syndrome. Critical Care, 2007, 11.1: 206. DOI: 10.1186/cc5159

[90] AL-RAWAS, Nawar, et al. Expiratory time constant for determinations of plateau pressure, respiratory system compliance, and total resistance. Critical care, 2013, 17.1: R23. DOI: 10.1186/cc12500

[91] FAJARDO-CAMPOVERDI, Aurio, et al. Stress, strain and mechanical power: let's not forget the shape of the flow. *Anaesthesia*, 2025, 80.7: 868-869. DOI: 10.1111/anae.16602

[92] ROUBIK, Karel, et al. Novel design of inspiratory flow generation and gas mixing for critical care ventilators suitable for rapid production and mass casualty incidents. *Scientific Reports*, 2023, 13.1: 7153. DOI: 10.1038/s41598-023-34300-x

[93] WALZEL, Simon, et al. Simple Design of Mechanical Ventilator for Mass Production May Offer Excellent Performance, Precise Monitoring, and Advanced Safety. *Applied Sciences*, 2025, 15.10: 5631. DOI: 10.3390/app15105631

[94] PELOSI, Paolo, et al. Personalized mechanical ventilation in acute respiratory distress syndrome. *Critical care*, 2021, 25.1: 250. DOI: 10.1186/s13054-021-03686-3

[95] WALZEL, Simon; ROUBIK, Karel. Effect of tissue viscoelasticity on delivered mechanical power in a physical respiratory system model: distinguishing between airway and tissue resistance. *Biomedical Physics & Engineering Express*, 2024, 11.1: 015026. DOI: 10.1088/2057-1976/ad974b

[96] GAVER III, Donald P., et al. Mechanical ventilation energy analysis: Recruitment focuses injurious power in the ventilated lung. *Proceedings of the National Academy of Sciences*, 2025, 122.10: e2419374122. DOI: 10.1073/pnas.2419374122

Appendix A: Mathematical derivations of simplified mechanical energy equations

We consider volume-controlled ventilation with constant inspiratory flow, linear compliance and linear airway flow resistance, and negligible inertance. Let VT be tidal volume, P_{aw} airway pressure, T total time, T_i inspiratory time, T_e expiratory time, RR respiratory rate, Q flow, C_{rs} respiratory-system compliance, R_{aw} airway flow resistance, $PEEP$ the end-expiratory pressure, P_{max} maximum pressure (end-inspiration, before the inspiratory hold), and P_{plat} plateau pressure (during end-inspiratory hold). A conversion factor of 0.098 was used to convert cmH_2O to Pa. E corresponds to the delivered mechanical energy during the inspiratory phase of the respiratory cycle, expressed in joules. Mechanical power is calculated by multiplying E by the respiratory rate, yielding units of $J \cdot min^{-1}$.

Gattinoni's energy equation (Eq. 10)

Starting from the equation of motion, at any given time, the pressure (P_{aw}) in the whole respiratory system is equal to:

$$P_{aw}(t) = \frac{VT(t)}{C_{rs}} + R_{aw} \cdot Q(t) + PEEP.$$

Integrating over volume during inspiration with constant flow yields:

$$E = 0.098 \cdot \left(\frac{VT^2}{2 \cdot C_{rs}} + R_{aw} \cdot \frac{VT^2}{T_i} + PEEP \cdot VT\right).$$

This produces Eq. (10) in the main text.

Comprehensive equation using P_{max} and P_{plat} (Eq. 12)

Knowing that airway resistance is given by

$$R_{aw} = \frac{P_{max} - P_{plat}}{Q},$$

Eq. (10) of the main manuscript can be rewritten to separate the elastic, resistive, and $PEEP$ components:

$$E = \frac{VT^2}{2 \cdot C_{\mathrm{rs}}} + \frac{P_{\max} - P_{\mathrm{plat}}}{Q} \cdot \frac{VT^2}{T_{\mathrm{i}}} + PEEP \cdot VT.$$

Since

$$C_{\mathrm{rs}} = \frac{VT}{P_{\mathrm{aw}}}$$

and

$$P_{\mathrm{aw}} = P_{\mathrm{plat}} - PEEP,$$

the expression becomes

$$E = \frac{VT \cdot (P_{\mathrm{plat}} - PEEP)}{2} + (P_{\max} - P_{\mathrm{plat}}) \cdot VT + PEEP \cdot VT.$$

After regrouping terms, this simplifies to:

$$E = 0.098 \cdot VT \cdot \left[(P_{\max} - 0.5 \cdot \left(P_{\mathrm{plat}} - PEEP\right)\right],$$

which is the Comprehensive Eq. (12) used when both $P_{\max}$ and P_{plat} are available.

Dynamic equation with no inspiratory hold (Eq. 13)

If P_{plat} is unavailable, it can be approximated by $P_{\max}$ in the Comprehensive Eq. (12). This requires only $P_{\max}$ and *PEEP* and no need for inspiratory hold to derive Eq. (13).

Surrogate equation with fixed resistance (Eq. 14)

Comprehensive Eq. (12) was used to derive Surrogate Eq. (14):

$$E = 0.098 \cdot VT \cdot \left[(P_{\max} - 0.5 \cdot \left(P_{\mathrm{plat}} - PEEP\right)\right],$$

where the part in the square brackets was replaced by the average of the endpoints of the inspiratory pressure to get the unadjusted equation:

$$E_{\text{unadjusted}} = 0.098 \cdot VT \cdot [0.5 \cdot (P_{\max} + PEEP)].$$

Approximating 0.098 ≈ 0.10 gives

$$E_{\text{unadjusted}} = VT \cdot \left(\frac{P_{\max}+PEEP}{20}\right).$$

The unadjusted equation underestimates by half the resistive component. The bias is

$$E_{\text{bias}} = VT \cdot \left(\frac{R_{\text{aw}} \cdot Q}{20}\right).$$

R_{aw} was replaced with a fixed constant of 10 $cmH_2O \cdot s \cdot L^{-1}$ and Q was converted to $L \cdot s^{-1}$:

$$E_{\text{bias}} = VT \cdot \left(\frac{10 \cdot \frac{Q}{60}}{20}\right)$$

Then, the correct Surrogate Eq. (14) is

$$E = E_{\text{unadjusted}} + E_{\text{bias}} = VT \cdot \left(\frac{P_{\max} + PEEP + \left(\frac{Q}{6}\right)}{20}\right).$$

Mean-airway-pressure equation (Eq. 15)

The mechanical energy delivered during inspiratory phase corresponds to the area under the pressure curve (A_{insp}) on a pressure-time graph, multiplied by inspiratory flow. Then

$$A_{\text{insp}} = \frac{E}{Q} = \frac{E \cdot T_{\text{i}}}{VT}.$$

Mean airway pressure is the average pressure during the entire respiratory cycle. P_{mean} can be calculated using the following equation:

$$P_{\text{mean}} \cdot T = A_{\text{insp}} + A_{\text{decay}} + PEEP \cdot T_{\text{e}},$$

where A_{decay} is the area of pressure decay from P_{max} to $PEEP$. Owing to its relatively small contribution, this part of the equation was excluded. A_{insp} was then substituted using Comprehensive Eq. (12) and divided by Q.

$$P_{\text{mean}} \cdot T = \frac{VT \cdot \left[(P_{\text{max}} - 0.5 \cdot \left(P_{\text{plat}} - PEEP\right)\right] \cdot T_{\text{i}}}{VT} + PEEP \cdot T_{\text{e}}$$

$$P_{\text{max}} - 0.5 \cdot \left(P_{\text{plat}} - PEEP\right) \cdot T_{\text{i}} \ = P_{\text{mean}} \cdot T - PEEP \cdot T_{\text{e}}$$

$$P_{\text{max}} - 0.5 \cdot \left(P_{\text{plat}} - PEEP\right) \ = \frac{P_{\text{mean}} \cdot T - PEEP \cdot T_{\text{e}}}{T_{\text{i}}}$$

$$P_{\text{max}} - 0.5 \cdot \left(P_{\text{plat}} - PEEP\right) \ = P_{\text{mean}} + (P_{\text{mean}} - PEEP) \cdot \frac{T_{\text{e}}}{T_{\text{i}}}$$

By multiplying by the tidal volume and the conversion factor, we obtain Eq. 15.

$$E = \ 0.098 \cdot VT \cdot \left((P_{\text{mean}}) + \frac{T_{\text{e}}}{T_{\text{i}}}(P_{\text{mean}} - PEEP)\right)$$

Appendix B: Results of the impact of frictional resistance between barrel and plunger of the glass syringe on measured pressure and flow

The data from No-resistance model was used as a benchmark. The glass syringe without the throttle valve was connected to No-resistance model and the same ventilation parameters and all setting as for the Testing section of the main Manuscript were used. No difference between No-resistance model and No-resistance model with the syringe connected was noticeable for either parameter at either setting, as documented in Fig. B1. Based on these results, we suggest that the impact of frictional resistance between barrel and plunger of the glass syringe is minimal and not affecting the results of the main experiment.

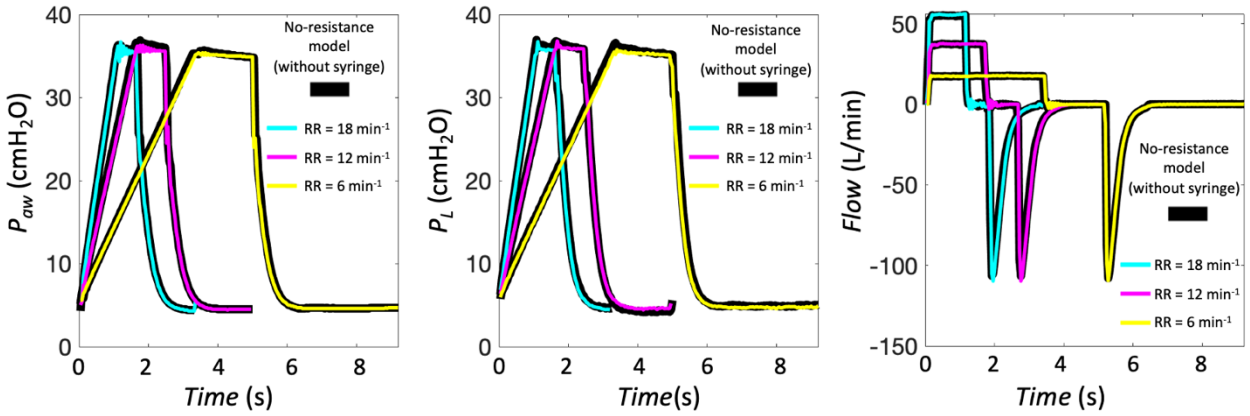

Figure B1: The impact of frictional resistance between barrel and plunger of the glass syringe on P_{aw}, P_L, and Q at respiratory rate settings RR = 6, 12 and 18 min^{-1}. The color-coded curves are for No-resistance model with the syringe connected and the black curves are for No-resistance model. Reproduced from [Walzel et al., 2025], published under the CC BY 4.0 license.

Appendix C: Calculated Respiratory Parameters and Mechanical Energy Estimates

Increase in P_{max}, R_{aw} and P_{mean} due to tissue resistance and increase in flow resistance with no effect on P_{plat} and C as shown in Table C1.

Table C1: Average parameters determined from pressure waveforms and set ventilation parameters for each model of the respiratory system.

Model of the respiratory system	P_{max} (cmH_2O)	P_{plat} (cmH_2O)	C ($mL \cdot cmH_2O^{-1}$)	R_{aw} ($cmH_2O \cdot s \cdot L^{-1}$)	P_{mean} with insp. hold (cmH_2O)
No-resistance	38.07	36.35	27.5	2.02	19.62
Flow resistance 5	41.38	36.46	27.4	5.79	19.99
Tissue resistance	41.30	36.52	27.4	5.62	20.33
Tissue + Flow resistance 5	44.26	36.40	27.5	9.25	20.84
Tissue + Flow resistance 10	47.51	36.40	27.5	13.07	21.33
Tissue + Flow resistance 15	51.1	36.40	27.5	17.29	22.42

Increase in mechanical energy (E) due to tissue resistance and flow resistance calculated by different simplified E calculation methods based on the obtained ventilation parameters (Table C2).

Table C2: Calculated average mechanical energy delivered to the model of the respiratory system by different simplified methods of E calculation based on the obtained ventilation parameters.

Model of the respiratory system	Simplified methods of E calculation for volume-controlled ventilation				
	Gattinoni Eq. (10)	Comprehensive Eq. (12)	Dynamic Eq. (13)	Surrogate Eq. (14)	Chi Eq. (15)
No-resistance	2.34 ± 0.03	2.19 ± 0.04	2.11 ± 0.03	2.58 ± 0.03	3.37 ± 0.07
Flow resistance 5	2.47 ± 0.01	2.51 ± 0.02	2.27 ± 0.01	2.74 ± 0.01	3.44 ± 0.02
Tissue resistance	2.46 ± 0.01	2.50 ± 0.01	2.27 ± 0.01	2.74 ± 0.01	3.51 ± 0.02
Tissue + Flow resistance 5	2.58 ± 0.01	2.80 ± 0.02	2.41 ± 0.01	2.89 ± 0.01	3.61 ± 0.02
Tissue + Flow resistance 10	2.70 ± 0.01	3.12 ± 0.01	2.57 ± 0.01	3.05 ± 0.01	3.71 ± 0.02
Tissue + Flow resistance 15	2.84 ± 0.01	3.47 ± 0.01	2.75 ± 0.01	3.23 ± 0.01	3.92 ± 0.03

The effect of inspiratory hold on P_{mean} and E calculated according to Chi et al. [70] for models of the respiratory system with tissue and different flow resistances (Table C3, Table C4).

Table C3: P_{mean} determined from pressure waveforms with/without inspiratory hold for each model of the respiratory system.

Model of the respiratory system	P_{mean} without inspiratory hold (cmH_2O)	P_{mean} with inspiratory hold (cmH_2O)
No-resistance	9.51	19.62
Flow resistance 5	10.11	19.99
Tissue resistance	10.10	20.33
Tissue + Flow resistance 5	10.72	20.83
Tissue + Flow resistance 10	11.35	21.33
Tissue + Flow resistance 15	12.09	22.41

Table C4: Calculated average mechanical energy delivered to the model of the respiratory system with/without inspiratory hold according to Chi et al. [70].

Model of the respiratory system	Without inspiratory hold Eq. (15)	With inspiratory hold Eq. (15)
No-resistance	1.38	3.37
Flow resistance 5	1.50	3.44
Tissue resistance	1.49	3.51
Tissue + Flow resistance 5	1.62	3.61
Tissue + Flow resistance 10	1.74	3.71
Tissue + Flow resistance 15	1.89	3.92

No difference between Tissue resistance model and Flow resistance 5 model without inspiratory hold compared to significant difference with inspiratory hold (Fig. C1).

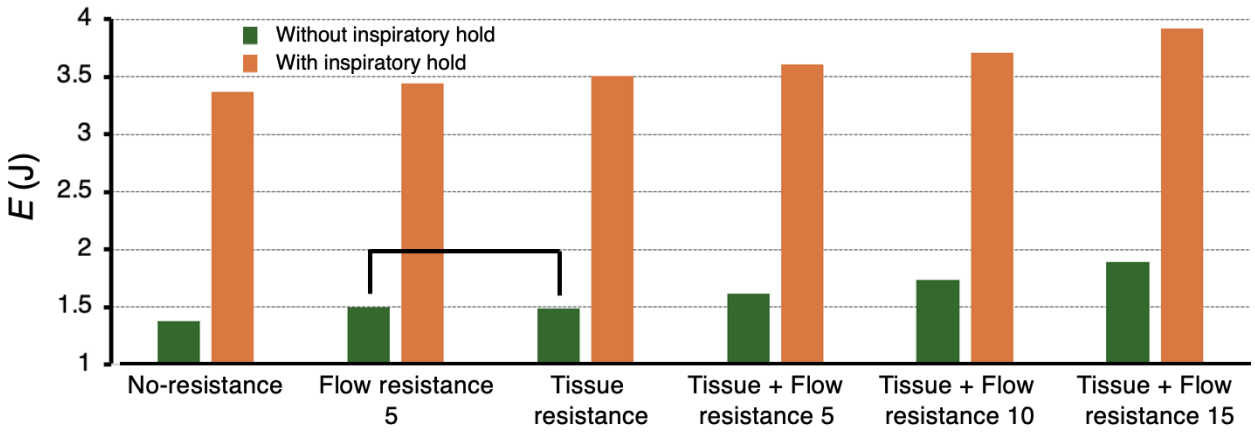

Figure C1: Calculated average mechanical energy delivered to the model of the respiratory system with/without inspiratory hold according to Chi et al. [70]. Reproduced from [Walzel et al., 2025], published under the CC BY 4.0 license.

Appendix D: Geometrical calculations of mechanical energy

The equations which were used to calculate mechanical and dissipated energy by the geometric method. The resulting values were obtained by numerical integration of the pressure–volume loop, with energy expressed for pressures measured at the airway opening with *PEEP* (E_{aw}), at the airway opening without *PEEP* (E_d), and at the artificial lung level without *PEEP* (E_L). The respective equations are listed below.

$$I_{\text{insp}} = \{\, i\colon VT_{i+1} > VT_i \,\},$$

where I_{insp} is the set of indices i that belong to the inspiratory part of the cycle.

$$E_{\text{aw}} = 0.098 \cdot \sum_{i \in I_{\text{insp}}} \left[0.5 \cdot (P_{\text{aw}_i} + P_{\text{aw}_{i+1}}) \cdot (VT_{i+1} - VT_i)\right],$$

where E_{aw} corresponds to the delivered mechanical energy during the inspiratory phase of the respiratory cycle in J, P_{aw} represents the measured pressure at a given time in cmH_2O at the airway opening, VT is the measured volume at a given time in L and i denotes the number of a sample in the inspiratory phase.

$$E_{\text{d}} = 0.098 \cdot \sum_{i \in I_{\text{insp}}} \left[0.5 \cdot ((P_{\text{aw}_i} + P_{\text{aw}_{i+1}}) - 2 \cdot PEEP) \cdot (VT_{i+1} - VT_i)\right],$$

where E_D corresponds to the delivered mechanical energy during the inspiratory phase of the respiratory cycle without *PEEP* in J, P_{aw} represents the measured pressure at a given time in cmH_2O at the airway opening, *PEEP* is the positive end-expiratory pressure in cmH_2O, VT is the measured volume at a given time in L and i denotes the number of a sample in the inspiratory phase.

$$E_{\text{L}} = 0.098 \cdot \sum_{i \in I_{\text{insp}}} \left[0.5 \cdot ((P_{\text{L}_i} + P_{\text{L}_{i+1}}) - 2 \cdot PEEP) \cdot (VT_{i+1} - VT_i)\right],$$

where E_L corresponds to the delivered mechanical energy during the inspiratory phase of the respiratory cycle at the artificial lung level in J, P_L represents the measured pressure at the artificial lung level at a given time in cmH_2O, VT is the measured volume at a given time in L and i denotes the number of a sample in the inspiratory phase.

Dissipated energy was obtained by calculating the difference between the total energy during inspiration and the total energy during expiration. In practice, this meant first summing the energy associated with the inspiratory part of the PV loop, then summing the energy associated with the expiratory part, and finally subtracting the latter from the former. The resulting value corresponds to the hysteresis area of the PV loop.

Appendix E: Clinical study registration

ClinicalTrials.gov PRS
Protocol Registration and Results System

ClinicalTrials.gov PRS DRAFT Receipt (Working Version)
Last Update: 05/28/2024 15:58

ClinicalTrials.gov ID: NCT06236685

Study Identification

Unique Protocol ID:	AVIM
Brief Title:	Optimizing the Assessment of Mechanical Ventilation by Integrating Advanced Monitoring Techniques [AVIM]
Official Title:	Optimizing the Assessment of Mechanical Ventilation by Integrating Advanced Monitoring Techniques
Secondary IDs:	

Study Status

Record Verification:	February 2024
Overall Status:	Enrolling by invitation
Study Start:	April 22, 2024 [Actual]
Primary Completion:	December 2027 [Anticipated]
Study Completion:	December 2027 [Anticipated]

Sponsor/Collaborators

Sponsor:	Czech Technical University in Prague
Responsible Party:	Sponsor
Collaborators:	Military University Hospital, Prague

Oversight

U.S. FDA-regulated Drug:	No
U.S. FDA-regulated Device:	No
U.S. FDA IND/IDE:	No
Human Subjects Review:	Board Status: Approved Approval Number: 108/19-1/2024 Board Name: Ethics Committee of Central Military Hospital Prague Board Affiliation: Military University Hospital Prague Phone: +420973203550 Email: eticka.komise@uvn.cz Address: U Vojenské nemocnice 1200 Praha 6, 169 02 Czech Republic

Data Monitoring:	No
FDA Regulated Intervention:	No

Study Description

Brief Summary: The aim of this study is to collect synchronized data from multiple monitoring techniques of mechanical ventilation (pressure/flow waves from the ventilator, electrical impedance tomography – EIT, esophageal pressure, capnography) in patients ventilated either on intensive care units or during anesthesia and evaluate the data by detailed mathematical analysis, to test three hypotheses:

1. Various published methods of calculation of the expiratory time constant provide different results in most cases.
2. Inhomogeneous ventilation (as described by EIT) affects the form of the expiratory flow curve and thus the calculated expiratory time constants.
3. The calculation of mechanical energy transferred to the lungs is affected by the chosen technique and length of the inspiratory pause maneuver.

This study does not test any new or non-standard methods and does not in any way interfere with the course of treatment indicated by the clinician, apart from extending the monitoring techniques.

Detailed Description: Mechanical ventilation is known to cause various complications, generally known as ventilator induced lung injury. Thus, detailed monitoring is essential. However, data interpretation is complicated in clinical practice. The investigators aim to collect synchronized data from multiple monitoring techniques of mechanical ventilation (pressure/flow waves from the ventilator, electrical impedance tomography – EIT, esophageal pressure, capnography) in patients ventilated either on intensive care units or during anesthesia and evaluate the data by detailed mathematical analysis. The results will be used to explore the complexity of seemingly simple and often used calculations describing the course of mechanical ventilation – mostly the expiratory time constant and amount of mechanical energy transferred to the lungs. The investigators primarily aim to test three hypotheses:

1. Various published methods of calculation of the expiratory time constant provide different results in most cases.
2. Inhomogeneous ventilation (as described by EIT) affects the form of the expiratory flow curve and thus the calculated expiratory time constants.
3. The calculation of mechanical energy transferred to the lungs is affected by the chosen technique and length of the inspiratory pause maneuver.

For this, the investigators plan to recruit 50 patients undergoing general anesthesia with controlled mechanical ventilation and 50 patients hospitalized on intensive care units. Monitoring of those patients will be protocolized and will in all cases include pressure/flow monitoring of the mechanical ventilator, capnography, and electrical impedance tomography. Esophageal pressure monitoring will be introduced where indicated by the clinician or where nasogastric tube insertion will be indicated (as the pressure can be measured by a combined catheter).

This study thus does not test any new or non-standard methods and does not in any way interfere with the course of treatment indicated by the clinician, apart from extending the monitoring techniques. Patient data will be anonymized and all the enrolled patients or their families will sign an informed consent as agreed by the ethical committee of our hospital.

Conditions

Conditions:	Mechanical Ventilation Complication Ventilator-Induced Lung Injury
Keywords:	electrical impedance tomography expiratory time constant mechanical energy lung protective ventilation ventilator-induced lung injury expiratory flow inspiratory hold maneuver

Study Design

Study Type:	Interventional
Primary Purpose:	Diagnostic
Study Phase:	N/A
Interventional Study Model:	Parallel Assignment The study will be conducted on patients provided with mechanical ventilation either on intensive care units or during anesthesia. Extended monitoring of ventilation, including electric impedance tomography and esophageal pressure readings will be applied.
Number of Arms:	2
Masking:	None (Open Label)
Allocation:	Non-Randomized
Enrollment:	100 [Anticipated]

Arms and Interventions

Arms	Assigned Interventions
Experimental: General anesthesia Patients undergoing general anesthesia with mechanical ventilation will be monitored by electrical impedance tomography in addition to standard monitoring. Moreover, esophageal pressure catheter will be used in cases where indicated by clinician or in case of an indication of nasogastric tube, as esophageal pressure can be measured by a combined catheter.	Device: Electric impedance tomography EIT is rarely used during general anesthesia for standard procedures. In the anesthesia arm, all patients will be monitored by EIT. Other Names: • EIT
Experimental: Intensive Care Unit Patients ventilated in the ICU for various reasons will receive standard care, including advanced monitoring of mechanical ventilation.	Device: Electric impedance tomography EIT is rarely used during general anesthesia for standard procedures. In the anesthesia arm, all patients will be monitored by EIT. Other Names: • EIT

Outcome Measures

Primary Outcome Measure:

1. Expiratory time constant

Time [in seconds], in which the lungs exhale 63% of the total volume.

[Time Frame: 2 minutes after an intervention or a change in the ventilator settings]

2. Mechanical energy transferred to the lungs
   Mechanical energy (alternatively referred to as mechanical work) [in Joules] is the energy delivered to the respiratory system during a single inspiration cycle.

   [Time Frame: 2 minutes after an intervention or a change in the ventilator settings]

Other Pre-specified Outcome Measures:

3. Regional signals of electrical impedance tomography
   Changes of regional signals of electrical impedance tomography throughout the respiratory cycle correspond to changes in lung aeration.

   [Time Frame: 2 minutes after an intervention or a change in the ventilator settings]

Appendix F: Example of raw data recorded from the vital signs monitor

Table D1: One second of data recorded from the vital signs monitor at a sampling rate of 100 Hz.

Time (s)	Pressure inside the lung model (cmH_2O)	Pressure at the airway opening (cmH_2O)	Flow ($L \cdot min^{-1}$)	Tidal volume increase (mL)
0	4.1	3.8	0.1	0.0
0.01	4.8	4.9	1.1	0.2
0.02	5.7	6.0	2.4	0.6
0.03	6.0	7.0	3.6	1.2
0.04	5.9	8.1	4.9	2.0
0.05	6.1	7.9	12.2	4.1
0.06	6.6	7.8	19.4	7.3
0.07	7.2	7.6	26.7	11.7
0.08	7.4	7.4	34.0	17.4
0.09	7.6	7.9	34.6	23.2
0.1	8.0	8.4	35.1	29.0
0.11	8.3	8.9	35.6	35.0
0.12	8.6	9.4	36.2	41.0
0.13	8.7	9.6	36.6	47.1
0.14	8.9	9.8	37.0	53.3
0.15	9.2	10.0	37.4	59.5
0.16	9.5	10.2	37.8	65.8
0.17	9.7	10.5	37.8	72.1
0.18	9.9	10.8	37.8	78.4
0.19	10.2	11.0	37.7	84.7
0.2	10.4	11.3	37.7	91.0
0.21	10.7	11.5	37.8	97.3
0.22	10.9	11.8	37.8	103.6
0.23	11.2	12.0	37.8	109.9
0.24	11.3	12.2	37.9	116.2
0.25	11.6	12.4	38.0	122.5
0.26	11.9	12.7	38.0	128.8
0.27	12.1	13.0	38.0	135.2
0.28	12.3	13.2	38.1	141.5
0.29	12.6	13.4	38.2	147.9
0.3	12.8	13.6	38.2	154.3
0.31	12.9	13.8	38.2	160.6
0.32	13.1	14.0	38.3	167.0
0.33	13.3	14.2	38.2	173.4
0.34	13.5	14.4	38.2	179.7
0.35	13.8	14.7	38.2	186.1
0.36	14.0	14.9	38.1	192.5
0.37	14.1	15.1	38.1	198.8
0.38	14.4	15.3	38.0	205.1
0.39	14.6	15.5	38.0	211.5
0.4	14.9	15.7	38.0	217.8
0.41	15.1	15.9	38.0	224.1
0.42	15.3	16.1	38.0	230.5
0.43	15.4	16.3	38.0	236.8
0.44	15.7	16.5	38.0	243.1
0.45	16.0	16.7	38.0	249.5
0.46	16.2	17.0	37.9	255.8
0.47	16.3	17.2	37.8	262.1
0.48	16.5	17.4	37.8	268.4
0.49	16.6	17.6	37.8	274.7
0.5	16.9	17.8	37.8	281.0
0.51	17.2	18.0	37.7	287.3
0.52	17.4	18.2	37.7	293.6
0.53	17.6	18.4	37.7	299.8
0.54	17.8	18.6	37.8	306.1
0.55	18.0	18.8	37.8	312.4

0.56	18.2	19.0	37.8	318.7
0.57	18.4	19.2	37.8	325.0
0.58	18.6	19.4	37.8	331.3
0.59	18.8	19.6	37.7	337.6
0.6	19.0	19.8	37.7	343.9
0.61	19.2	20.0	37.7	350.2
0.62	19.3	20.2	37.7	356.5
0.63	19.6	20.4	37.7	362.8
0.64	19.8	20.6	37.7	369.0
0.65	20.0	20.6	37.7	375.3
0.66	20.2	20.6	37.7	381.6
0.67	20.4	20.6	37.7	387.9
0.68	20.6	21.4	37.9	394.2
0.69	20.7	21.6	37.9	400.5
0.7	20.9	21.8	37.9	406.8
0.71	21.1	22.0	37.9	413.2
0.72	21.3	22.2	37.9	419.5
0.73	21.6	22.4	37.9	425.8
0.74	21.8	22.6	37.9	432.1
0.75	22.0	22.7	37.9	438.4
0.76	22.2	22.9	37.9	444.7
0.77	22.3	23.1	37.9	451.1
0.78	22.5	23.3	37.8	457.4
0.79	22.6	23.5	37.8	463.7
0.8	22.9	23.7	37.8	470.0
0.81	23.2	23.9	37.8	476.3
0.82	23.4	24.1	37.7	482.5
0.83	23.5	24.3	37.6	488.8
0.84	23.7	24.5	37.6	495.1
0.85	23.9	24.7	37.6	501.3
0.86	24.1	24.9	37.7	507.6
0.87	24.3	25.1	37.8	513.9
0.88	24.5	25.3	37.8	520.2
0.89	24.7	25.5	37.8	526.5
0.9	24.9	25.7	37.9	532.8
0.91	25.1	25.9	38.0	539.2
0.92	25.4	26.1	38.0	545.5
0.93	25.4	26.3	38.0	551.8
0.94	25.6	26.6	38.0	558.2
0.95	25.8	26.8	38.0	564.5
0.96	26.0	27.0	38.0	570.8
0.97	26.2	27.2	38.0	577.2
0.98	26.4	27.4	38.0	583.5
0.99	26.7	27.5	37.9	589.8
1	26.8	27.7	37.9	596.1

Appendix G: List of publications with a relation to the dissertation

- Walzel, S. & Roubik, K. (2025). Effect of tissue viscoelasticity on delivered mechanical power in a physical respiratory system model: Distinguishing between airway and tissue resistance. *Biomedical Physics & Engineering Express, 11*(1), 015026. DOI: 10.1088/2057-1976/ad974b. *(IF = 1.6)*

- Walzel, S., Bis, L., Ort, V. & Roubik, K. (2025). Simple design of mechanical ventilator for mass production may offer excellent performance, precise monitoring, and advanced safety. *Applied Sciences, 15*(10), 5631. DOI: 10.3390/app15105631. (IF = 2.5)

- Roubik, K., Ort, V., Horakova, L. & Walzel, S. (2023). Novel design of inspiratory flow generation and gas mixing for critical care ventilators suitable for rapid production and mass casualty incidents. *Scientific Reports, 13*(1), 7153. DOI: 10.1038/s41598-023-34300-x. *(IF = 3.9)*

- Walzel, S. & Roubik K. (2025). Evaluation of simplified mechanical power and dissipated energy calculations in physical respiratory models with tissue and airway resistance. *Lékař a technika-Clinician and Technology,* 55(1). DOI: 10.14311/CTJ.2025.1.03. (in print).

Appendix H: List of publications without a relation to the dissertation

Journal articles with impact factor

- Walzel, S., Mikus, R., Rafl-Huttova, V., Rozanek, M., Bachman, T. E. & Rafl, J. (2023). Evaluation of leading smartwatches for the detection of hypoxemia: Comparison to reference oximeter. *Sensors, 23*(22), 9164. DOI 10.3390/s23229164. (IF = 3.5)

- Rafl, J., Bachman, T. E., Rafl-Huttova, V., Walzel, S. & Rozanek, M. (2022). Commercial smartwatch with pulse oximeter detects short-time hypoxemia as well as standard medical-grade device: Validation study. *Digital Health, 8*, 20552076221132127. DOI 10.1177/20552076221132127. (IF = 3.3)

- Roubik, K., Sykora, K., Sieger, L., Ort, V., Horakova, L. & Walzel, S. (2022). Perlite is a suitable model material for experiments investigating breathing in high density snow. *Scientific Reports, 12*(1), 2070. DOI 10.1038/s41598-022-06015-y. (IF = 3.9)

- Walzel, S., Rozanek, M. & Roubik, K. (2023). Perlite has similar diffusion properties for oxygen and carbon dioxide to snow: Implications for avalanche safety equipment testing and breathing studies. *Applied Sciences, 13*(23), 12569. DOI 10.3390/app132312569. (IF = 2.5)

- Walzelova, K., Walzel, S. & Hovorka, J. (2025). Simultaneous mobile PM10 monitoring provides high definition spatial and time localization of hotspots of poor air quality in an urban environment. *European Journal of Environmental Sciences*, *15*(1), 34-42. DOI 10.14712/23361964.2025.5. (IF = 1.0)

Journal articles

- Roubik, K., Walzel, S., Horakova, L., Refalo, A., Sykora, K., Ort, V. & Sieger, L. (2020). Materials suitable to simulate snow during breathing experiments for avalanche survival research. *Lékař a technika-Clinician and Technology, 50*(1), 32–39. DOI: 10.14311/CTJ.2020.1.05.

- Etxeberria-Arteun, M. P. & Walzel, S. (2024). Perfusion index values are consistent across common lying surgical positions. *Lékař a technika-Clinician and Technology*, *54*(3), 101–105. DOI 10.14311/CTJ.2024.3.05.

Conference proceedings

- Walzel, S. (2023). Comparing Perfusion Index Between Fingers During Short-Term Hypoxemia: Implications for SpO2 Monitoring. In *International Conference on e-Health and Bioengineering* (pp. 22-29). Cham: Springer Nature Switzerland. DOI 10.1007/978-3-031-62502-2_3.

- Sebestova, H., Walzel, S. & Kudrna, P. (2022). Educational pulse oximeter controlled by microprocessor. In *Proceedings of the 2022 E-Health and Bioengineering Conference (EHB)*. DOI 10.1109/EHB55594.2022.9991740.

- Roubik, K., Skola, J., Horakova, L., Ort, V. & Walzel, S. (2021). First clinical use of rapidly designed and manufactured mechanical lung ventilator CoroVent for COVID-19 patients. In *Proceedings of the 2021 International Conference on E-Health and Bioengineering (EHB)*. DOI 10.1109/EHB52898.2021.9657608.

- Walzel, S. & Roubik, K. (2021). Decrease in brain oxygenation is significantly less pronounced than decrease in SpO_2 during short-time breathing experiments in simulated avalanche snow. In *Proceedings of the 2021 International Conference on E-Health and Bioengineering (EHB)* (pp. 1–6). IEEE. DOI 10.1109/EHB52898.2021.9657655.

- Ort, V., Bis, L. & Walzel, S. (2023). Practice-oriented education of biomedical engineers. In *The International Scientific Conference eLearning and Software for Education* (Vol. 1, pp. 418-424). "Carol I" National Defence University. DOI 10.12753/2066-026X-23-039.